NIST Technical Note 1858

Impact Characterization of 4340 and T200 Steels by Means of Standard, Sub-Size and Miniaturized Charpy Specimens

Enrico Lucon
Chris N. McCowan
Ray L. Santoyo

This publication is available free of charge from:
http://dx.doi.org/10.6028/NIST.TN.1858

NIST Technical Note 1858

Impact Characterization of 4340 and T200 Steels by Means of Standard, Sub-Size and Miniaturized Charpy Specimens

Enrico Lucon
Chris N. McCowan
Ray L. Santoyo

Applied Chemicals and Materials Division
Material Measurement Laboratory

This publication is available free of charge from:
http://dx.doi.org/10.6028/NIST.TN.1858

February 2015

U.S. Department of Commerce
Penny Pritzker, Secretary

National Institute of Standards and Technology
Willie May, Acting Under Secretary of Commerce for Standards and Technology and Acting Director

National Institute of Standards and Technology Technical Note 1858
Natl. Inst. Stand. Technol. Tech. Note 1858, 61 Pages (February 2015)
CODEN: NTNOEF

This publication is available free of charge from:
http://dx.doi.org/10.6028/NIST.TN.1858

Abstract

In this investigation, we performed instrumented Charpy tests in order to characterize the impact properties of three steels, used by NIST for the production of Charpy reference specimens (4340 quenched and tempered with two energy levels, and T200 18Ni maraging steel). For each of the steels, tests were performed on standard E23 Charpy specimens, sub-size specimens of three types (3/4-size, 1/2-size and 1/4-size), and miniaturized specimens of Reduced Half-Size (RHS) geometry. For every combination of steel and specimen type, full transition curves and corresponding transition temperatures were established for absorbed energy, lateral expansion and shear fracture appearance.
Topics addressed in this study include:

- the relationship between different measures of ductile-to-brittle transition temperature;
- comparisons between, and normalization of, characteristic instrumented forces obtained from different specimen types;
- the relationship between different measures of absorbed energy;
- the relationship between transition temperatures and upper shelf energies calculated from different specimen types; and
- the relationship between shear fracture appearance optically measured and estimated from characteristic impact forces.

Among the most interesting conclusions emerging from this investigation, we mention the following.

– The use of 1/4-size sub-size specimens (thickness = 2.5 mm) has pointed out several issues from the experimental and analytical point of view, and therefore, the use of miniaturized specimens might be preferable instead for the characterization of thin-walled structures or components.
– The results of this investigation, in terms of the relationships between test data measured from specimens of different type (full-size Charpy, sub-size Charpy, miniaturized Charpy) and size, were partially complicated by large uncertainties in some of the measured ductile-to-brittle transition temperatures and upper shelf energies.
– It looks feasible to obtain conservative predictions of shear fracture appearance (*SFA*) and *SFA*-based transition temperatures through the use of empirical formulae based on characteristic instrumented forces.
– The comparison between our results and the data from Table 9 of ASTM A370-14 (*Charpy V-Notch Test Acceptance Criteria for Various Sub-Size Specimens*) clearly shows that the approach proposed by the standard can work only if the different specimens tested correspond to the same material's fracture behavior (brittle/transition/ductile). If this is not the case, a completely different approach must be sought for correlating Charpy acceptance criteria between full-size and sub-size specimens.

Keywords

ASTM A370; Charpy acceptance criteria; ductile-to-brittle transition temperature; instrumented Charpy tests; miniaturized Charpy specimens; NIST reference steels; size-normalization; sub-size Charpy specimens; shear fracture appearance; upper shelf energy.

Table of Contents

1. Introduction

Many modern structural steels are characterized by a continuously increasing ratio between ductility and mechanical strength, which makes it difficult to interpret the results of conventional mechanical characterization tests, such as Charpy impact tests. In these steels, the improvement in fracture resistance is due to various refinements of the manufacturing process, which lead to smaller gran sizes, reduced inclusion contents, a fine bainitic structure, etc. For steels exhibiting this combination of toughness and ductility, the usefulness and significance of conventional mechanical tests are nowadays seriously questioned, as well as the possibility of predicting fracture scenarios in full-scale tests based on the outcome of small-scale laboratory tests.

According to current Charpy test standards (ASTM E23-12c and ISO 148-1:2009), absorbed energy (*KV*) results from partially fractured test specimens can be averaged with the results from fully fractured specimens. However, most researchers agree that if a specimen does not fully fracture at the end of a Charpy test, a significant fraction of the work spent was employed to bend/plastically deform the sample rather than fracture it. Therefore, in principle, *KV* from partially and fully fractured specimens is not directly comparable and should not be averaged. In the case of very high-ductility materials such as modern line pipe steels, the situation is exacerbated by the very limited amount of tearing (actual fracture) observed on tested specimens. The extremely high *KV* values recorded from these tests can be attributed mostly to bending of the sample and friction between specimen and anvils. The reliability and usefulness of conventional Charpy tests under these circumstances are therefore questionable.

In the work presented here, we characterized the impact properties of three steels that are used at NIST for the production of reference Charpy specimens for the indirect verification of impact testing machines in accordance with ASTM E23-12c: two quenched and tempered 4340 steels (with different mechanical properties induced by different thermal treatments) and a T200 18Ni maraging steel.

For each of the steels investigated, we performed tests on standard full-size Charpy specimens (10 × 10 × 55 mm), CVN, sub-size specimens corresponding to different fractions of the thickness of a standard Charpy specimen (3/4, 1/2, 1/4), SCVN, and scaled miniaturized specimens (Reduced Half-Size, RHS, geometry), MCVN. All tests were performed as instrumented impact tests, recording the force applied to the specimen during impact, at temperatures ranging from lower shelf conditions (fully brittle behavior) to upper shelf conditions (fully ductile behavior). Ductile-to-Brittle Transition Temperatures (*DBTT*s) calculated from absorbed energy, lateral expansion, and shear fracture appearance were compared among the different specimen types, and empirical correlations between full-size, sub-size, and miniaturized specimens were established.

For many materials of recent production, it is often very difficult to correctly interpret the fracture surface when performing optical measurements of Shear Fracture Appearance (*SFA*) because of the complex appearance of the microstructure and the intermixing of brittle (cleavage) and ductile features. Under these circumstances, the conventional methods of *SFA* measurement are associated to a very high degree of uncertainty and the availability of an instrumented test record is extremely useful. Characteristic force values, which correspond to specific events such as general yield, maximum force, initiation of brittle fracture and crack arrest, can be correlated to the percentage of ductility on the fracture surface, and reasonable estimates of *SFA* can be obtained by correlation of these characteristic force values.

An additional incentive to conduct this investigation came from a request formulated to NIST by a Task Group of ASTM Subcommittee A01.13 (*Mechanical and Chemical Testing and Processing Methods of Steel*

Products and Processes). Task Group A01.13 on *A370 Table 9 Use and Accuracy* is working on a possible revision of ASTM A370-14 [1], and specifically on the revision of Table 9 (reproduced in Figure 1), which provides the equivalence between Charpy acceptance criteria for CVN and SCVN specimens. NIST and the ASTM Task Group planned the activity described herein, as a way to verify the numbers provided in Table 9 (the original reference for the Table 9 is unknown), as well as investigate the possibility of extending its applicability to full-size values above 40 ft-lbf (54 J), which is currently excluded by Note A of the Table.

TABLE 9 Charpy V-Notch Test Acceptance Criteria for Various Sub-Size Specimens

Full Size, 10 by 10 mm		¾ Size, 10 by 7.5 mm		⅔ Size, 10 by 6.7 mm		½ Size, 10 by 5 mm		⅓ Size, 10 by 3.3 mm		¼ Size, 10 by 2.5 mm	
ft·lbf	[J]	ft·lbf	[J]	ft·lbf	[J]	ft·lbf	[J]	ft·lbf	[J]	ft·lbf	[J]
40[A]	[54]	30	[41]	27	[37]	20	[27]	13	[18]	10	[14]
35	[48]	26	[35]	23	[31]	18	[24]	12	[16]	9	[12]
30	[41]	22	[30]	20	[27]	15	[20]	10	[14]	8	[11]
25	[34]	19	[26]	17	[23]	12	[16]	8	[11]	6	[8]
20	[27]	15	[20]	13	[18]	10	[14]	7	[10]	5	[7]
16	[22]	12	[16]	11	[15]	8	[11]	5	[7]	4	[5]
15	[20]	11	[15]	10	[14]	8	[11]	5	[7]	4	[5]
13	[18]	10	[14]	9	[12]	6	[8]	4	[5]	3	[4]
12	[16]	9	[12]	8	[11]	6	[8]	4	[5]	3	[4]
10	[14]	8	[11]	7	[10]	5	[7]	3	[4]	2	[3]
7	[10]	5	[7]	5	[7]	4	[5]	2	[3]	2	[3]

[A] Table is limited to 40 ft-lbf because the relationship between specimen size and test results has been reported to be non-linear for higher values.

Figure 1 - Table 9 from ASTM A370-14, used with permission.

2. Materials and experimental procedure

Three steels, currently used by NIST for the production of reference Charpy specimens for the indirect verification of impact machines, were considered in this study. Two of the steels correspond to quenched and tempered AISI 4340 structural steel, which by way of different thermal treatments can be given significantly different mechanical properties; these are used for the production of low-energy specimens (approximately 15 J to 20 J Charpy absorbed energy at -40 °C) and high-energy specimens (approximately 100 J at -40 °C). The third steel is an 18 Ni maraging steel designated T200, a low-carbon ultra-high-strength steel which derives its strength from the precipitation of intermetallic compounds; it is used for the production of super-high energy specimens (approximately 200 J at room temperature). The chemical composition of the steels is shown in Table 1. Table 2 provides the measured hardness (Rockwell C, HRC) and the corresponding tensile strength, σ_{TS}, which was estimated through the use of standardized conversion tables [2].

Table 1 - Chemical composition (weight %) of the investigated steels. (n/a = not applicable.)

Steel	C	Mn	Si	S	P	Al	Ni	Cr	Mo	Ti	Co
4340	0.4	0.66	0.28	0.001	0.004	n/a	1.77	0.83	0.28	n/a	n/a
T200	≤0.01	≤0.01	≤0.01	≤0.01	≤0.01	0.1	18.5	n/a	3.0	0.7	≤0.5

Table 2 – Rockwell hardness and estimated tensile strength for the investigated steels.

Steel	HRC	σ_{TS} (MPa)
4340 – low energy	45.0	1480
4340 – high energy	30.0	952
T200	36.2	1134

Additional information on the materials and the heat treatment and machining process can be found in [3] and [4] for 4340 and T200, respectively.

Charpy specimens of five different geometries were tested:

- full-size Charpy V-notch specimens (CVN);
- sub-size Charpy V-notch specimens (SCVN) with thicknesses B = 7.5 mm (3/4-size), 5 mm (1/2-size), and 2.5 mm (1/4-size) (Figure 2);
- miniaturized Charpy V-notch specimens (MCVN) of the RHS (*Reduced Half-Size*) type, with cross-section dimensions 4.83 mm × 4.83 mm and length 24.13 mm; this is the reference specimen type in ASTM E2248-13 [5] (Figure 3).

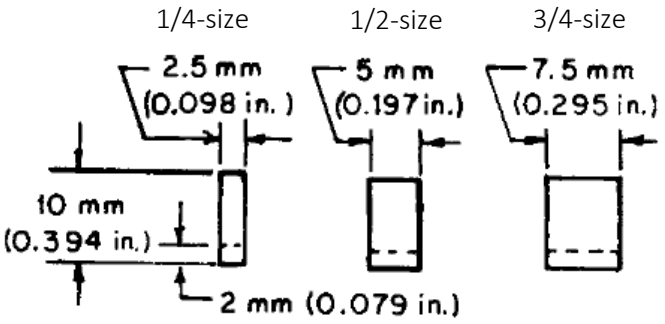

Figure 2 - Cross-sectional dimensions of the SCVN specimens used in this study.

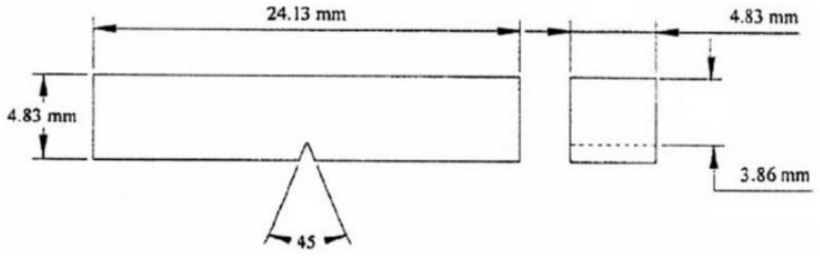

Figure 3 – Miniaturized specimens of RHS type.

Specimens were fabricated from the following NIST reference specimen lots: LL-141 (4340 low energy), HH-143 (4340 high energy), and SH-38 (T200 super-high energy). SCVN and RHS specimens were machined out of CVN specimens of the corresponding materials.

For every material and specimen type, between 9 and 13 instrumented Charpy tests were performed at temperatures which allowed a complete definition of transition curves for absorbed energy, lateral expansion (*LE*) and shear fracture appearance (*SFA*).

CVN and SCVN tests were performed on a large-scale impact machine with capacity of 953.56 J and impact speed of 5.47 m/s. The machine was equipped with an instrumented striker conforming to ASTM E23-12c (radius of striking edge = 8 mm). For tests above room temperature, specimens were heated by means of an electric plate; for tests below room temperature down to -90 °C, specimens were refrigerated by means of a cooling bath of ethyl alcohol. Below -90 °C, specimens were positioned on a steel block partially immersed in liquid nitrogen inside an insulated container. In all cases, the time required to transfer the specimen from the conditioning medium and striker impact was well below 5 s (typically around 3 s). During conditioning, temperature was monitored by means of a dummy specimen instrumented with a K-type thermocouple.

In order to maintain the position of the center of strike when SCVN specimens were tested, shims were attached to the supports of the impact machine by means of double-sided tape. The thickness of the shims was 1.25

mm, 2.5 mm, and 3.75 mm for 3/4-size, 1/2-size, and 1/4-size specimens, respectively, so that the centerline of the SCVN specimen at impact coincided with the centerline of a CVN specimen.

RHS specimens were tested on a small-scale impact tester with a capacity of 50.8 J, impact speed of 3.5 m/s and equipped with an instrumented striker with a striking edge radius of 3.86 mm (nominal 4-mm striker, in accordance with E2248-13). For high-temperature tests, specimens were heated by means of an electric plate. For low-temperature tests, the samples were individually immersed in liquid nitrogen (LN_2) until their temperature was stable between -180 °C and -190 °C. Specially-made tongs were used to remove the specimen from the LN_2 bath and position it on the machine supports and anvils. When the specimen reached the desired test temperature (within approximately ± 3 °C), the hammer was released and the specimen impacted. The actual specimen temperature at the moment of impact was recorded*. Each sample was individually instrumented with a K-type thermocouple that had been spot-welded on the specimen surface in the vicinity of the notch tip (within 1 mm). To minimize temperature gradients induced by the small size of the specimens, the anvils and supports of the machine were kept at low temperature (between -30 °C and -60 °C) by a constant flow of LN_2 vapors through copper blocks insulated with Styrofoam.

For all tests, absorbed energy (*KV*) values were provided by the machine encoder. Lateral expansion (*LE*) on CVN and SCVN specimens was measured by the use of a gage similar to the one recommended by ASTM E23-12c, Fig. 7. On RHS specimens, *LE* measurements were executed with the aid of a caliper.

Shear fracture appearance (*SFA*) was measured directly on the specimen fracture surface in accordance with ASTM E23-12c and ISO 148-1:2009. Optical measurements were also compared with estimates obtained from the instrumented test records, by means of empirical formulae that are included in both ISO 14556:2000 [6] and ASTM E2298-13a [7]. These formulae utilize characteristic instrumented forces (general yield, maximum force, brittle fracture initiation and crack arrest) to quantify the percentage of brittle fracture for the specimen tested. Results and analyses are reported elsewhere [8].

3. Data analyses

3.1 Conventional Charpy parameters (*KV*, *LE*, *SFA*)

Absorbed energy, lateral expansion and shear fracture appearance values were fitted as a function of test temperature with the widely used, hyperbolic tangent model, given by:

$$Y = A + B \tanh \frac{X - DBTT}{C} \quad , \tag{1}$$

where the variable X is temperature (in °C) and Y is *KV*, *LE*, or *SFA*, and A, B, *DBTT*, and C are fitting coefficients that are calculated by the least-square method [9]. The fitting coefficients in eq.(1) have the following physical interpretation:

- $A + B$ corresponds to the upper shelf value (asymptotic Y level that the curve approaches for $X \rightarrow +\infty$);
- $A - B$ corresponds to the lower shelf value (asymptotic Y level that the curve approaches for $X \rightarrow -\infty$);
- C corresponds to the half-width of the transition region (portion of the curve between lower and upper shelf), in °C;

*The same procedure was followed for tests above room temperature.

- *DBTT* (Ductile-to-Brittle Transition Temperature) corresponds to the *X* value of the midpoint between lower and upper shelf, in °C;
- *B*/*C* corresponds to the slope of the fitted curve in the transition region.

Data fitting for *KV* and *LE* values was performed with the following constraint applied:

- the upper shelf value (*A* + *B*) was set as the average *KV* or *LE* for all specimens having *SFA* ≥ 95 %.

Data fitting for *SFA* values was performed with the following constraint applied:

- *A* and *B* were both set at 50 %, so that lower and upper shelf levels always equal 0 % and 100 %, respectively; as a consequence, the value of *DBTT* (designated as $FATT_{50}$[†]) always corresponds to *SFA* = 50 %.

For each data set analyzed (material/specimen type), the following parameters are reported:

- *DBTT*s calculated from the transition curves of absorbed energy ($DBTT_{KV}$), lateral expansion ($DBTT_{LE}$), and shear fracture appearance ($FATT_{50}$);
- upper shelf energy (*USE*) from the *KV* transition curve.

3.2 Instrumented Charpy parameters

From the analysis of each instrumented Charpy test record, conducted in accordance with both ISO 14556:2000 [6] and ASTM E2298-13a [7], the following values of force (*F*) and absorbed energy (*W*)[‡] were determined:

- general yield (F_{gy}, W_{gy});
- maximum force (F_m, W_m);
- initiation of brittle fracture (F_{bf}, W_{bf})[§];
- crack arrest (F_a, W_a);
- test termination (W_t).

In case of fully brittle behavior (curve of Type A according to ASTM E2298-13a, curve of Type A or B according to ISO 14556:2000), F_{gy} is not defined. In case of fully ductile behavior (curve of Type A according to ASTM E2298-13a, curve of Type A or B according to ISO 14556:2000), F_{bf} and F_a are not defined.

Additionally, the ratio between the two independent measures of absorbed energy (*KV* and W_t) was calculated and reported. *KV* and W_t should ideally be in agreement within ± 15 % [7], and their ratio should be reasonably consistent from test to test and from material to material (since it depends only on the machine characteristics and the calibration of the instrumented striker), see Section 4.3.

[†] *FATT* stands for Fracture Appearance Transition Temperature.
[‡] In terms of absorbed energy, *KV* is the value provided by the machine encoder, whereas *W* is calculated from the instrumented force-displacement curve.
[§] The identification used here and in the rest of this document ("*bf*") is from ASTM E2298-13a; ISO 14556:2000 uses "*iu*" as a subscript.

4. Test results

4.1 Conventional Charpy parameters (*KV*, *LE*, *SFA*)

Conventional test results for CVN, SCVN and RHS specimens are provided in Tables 3 to 7.

Table 3 - Charpy test results for CVN specimens.

4340 – Low energy					4340 – High energy					T200 – Super-high energy[**]				
Specimen id	**T (°C)**	***KV* (J)**	***LE* (mm)**	***SFA* (%)**	**Specimen id**	**T (°C)**	***KV* (J)**	***LE* (mm)**	***SFA* (%)**	**Specimen id**	**T (°C)**	***KV* (J)**	***LE* (mm)**	***SFA* (%)**
1435	-198	6.02	0.129	2	468	-198	12.27	0.152	6	825	-198	35.13	0.230	26
1542	-150	7.09	0.112	2	298	-150	24.61	0.149	9	714	-150	41.96	0.463	32
1875	-121	8.53	0.121	3	296	-120	27.44	0.136	18	147	-120	74.29	0.598	54
1730	-90	9.52	0.110	4	467	-90	64.04	0.639	72	61	-90	117.50	1.068	68
1527	-60	16.67	0.108	8	292	-60	96.89	1.309	100	874	-60	144.84	1.535	88
1590	-30	18.77	0.120	15	300	-30	106.24	1.427	100	624	-30	144.39	1.605	80
1516	21	21.65	0.163	31	294	21	107.82	1.320	100	101	21	169.53	1.799	100
1937	50	23.28	0.198	42	469	50	120.44	1.535	100	1109	21	175.22	1.996	100
1500	100	28.23	0.218	100	299	100	125.83	1.561	100	442	21	186.37	1.911	100
1640	150	30.06	0.236	100						686	21	187.22	2.087	100
2743	200	34.67	0.218	100						963	21	178.11	1.957	100
1563	300	34.89	0.257	100						204	50	166.03	1.876	100
										49	100	177.79	1.964	100

Table 4 - Charpy test results for 3/4-size specimens.

4340 – Low energy					4340 – High energy					T200 – Super-high energy				
Specimen id	**T (°C)**	***KV* (J)**	***LE* (mm)**	***SFA* (%)**	**Specimen id**	**T (°C)**	***KV* (J)**	***LE* (mm)**	***SFA* (%)**	**Specimen id**	**T (°C)**	***KV* (J)**	***LE* (mm)**	***SFA* (%)**
2992	-198	4.13	0.152	3	714	-198	13.20	0.106	7	776	-198	23.28	0.137	29
2795	-150	4.13	0.116	4	715	-150	17.51	0.180	10	916	-150	30.84	0.277	41
2575	-121	6.48	0.051	4	754	-120	20.23	0.237	21	162	-120	49.84	0.526	59
2759	-90	8.68	0.094	7	720	-100	33.29	0.589	*36*[††]	1459	-90	98.85	1.495	64
1504	-60	12.05	0.099	14	718	-90	56.57	0.523	84	1093	-60	105.98	1.821	70
2912	-30	11.97	0.098	18	712	-60	71.12	1.124	100	531	-30	125.32	1.804	81
2780	21	15.21	0.117	44	717	-30	78.40	1.794	100	201	21	135.76	1.858	100
1596	50	18.83	0.121	57	781	21	79.84	1.372	100	329	50	144.97	2.217	100
2801	100	21.32	0.181	100	713	50	87.16	1.915	100	387	100	138.44	2.158	100
2757	150	25.02	0.268	100										
2812	200	23.76	0.308	100										
2944	300	30.99	0.336	100										
2788	300	27.67	0.304	100										

[**]For this material, 5 tests were available at 21 °C (room temperature) from the latest indirect verification of the machine.

[††]For this test, it was not possible to estimate the value of *SFA* through optical measurements. The reported value is therefore the average of the estimations obtained from the instrumented test records.

Table 5 - Charpy test results for 1/2-size specimens.

4340 – Low energy					4340 – High energy					T200 – Super-high energy				
Specimen id	**T (°C)**	***KV* (J)**	***LE* (mm)**	***SFA* (%)**	**Specimen id**	**T (°C)**	***KV* (J)**	***LE* (mm)**	***SFA* (%)**	**Specimen id**	**T (°C)**	***KV* (J)**	***LE* (mm)**	***SFA* (%)**
48	-198	3.00	0.063	3	5-10	-198	10.82	0.113	11	74	-198	17.05	0.120	41
21	-150	2.93	0.086	3	5-6	-150	10.97	0.121	13	446	-150	23.98	0.397	59
20	-123	4.36	0.091	4	5-5	-120	14.73	0.359	33	376	-120	42.20	0.763	77
2	-90	5.12	0.060	9	72	-100	21.55	0.547	*36*[‡‡]	50	-90	55.75	1.177	100
97	-60	7.70	0.087	19	5-4	-90	40.19	1.081	100	929	-60	65.08	1.656	100
50	-30	7.85	0.059	28	5-3	-60	45.06	0.962	100	558	-30	71.79	1.522	100
586	21	10.90	0.067	60	5-2	-30	45.79	1.249	100	687	21	80.01	1.588	100
7	50	13.58	0.170	74	5-72	21	47.90	1.371	100	418	50	81.68	1.823	100
11	100	14.81	0.267	100	5-9	50	51.97	1.214	100	1088	100	85.47	2.013	100
2890	150	16.91	0.240	100										
1141	200	18.46	0.247	100										
63	300	18.36	0.272	100										

Table 6 - Charpy test results for 1/4-size specimens. NOTE: results highlighted in yellow were obtained from specimens most likely altered by the machining process (see the text for further details).

4340 – Low energy					4340 – High energy					T200 – Super-high energy				
Specimen id	**T (°C)**	***KV* (J)**	***LE* (mm)**	***SFA* (%)**	**Specimen id**	**T (°C)**	***KV* (J)**	***LE* (mm)**	***SFA* (%)**	**Specimen id**	**T (°C)**	***KV* (J)**	***LE* (mm)**	***SFA*[§] (%)**
5-15	-198	1.20	0.075	6	5-3	-198	5.57	0.144	11	132	-198	12.35	0.271	*60*
5-1	-150	2.33	0.087	7	5-5	-150	5.87	0.215	27	375	-150	14.50	0.491	*65*
5-2	-123	3.61	0.056	8	SS3_4	-135	0.75	0.000	0	535	-123	17.67	0.725	*57*
5-3	-90	3.61	0.088	17	SS3_3	-130	1.35	0.000	0	257	-90	18.37	0.968	*71*
5-4	-60	3.76	0.030	28	5-6	-120	13.43	0.503	93	28	-60	23.68	0.714	*87*
25-2	-30	4.44	0.060	81	5-7	-90	15.81	0.949	100	1285	-30	20.40	1.117	*79*
5-12	21	6.86	0.100	58	5-8	-60	18.30	0.575	100	414	21	21.18	1.175	*100*
5-5	50	8.00	0.132	100	5-2	-30	17.76	n/a	100	153	50	22.42	1.204	n/a[§§]
5-6	100	8.30	0.317	100	SS3_1	-25	4.98	0.071	17	745	100	24.94	1.188	*100*
10	150	7.79	0.354	100	SS3_2	-25	9.90	0.016	11					
9	200	8.32	0.382	100	5-1	21	16.67	0.998	97					
13	300	8.83	0.485	100	5-4	50	19.07	0.672	100					

Table 7 - Charpy test results for RHS specimens.

4340 – Low energy					4340 – High energy					T200 – Super-high energy				
Specimen id	**T (°C)**	***KV* (J)**	***LE* (mm)**	***SFA* (%)**	**Specimen id**	**T (°C)**	***KV* (J)**	***LE* (mm)**	***SFA* (%)**	**Specimen id**	**T (°C)**	***KV* (J)**	***LE* (mm)**	***SFA* (%)**
LL-R12	-186	1.08	0.020	3	HH-R1	-181	4.16	0.110	17	SH-R2	-194	6.41	0.140	42
LL-R3	-159	1.08	0.040	5	HH-R4	-147	4.52	0.140	22	SH-R12	-164	8.45	0.210	43
LL-R7	-118	1.94	0.020	9	HH-R10	-130	6.71	0.250	50	SH-R9	-152	14.52	0.450	65
LL-R5	-101	2.57	0.040	9	HH-R8	-121	9.17	0.350	71	SH-R6	-143	15.44	0.490	67
LL-R4	-74	2.58	0.030	12	HH-R2	-98	12.84	0.420	92	SH-R3	-125	17.84	0.600	71
LL-R2	-50	2.97	0.030	19	HH-R6	-76	13.61	0.420	100	SH-R10	-115	16.34	0.480	75
LL-R6	-25	3.08	0.050	28	HH-R7	-50	14.86	0.530	100	SH-R4	-100	22.19	0.680	100
LL-R9	0	3.47	0.070	48	HH-R11	-30	14.75	0.660	100	SH-R11	-76	24.39	0.780	100
LL-R1	22	3.99	0.090	58	HH-R12	-20	14.64	0.630	100	SH-R1	-50	24.61	0.840	100
LL-R11	99	4.87	0.110	100	HH-R9	22	16.50	0.700	100	SH-R8	-20	26.21	0.860	100
LL-R10	197	5.82	0.170	100	HH-R5	101	17.80	0.710	100	SH-R5	22	27.87	0.970	100
LL-R8	292	6.02	0.210	100	HH-R3	235	19.01	0.770	100	SH-R7	101	29.83	0.960	100

[‡‡] For this test, it was not possible to estimate the value of *SFA* through optical measurements. The reported value is therefore the average of the estimations obtained from the instrumented test records.
[§§] Instrumented signal not acquired.

In reference to Table 6, the cells highlighted in yellow indicate four 1/4-size specimens of 4340 high energy, which exhibited clear signs of overheating caused by the machining process as evidenced by "bluing" of the specimen. This phenomenon clearly altered the properties of the material, and induced a significant embrittlement which can be appreciated in Figure 4 both in terms of the increase in *DBTT* and the reduction of upper shelf levels. The results from these four tests were not used in further analyses.

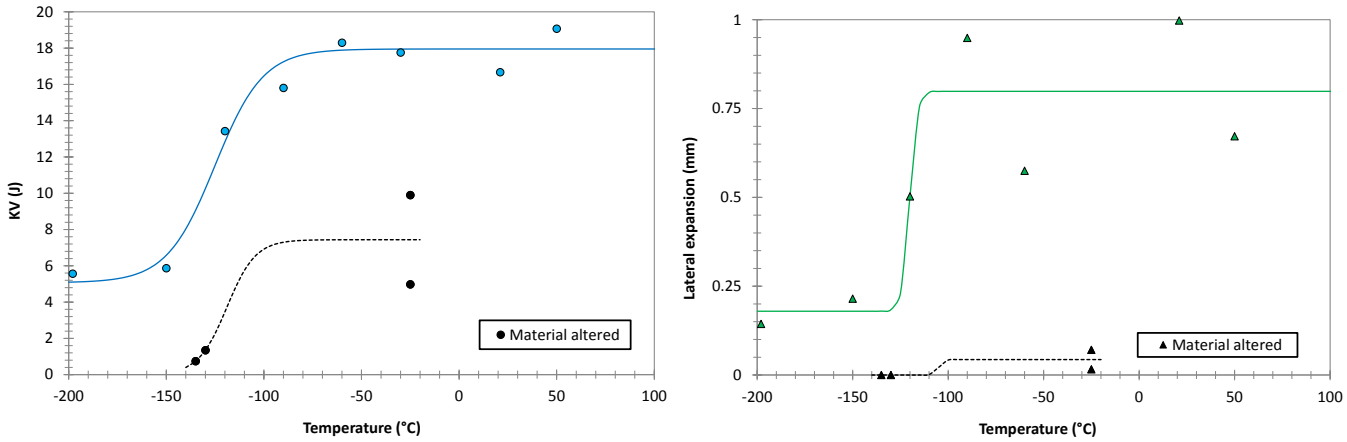

Figure 4 - Absorbed energy and lateral expansion data for 1/4-size specimens of 4340 high energy. Specimens altered by the machining process are indicated by black symbols.

Examination of the transition curves obtained leads to the following observations:

(a) For 4340 low energy, absorbed energy and lateral expansion in fully ductile conditions tend to increase up to the highest test temperature (300 °C) and often a plateau is not observed, see for example the *KV* transition curves for CVN and 3/4-size specimens in Figure 5. The calculated values of $DBTT_{KV}$, *USE* and $DBTT_{LE}$ are, therefore, associated to significant uncertainty related to the uncertainty in the corresponding upper shelf levels.

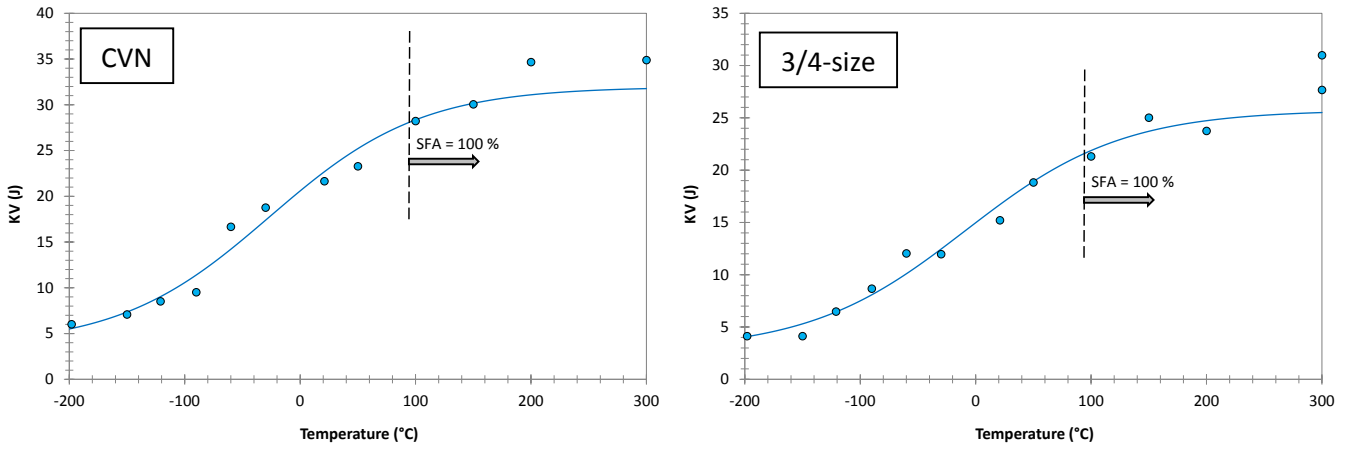

Figure 5 - Absorbed energy transition curves for CVN and 3/4-size specimens of 4340 low energy.

(b) For T200, both measurements and estimates of *SFA* in lower shelf conditions indicate a significant amount of ductility (≥ 25 %) down to the lowest test temperature which could be attained (-198 °C) (see, for example, the *SFA* transition curves for CVN and 3/4-size specimens shown in Figure 6) As a consequence, the corresponding values of $FATT_{50}$ are poorly defined, and possibly underestimated.

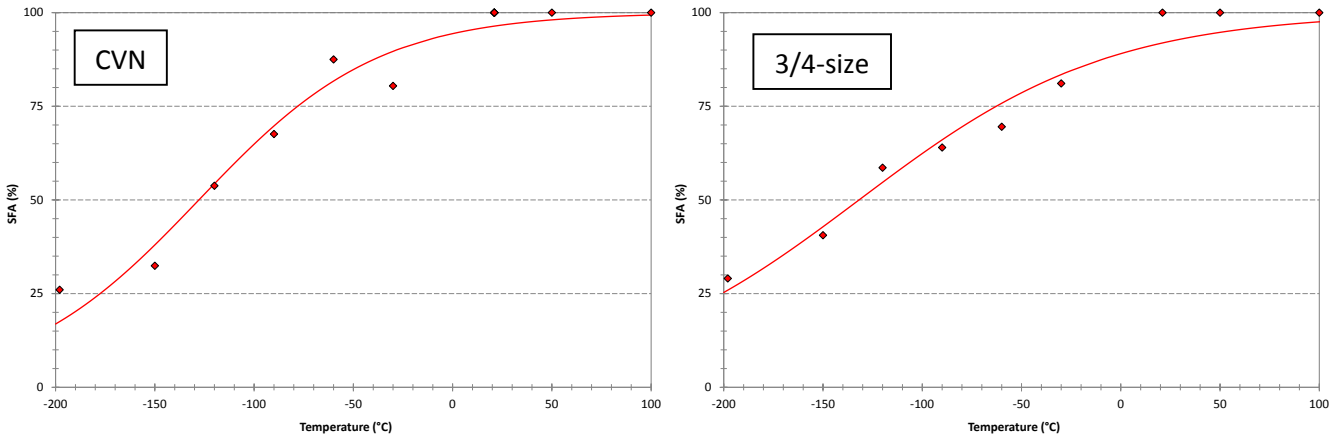

Figure 6 – Shear Fracture Appearance transition curves for CVN and 3/4-size specimens of T200.

(c) In general, all three materials exhibit high lower shelf levels of *KV* and *LE*, as compared with what is typically observed. Namely, for CVN specimens of 4340 low energy, 4340 high energy, and T200, the calculated Lower Shelf Energy (*LSE* = *A*-*B*) is 3.6 J, 15.6 J, and 25.6 J, respectively. For lateral expansion, the lower shelf values are 0.12 mm, 0.13 mm, and 0.22 mm, respectively. For comparison, ORNL found 2.7 J and 0.061 mm as the lower shelf mean values from a large database of Charpy data consisting of ferritic, structural and pressure vessel steels [10].

The values of $DBTT_{KV}$, *USE*, $DBTT_{LE}$, and $FATT_{50}$ calculated from the transition curves for all materials and specimen types are summarized in Table 8. All the individual transition curves and their regression coefficients (*A*, *B*, *C*, *DBTT*) are collected in Annex 1.

Table 8 - Values of *DBTT* and *USE* calculated from the transition curves.

Steel	Specimen type	$DBTT_{KV}$ (°C)	*USE* (J)	$DBTT_{LE}$ (°C)	$FATT_{50}$ (°C)
4340 low energy	CVN	-26.1	32.0	31.0	47.1
	3/4-size	-8.5	25.8	116.5	27.2
	1/2-size	-6.5	17.1	49.7	3.6
	1/4-size	-33.2	8.2	75.3	-40.6
	RHS	-46.2	5.6	45.4	5.0
4340 high energy	CVN	-89.8	111.4	-85.0	-102.1
	3/4-size	-93.5	79.1	-78.4	-99.4
	1/2-size	-96.2	46.2	-97.9	-107.0
	1/4-size	-125.1	18.0	-120.2	-141.6
	RHS	-115.0	15.9	-111.1	-131.4
T200	CVN	-97.6	177.2	-88.5	-127.8
	3/4-size	-98.1	139.7	-100.8	-131.9
	1/2-size	-113.4	73.3	-113.9	-176.4
	1/4-size	-126.6	22.8	-137.1	-208.3
	RHS	-143.4	25.9	-144.5	-168.8

The uncertainties in the transition temperatures, particularly for the low-energy material, are confirmed by Figures 7 to 10, which compare values of $DBTT_{KV}$, *USE*, $DBTT_{LE}$, and $FATT_{50}$ that were measured from the different specimen types. It can be noted that oftentimes *DBTT* data do not conform to the typical and expected pattern of decreasing transition temperature (*i.e.*, more ductile behavior) with decreasing specimen size.

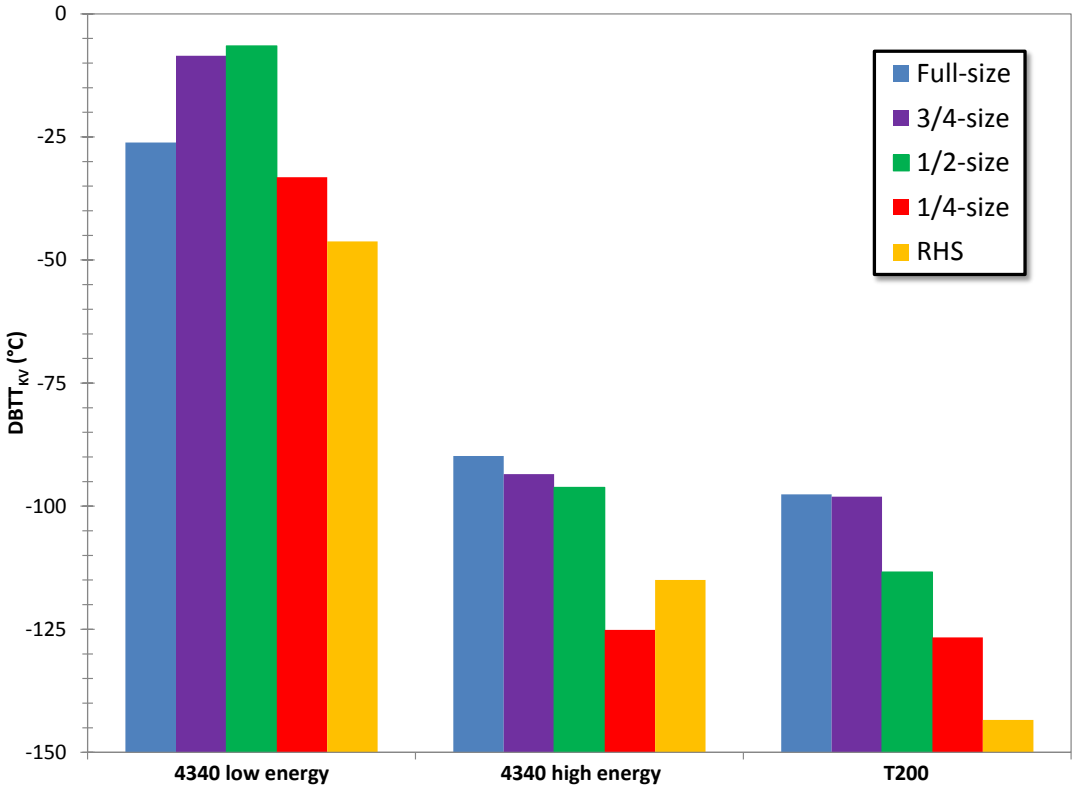

Figure 7 - *DBTT$_{KV}$* values measured from different specimen types.

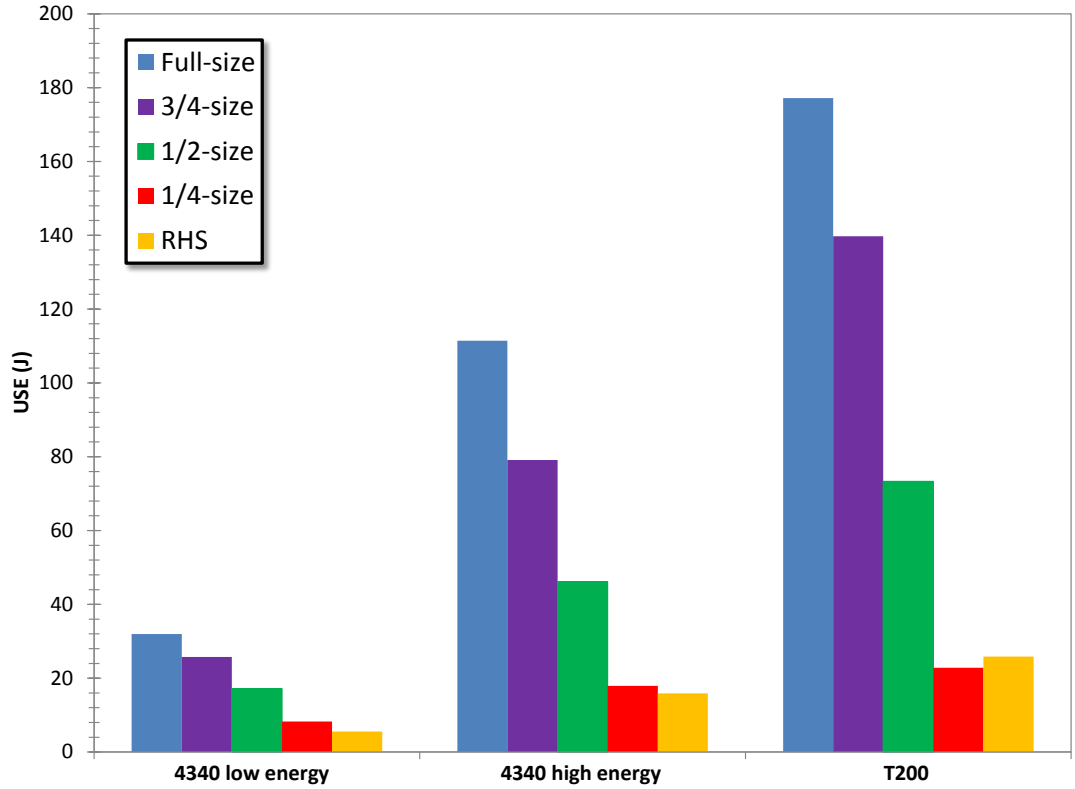

Figure 8 - *USE* values measured from different specimen types.

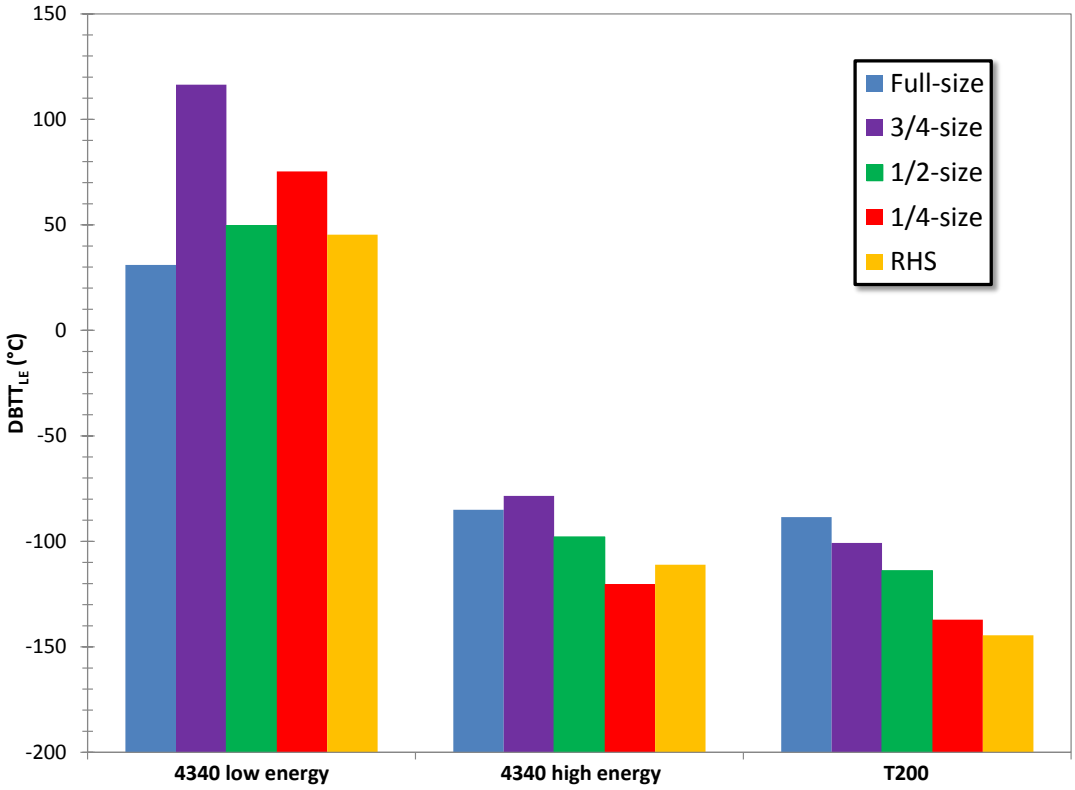

Figure 9 - *DBTT$_{LE}$* values measured from different specimen types.

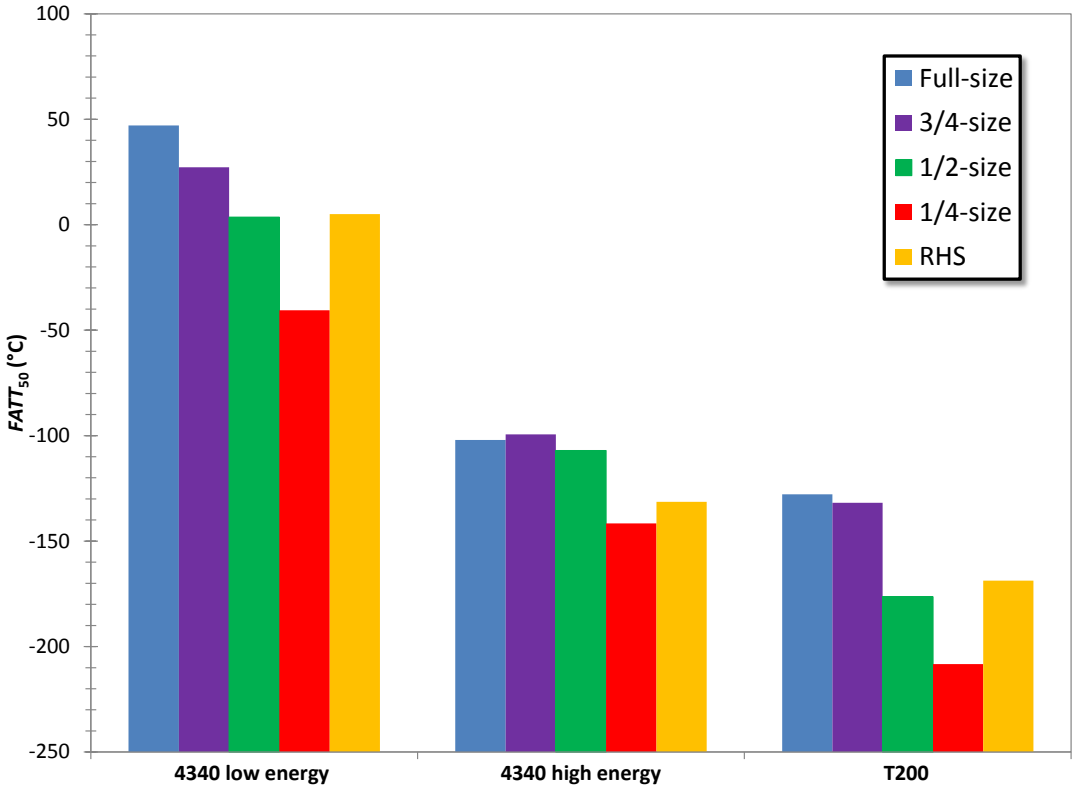

Figure 10 - *FATT$_{50}$* values measured from different specimen types.

It is interesting to briefly dwell upon the relationship between the two smallest specimens investigated, the 1/4-size (ligament cross-section: 20 mm²) and the RHS (ligament cross-section: 18.6 mm²). Based on the data shown in Figures 7 to 10, there is no consistency between transition temperature values measured from the two specimen types:

- for 4340 low energy and T200, the lowest *DBTT*s correspond to RHS, except in the case of $FATT_{50}$;
- for 4340 high energy, there is an inversion between 1/4-size and RHS, with the former providing the lowest *DBTT*s for the investigated parameters, *KV*, *LE*, and *SFA*;
- in most cases, the numerical differences are relatively small and well within the experimental uncertainties correlated with both the individual test data and the analyses of the results;
- *USE* values for 1/4-size are higher than for RHS for both 4340 low energy and 4340 high energy, but lower for T200; differences are small in all cases.

Another illustration of the inherent uncertainties that are associated with transition temperatures, as measured for the lowest energy material (for all parameters) and for T200 (in terms of *SFA*) is provided by Figure 11, where values of $DBTT_{KV}$, $DBTT_{LE}$ and $FATT_{50}$ for the different materials and specimen types are compared. In the Figure, the dotted lines correspond to ±25 °C tolerance bounds. In Figure 11, square and round symbols represent values of $DBTT_{LE}$ and $FATT_{50}$ respectively, whereas the colors indicate the type of Charpy specimen.

Ideally, all the different measures of ductile-to-brittle transition temperature should be in mutual agreement within a narrow tolerance band, typically in the order of ±15 °C. In the Figure, more lenient acceptability limits were used, which corresponded to ±25 °C, and used $DBTT_{KV}$ as the "reference" measure of transition temperature.

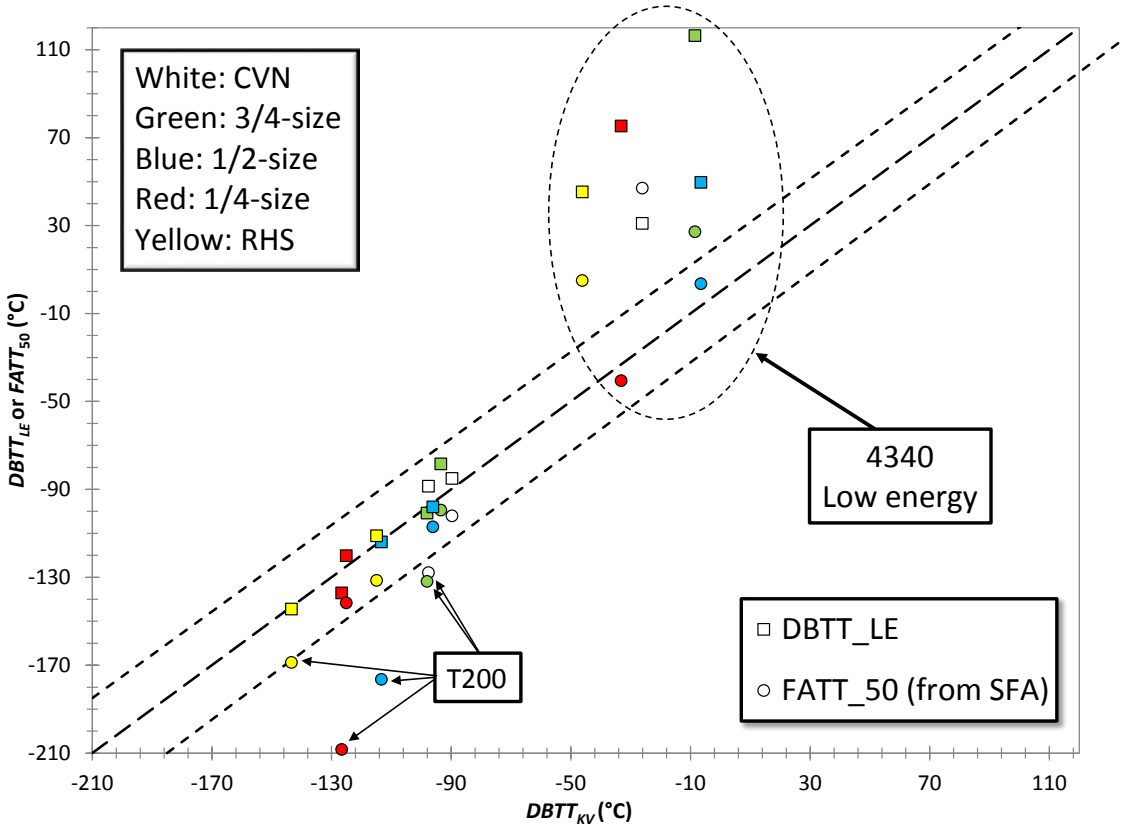

Figure 11 - Comparison between different measures of ductile-to-brittle transition temperature.

For 4340 low energy, in just two instances $DBTT_{KV}$ and $FATT_{50}$ agree within ±25 °C (1/2-size and 1/4-size specimens). The few additional data points falling outside the ±25 °C bounds for $DBTT_{KV}$ in the range -150 °C to -90 °C are all $FATT_{50}$ values from T200. These latter discrepancies stem from the poor definition of the $FATT_{50}$ caused by high percentages of shear (ductile) fracture measured even at very low temperatures, as previously illustrated in Figure 6.

All data points which fall outside the ±25 °C tolerance bounds in Figure 11 will be excluded from further analyses.

4.1.1 Differences between the materials investigated

Figures 12, 13, and 14 present a comparison between *KV*, *LE*, and *SFA* transition curves established for the investigated steels by means of CVN specimens. These figures clearly illustrate the expected ranking of the three materials in terms of impact toughness (*DBTT*s and *USE*). Note also that the difference in *DBTT* between the high-energy and super-high energy materials appears slightly larger for *KV* than for *LE* and *SFA*.

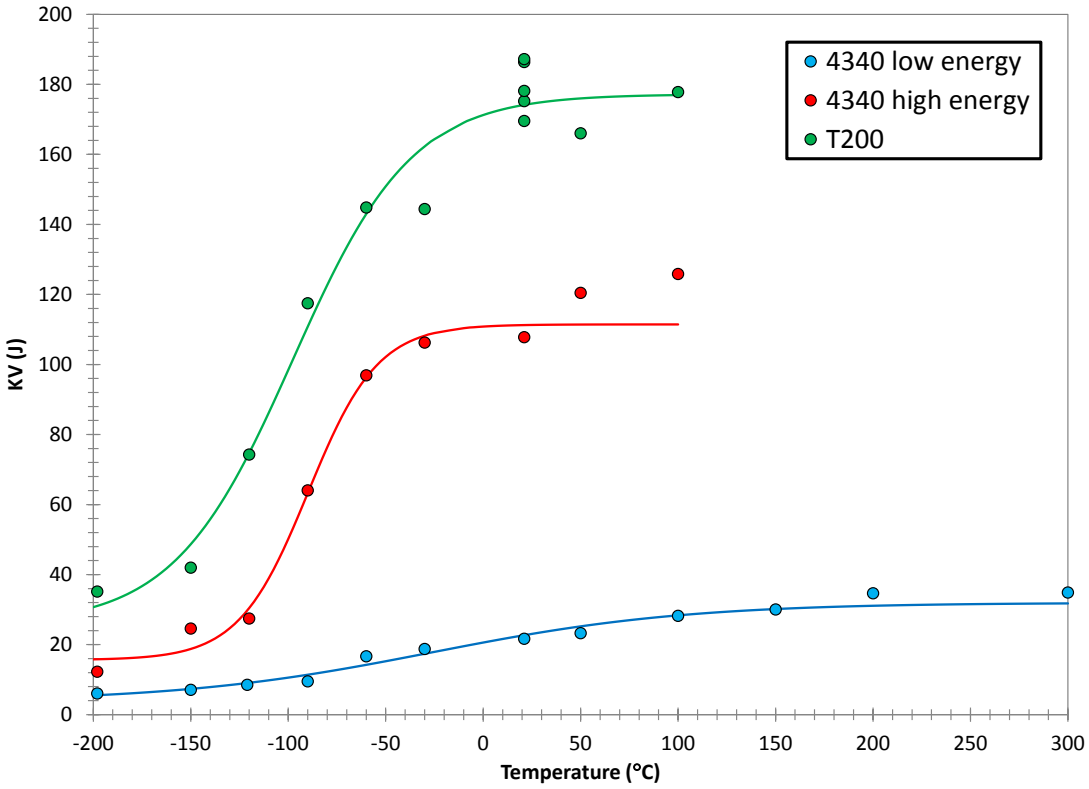

Figure 12 - Comparison between CVN transition curves for absorbed energy.

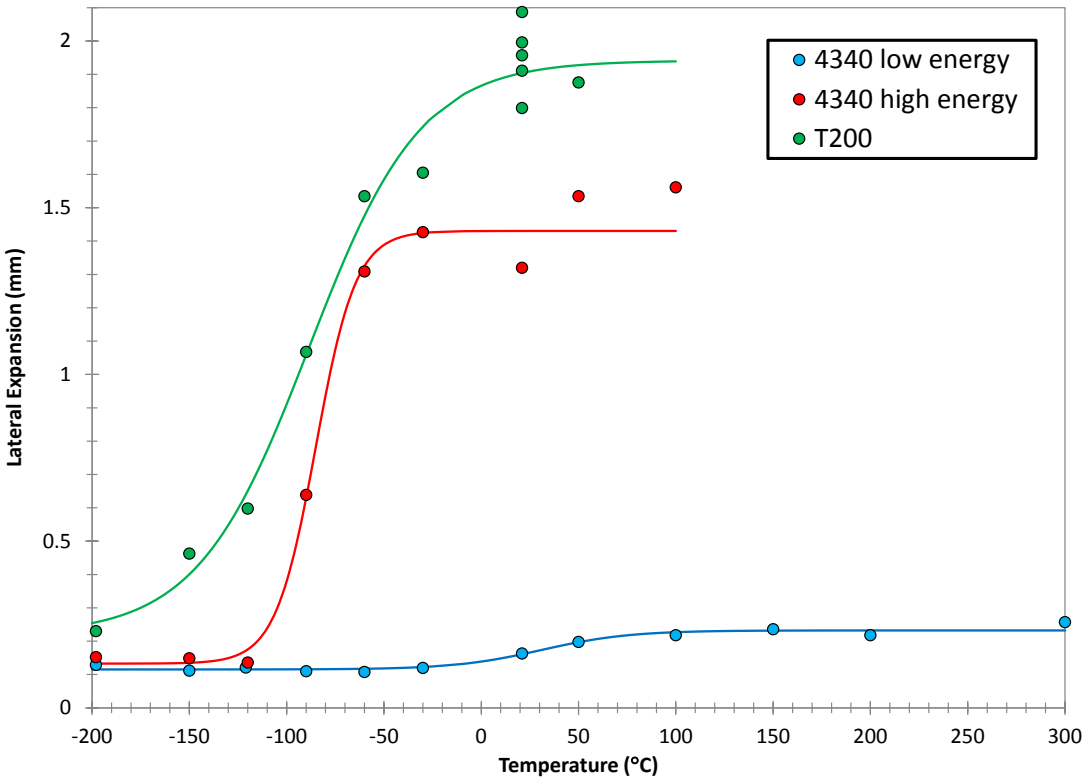

Figure 13 - Comparison between CVN transition curves for lateral expansion.

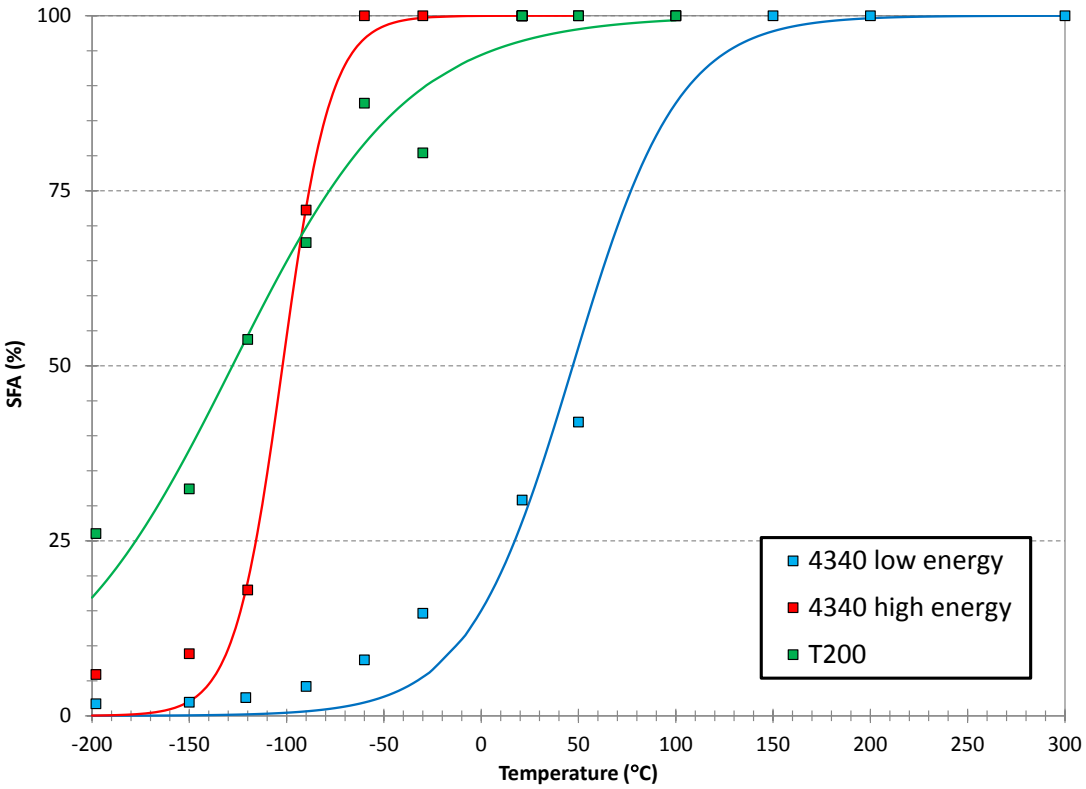

Figure 14 - Comparison between CVN transition curves for shear fracture appearance.

4.2 Instrumented Charpy parameters

Characteristic force and absorbed energy values are reported in Tables 9 to 13 for the different specimen types. Tables also include the ratio between the two measures of absorbed energy (KV/W_t).

Table 9 - Instrumented impact results obtained from CVN specimens.

4340 Low Energy									
Specimen id	**T (°C)**	F_{gy} **(kN)**	F_m **(kN)**	F_{bf} **(kN)**	F_a **(kN)**	W_m **(J)**	W_t **(J)**	KV **(J)**	$\frac{KV}{W_t}$
1435	-198	18.90	18.90	18.90	0.00	3.12	5.24	6.02	1.149
1542	-150	20.52	20.52	20.52	0.00	5.85	6.25	7.09	1.134
1875	-121	27.52	27.52	27.52	0.02	7.00	7.74	8.53	1.102
1730	-90	26.67	26.67	26.67	0.00	7.93	8.75	9.52	1.088
1527	-60	34.04	34.04	34.04	0.00	14.61	15.77	16.67	1.057
1590	-30	32.19	32.19	32.19	0.00	16.27	17.77	18.77	1.056
1516	21	26.29	31.36	31.12	0.00	18.12	19.79	21.65	1.094
1937	50	26.24	30.89	28.73	0.69	17.22	20.27	23.28	1.148
1500	100	25.57	29.22	-	-	14.33	25.85	28.23	1.092
1640	150	24.28	28.44	-	-	14.01	28.79	30.06	1.044
2743	200	24.00	28.66	-	-	15.60	33.08	34.67	1.048
1563	300	22.82	27.01	-	-	13.99	33.67	34.89	1.036
4340 High Energy									
Specimen id	**T (°C)**	F_{gy} **(kN)**	F_m **(kN)**	F_{bf} **(kN)**	F_a **(kN)**	W_m **(J)**	W_t **(J)**	KV **(J)**	$\frac{KV}{W_t}$
468	-198	28.63	28.63	26.59	0.00	8.26	11.31	12.27	1.085
298	-150	27.35	31.78	29.93	0.00	22.23	23.46	24.61	1.049
296	-120	25.58	29.65	29.19	0.00	24.01	26.25	27.44	1.045
467	-90	24.30	27.82	25.35	9.28	26.48	61.61	64.04	1.039
292	-60	23.11	26.97	-	-	29.28	93.78	96.89	1.033
300	-30	22.35	26.43	-	-	32.64	103.98	106.24	1.022
294	21	20.87	25.27	-	-	36.12	107.05	107.82	1.007
469	50	20.24	24.72	-	-	36.84	115.31	120.44	1.044
299	100	15.84	23.92	-	-	40.65	124.43	125.83	1.011
T200									
Specimen id	**T (°C)**	F_{gy} **(kN)**	F_m **(kN)**	F_{bf} **(kN)**	F_a **(kN)**	W_m **(J)**	W_t **(J)**	KV **(J)**	$\frac{KV}{W_t}$
825	-198	25.97	36.48	35.69	0.00	31.60	32.68	35.13	1.075
714	-150	26.62	36.57	34.78	0.00	38.74	40.09	41.96	1.047
147	-120	26.54	35.71	33.21	6.93	45.37	71.8	74.29	1.035
61	-90	27.00	35.24	26.91	13.00	52.31	117.9	117.5	0.997
874	-60	29.12	34.78	12.30	7.31	59.67	148.82	144.84	0.973
624	-30	25.93	34.09	11.63	6.93	60.49	148.12	144.39	0.975
101	21	***Signal not acquired***						169.53	
1109	21	24.52	32.09	-	-	63.93	177.76	175.22	0.986
442	21	24.32	32.32	-	-	64.43	187.46	186.37	0.994
686	21	24.08	32.26	-	-	64.66	187.79	187.22	0.997
963	21	24.32	32.07	-	-	65.75	181.09	178.11	0.984
204	50	***Signal not acquired***						460.94	
49	100	12.82	19.92	-	-	75.43	414.89	439.74	1.06

Table 10 - Instrumented impact results obtained from 3/4-size specimens.

Specimen id	T (°C)	F_{gy} (kN)	F_m (kN)	F_{bf} (kN)	F_a (kN)	W_m (J)	W_t (J)	KV (J)	$\frac{KV}{W_t}$
4340 Low Energy									
2992	-198	14.69	14.69	14.69	0.00	2.56	3.58	4.13	1.15
2795	-150	13.51	13.51	13.51	0.05	2.45	3.43	4.13	1.20
2575	-121	15.47	15.47	15.47	0.00	4.82	5.22	6.48	1.24
2759	-90	20.94	20.94	20.94	0.00	7.50	8.06	8.68	1.08
1504	-60	23.82	23.82	23.82	0.00	10.20	11.36	12.05	1.06
2912	-30	24.00	24.00	24.00	0.00	9.82	11.54	11.97	1.04
2780	21	22.57	25.78	25.78	0.00	11.64	15.20	15.21	1.00
1596	50	18.92	21.43	20.51	5.41	11.89	17.02	18.83	1.11
2801	100	19.33	22.15	-	-	11.39	19.64	21.32	1.09
2757	150	17.96	20.58	-	-	10.28	23.62	25.02	1.06
2812	200	16.48	18.61	-	-	9.25	21.03	23.76	1.13
2944	300	14.72	20.09	-	-	11.29	27.42	30.99	1.13
2788	300	17.00	19.32	-	-	9.63	26.39	27.67	1.05
4340 High Energy									
Specimen id	**T (°C)**	F_{gy} (kN)	F_m (kN)	F_{bf} (kN)	F_a (kN)	W_m (J)	W_t (J)	KV (J)	$\frac{KV}{W_t}$
714	-198	20.55	23.90	22.02	0.00	11.46	12.16	13.20	1.09
715	-150	19.96	22.48	21.01	0.00	15.43	16.25	17.51	1.08
754	-120	17.85	21.36	20.86	0.00	17.07	17.97	20.23	1.13
720	-100	14.06	20.42	18.85	4.29	17.55	31.18	33.29	1.07
718	-90	17.11	19.7	13.76	8.69	18.67	52.52	56.57	1.08
712	-60	16.61	19.15	-	-	20.66	67.94	71.12	1.05
717	-30	16.3	18.67	-	-	22.48	74.18	78.40	1.06
781	21	15.29	18.05	-	-	25.85	77.48	79.84	1.03
713	50	14.64	17.57	-	-	25.28	85.03	87.16	1.03
T200									
Specimen id	**T (°C)**	F_{gy} (kN)	F_m (kN)	F_{bf} (kN)	F_a (kN)	W_m (J)	W_t (J)	KV (J)	$\frac{KV}{W_t}$
776	-198	19.29	25.64	24.97	0.00	20.46	21.28	23.28	1.09
916	-150	19.36	25.37	24.28	0.00	25.93	27.83	30.84	1.11
162	-120	19.26	25.06	24.83	7.02	31.37	46.25	49.84	1.08
1459	-90	19.30	24.37	-	-	36.59	93.35	98.85	1.06
1093	-60	19.05	23.70	-	-	37.82	100.81	105.98	1.05
531	-30	18.22	23.43	-	-	43.49	122.86	125.32	1.02
201	21	17.82	22.29	-	-	43.20	130.40	135.76	1.04
329	50	16.93	21.60	-	-	41.30	139.32	144.97	1.04
387	100	16.67	20.79	-	-	42.58	134.72	138.44	1.03

Table 11 - Instrumented impact results obtained from 1/2-size specimens.

4340 Low Energy									
Specimen id	**T (°C)**	F_{gy} **(kN)**	F_m **(kN)**	F_{bf} **(kN)**	F_a **(kN)**	W_m **(J)**	W_t **(J)**	KV **(J)**	$\frac{KV}{W_t}$
48	-198	10.45	10.45	10.45	0.00	1.91	2.53	3.00	1.19
21	-150	9.08	9.08	9.08	0.00	1.68	2.16	2.93	1.36
20	-123	14.07	14.07	14.07	0.00	3.62	3.89	4.36	1.12
2	-90	14.24	14.24	14.24	0.00	3.55	4.47	5.12	1.15
97	-60	16.38	16.38	16.38	0.00	6.37	7.57	7.70	1.02
50	-30	16.40	16.40	16.40	0.86	6.23	7.52	7.85	1.04
586	21	10.87	13.15	13.15	2.51	5.75	8.19	10.90	1.33
7	50	13.10	14.68	13.95	4.95	7.60	12.02	13.58	1.13
11	100	12.29	13.79	-	-	7.00	13.91	14.81	1.06
2890	150	12.34	13.20	-	-	5.92	16.27	16.91	1.04
1141	200	12.52	13.31	-	-	5.54	18.68	18.46	0.99
63	300	12.06	12.83	-	-	6.09	17.42	18.36	1.05
4340 High Energy									
Specimen id	**T (°C)**	F_{gy} **(kN)**	F_m **(kN)**	F_{bf} **(kN)**	F_a **(kN)**	W_m **(J)**	W_t **(J)**	KV **(J)**	$\frac{KV}{W_t}$
5-10	-198	13.53	15.17	14.54	0.00	9.61	10.11	10.82	1.07
5-6	-150	12.66	14.72	13.72	0.73	9.30	10.35	10.97	1.06
5-5	-120	12.45	13.82	13.59	0.00	10.97	12.44	14.73	1.18
72	-100	12.21	13.25	12.98	4.36	12.01	20.32	21.55	1.06
5-4	-90	11.24	12.55	-	-	11.16	37.15	40.19	1.08
5-3	-60	10.99	12.26	-	-	13.15	41.69	45.06	1.08
5-2	-30	10.45	11.93	-	-	13.05	42.73	45.79	1.07
5-72	21	9.90	11.47	-	-	14.20	45.06	47.90	1.06
5-9	50	9.35	11.24	-	-	14.98	49.45	51.97	1.05
T200									
Specimen id	**T (°C)**	F_{gy} **(kN)**	F_m **(kN)**	F_{bf} **(kN)**	F_a **(kN)**	W_m **(J)**	W_t **(J)**	KV **(J)**	$\frac{KV}{W_t}$
74	-198	12.66	16.58	15.90	0.00	15.13	15.85	17.05	1.08
446	-150	12.63	16.24	15.16	1.70	17.52	21.01	23.98	1.14
376	-120	12.85	15.86	-	-	19.06	38.75	42.20	1.09
50	-90	12.79	15.58	13.85	12.60	21.10	52.92	55.75	1.05
929	-60	12.59	15.13	-	-	23.55	62.02	65.08	1.05
558	-30	12.52	14.62	-	-	23.06	68.47	71.79	1.05
687	21	11.61	13.97	-	-	24.43	76.16	80.01	1.05
418	50	11.22	13.66	-	-	23.79	78.87	81.68	1.04
1088	100	10.77	12.73	-	-	23.50	81.65	85.47	1.05

Table 12 - Instrumented impact results obtained from 1/4-size specimens.

4340 Low Energy									
Specimen id	**T (°C)**	F_{gy} **(kN)**	F_m **(kN)**	F_{bf} **(kN)**	F_a **(kN)**	W_m **(J)**	W_t **(J)**	KV **(J)**	$\frac{KV}{W_t}$
5-15	-198	4.94	4.94	4.94	0.00	0.87	1.17	1.20	1.03
5-1	-150	5.84	5.84	5.84	0.00	1.07	1.26	2.33	1.85
5-2	-123	7.30	7.30	7.30	0.00	3.33	4.30	3.61	0.84
5-3	-90	6.92	8.11	8.11	0.00	3.20	3.42	3.61	1.06
5-4	-60	5.74	7.59	7.58	0.00	3.10	3.89	3.76	0.97
25-2	-30	***Specimen not against anvils – trace can't be analyzed***						7.85	
5-12	21	6.23	7.28	6.82	3.07	3.54	6.68	6.86	1.03
5-5	50	***Signal not acquired***						13.58	
5-6	100							14.81	
10	150	5.97	6.53	-	-	3.40	7.23	7.79	1.08
9	200	***Signal not acquired***						18.46	
13	300	5.74	6.28	-	-	3.29	8.39	8.83	1.05
4340 High Energy									
Specimen id	**T (°C)**	F_{gy} **(kN)**	F_m **(kN)**	F_{bf} **(kN)**	F_a **(kN)**	W_m **(J)**	W_t **(J)**	KV **(J)**	$\frac{KV}{W_t}$
5-3	-198	5.36	7.61	7.53	0.00	5.02	5.18	5.57	1.08
5-5	-150	6.15	6.73	6.15	0.00	5.12	5.37	5.87	1.09
SS3_4	-135	2.98	2.98	2.98	0.00	0.43	0.50	0.75	1.50
SS3_3	-130	***Signal not acquired***						1.35	
5-6	-120	5.96	6.63	1.71	0.51	5.14	11.54	13.43	1.16
5-7	-90	***Signal not acquired***						15.81	
5-8	-60							18.30	
5-2	-30							17.76	
SS3_1	-25	9.06	10.44	10.44	0.00	4.75	4.96	4.98	1.00
SS3_2	-25	8.23	10.59	10.39	1.00	9.62	9.77	9.90	1.01
5-1	21	***Signal not acquired***						16.67	
5-4	50							19.07	
T200									
Specimen id	**T (°C)**	F_{gy} **(kN)**	F_m **(kN)**	F_{bf} **(kN)**	F_a **(kN)**	W_m **(J)**	W_t **(J)**	KV **(J)**	$\frac{KV}{W_t}$
132	-198	6.03	7.80	7.57	4.01	6.06	11.09	12.35	1.11
375	-150	6.17	7.52	6.97	4.01	6.95	12.72	14.50	1.14
535	-123	6.49	7.43	7.43	3.83	8.16	15.58	17.67	1.13
257	-90	5.88	7.08	6.68	4.39	6.40	15.46	18.37	1.19
28	-60	5.93	6.97	6.26	5.20	6.99	21.62	23.68	1.10
1285	-30	5.51	6.65	6.05	4.48	7.17	18.10	20.40	1.13
414	21	5.56	6.34	-	-	7.49	19.45	21.18	1.09
153	50	***Signal not acquired***						22.42	
745	100	4.01	5.87	-	-	6.47	24.09	24.94	1.04

Table 13 - Instrumented impact results obtained from RHS specimens.

4340 Low Energy									
Specimen id	**T (°C)**	F_{gy} **(kN)**	F_m **(kN)**	F_{bf} **(kN)**	F_a **(kN)**	W_m **(J)**	W_t **(J)**	KV **(J)**	$\frac{KV}{W_t}$
LL-R12	-186	***Signal not acquired***						4.13	
LL-R3	-159	6.14	6.43	6.27	0.00	1.09	1.16	1.08	0.93
LL-R7	-118	8.19	8.34	8.24	0.00	1.91	2.07	1.94	0.94
LL-R5	-101	7.63	8.77	8.61	0.00	2.61	2.73	2.57	0.94
LL-R4	-74	7.46	8.65	8.48	0.00	2.50	2.67	2.58	0.97
LL-R2	-50	7.53	8.88	8.69	0.00	3.04	3.19	2.97	0.93
LL-R6	-25	7.30	8.62	8.18	0.00	3.06	3.25	3.08	0.95
LL-R9	0	7.46	8.33	7.98	0.10	3.07	3.40	3.47	1.02
LL-R1	22	6.72	8.19	8.19	1.31	3.01	3.79	3.99	1.05
LL-R11	99	6.46	7.88	-	-	2.62	5.14	4.87	0.95
LL-R10	197	6.28	7.48	-	-	2.52	6.07	5.82	0.96
LL-R8	292	6.09	7.42	-	-	2.49	6.39	6.02	0.94
4340 High Energy									
Specimen id	**T (°C)**	F_{gy} **(kN)**	F_m **(kN)**	F_{bf} **(kN)**	F_a **(kN)**	W_m **(J)**	W_t **(J)**	KV **(J)**	$\frac{KV}{W_t}$
HH-R1	-181	6.74	8.06	7.59	0.00	3.42	4.40	4.16	0.95
HH-R4	-147	6.67	8.05	7.65	0.00	3.36	4.73	4.52	0.96
HH-R10	-130	6.77	7.61	7.32	0.27	4.04	6.12	6.71	1.10
HH-R8	-121	6.58	7.32	6.52	1.48	4.31	9.95	9.17	0.92
HH-R2	-98	5.97	7.18	3.18	2.06	4.71	14.08	12.84	0.91
HH-R6	-76	5.85	7.03	-	-	4.27	14.99	13.61	0.91
HH-R7	-50	5.68	6.96	-	-	5.05	15.95	14.86	0.93
HH-R11	-30	5.90	6.93	-	-	5.26	16.64	14.75	0.89
HH-R12	-20	5.75	6.71	-	-	5.15	15.81	14.64	0.93
HH-R9	22	5.23	6.45	-	-	5.59	17.62	16.50	0.94
HH-R5	101	4.97	6.23	-	-	5.83	18.79	17.80	0.95
HH-R3	235	4.49	5.82	-	-	5.51	20.47	19.01	0.93
T200									
Specimen id	**T (°C)**	F_{gy} **(kN)**	F_m **(kN)**	F_{bf} **(kN)**	F_a **(kN)**	W_m **(J)**	W_t **(J)**	KV **(J)**	$\frac{KV}{W_t}$
SH-R2	-194	6.39	9.05	9.01	0.00	5.68	6.23	6.41	1.03
SH-R12	-164	6.56	9.20	8.87	0.61	6.65	8.40	8.45	1.01
SH-R9	-152	7.16	9.12	7.78	2.99	8.21	15.56	14.52	0.93
SH-R6	-143	6.98	9.13	7.40	3.01	8.17	16.81	15.44	0.92
SH-R3	-125	7.02	9.01	6.33	3.96	8.53	19.26	17.84	0.93
SH-R10	-115	6.96	8.86	6.56	4.93	7.36	17.46	16.34	0.94
SH-R4	-100	7.01	8.93	-	-	9.02	24.06	22.19	0.92
SH-R11	-76	6.92	8.65	-	-	8.58	26.24	24.39	0.93
SH-R1	-50	6.65	8.40	1.90	1.34	8.81	26.43	24.61	0.93
SH-R8	-20	6.68	8.28	-	-	9.25	30.19	26.21	0.87
SH-R5	22	5.95	7.78	-	-	8.89	29.49	27.87	0.95
SH-R7	101	5.70	7.43	-	-	9.00	31.06	29.83	0.96

The tests performed on 1/4-size specimens (Table 12) exhibited by far the highest failure rate in terms of acquisition of the instrumented signal (30 %)[***], as compared with any other geometry (6 % for CVN, 0 % for 3/4-size and 1/2-size, 3 % for RHS). This was due to the relatively low level of the instrumented signals that were recorded during those tests. This forced the operator to lower the acquisition trigger level, to a point where random electrical spikes in the background noise would sometimes cause a false trigger of the acquisition. This did not occur for RHS specimens, even though the magnitude of the instrumented forces was similar, because a different instrumented striker, specifically designed for miniaturized specimens, was used and a low trigger level was not required. The lesson learned here is that an instrumented striker designed and built for larger specimens (and higher strain-gage signals) is not recommended for use with relatively small sub-sized specimens, and leads to a high percentage of failed acquisitions.

4.2.1 Effect of specimen type

The values of force at general yield (F_{gy}) and maximum force (F_m) are plotted as a function of test temperature for the investigated steels in Figures 15-20. In the Figures, data points are fitted by 3rd or 4th order polynomials simply as a guide for the eye.

As expected (and similar to the well-established trend of mechanical strength with test temperature), characteristic forces tend to decrease with both specimen cross-section/size and test temperature.

1/4-size specimens yield characteristic forces which are generally slightly lower than RHS specimens.

[***] The instrumented curve of another 1/4-size specimen of 4340 low-energy (id: 25-2) was also impossible to analyze, although the signal was acquired. In this case, the sample was not properly positioned against the anvils, and the huge oscillations in the early part of the test concealed the true mechanical behavior of the specimen.

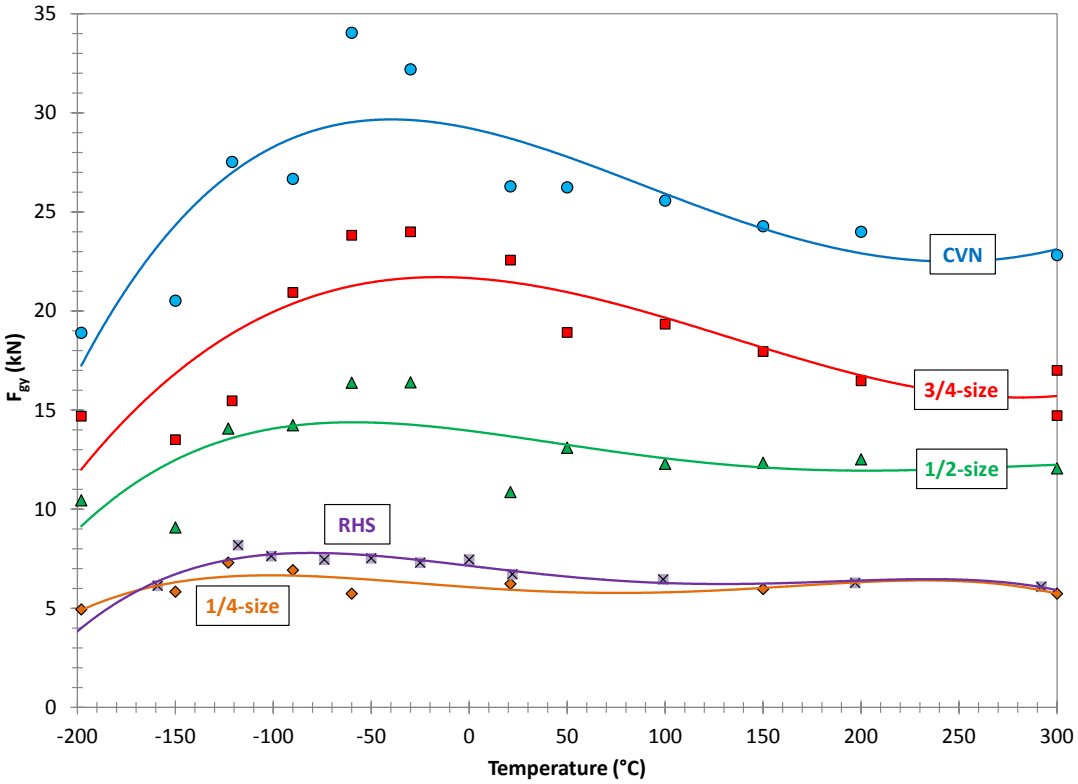

Figure 15 - Forces at general yield for 4340 low energy.

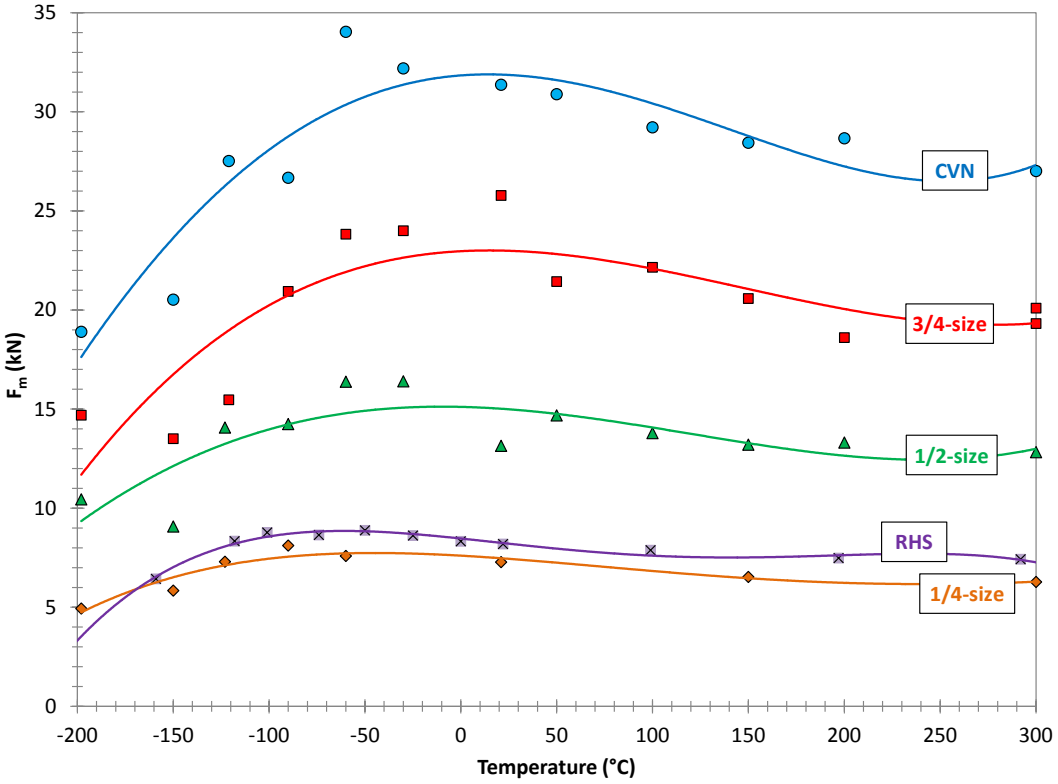

Figure 16 – Maximum forces for 4340 low energy.

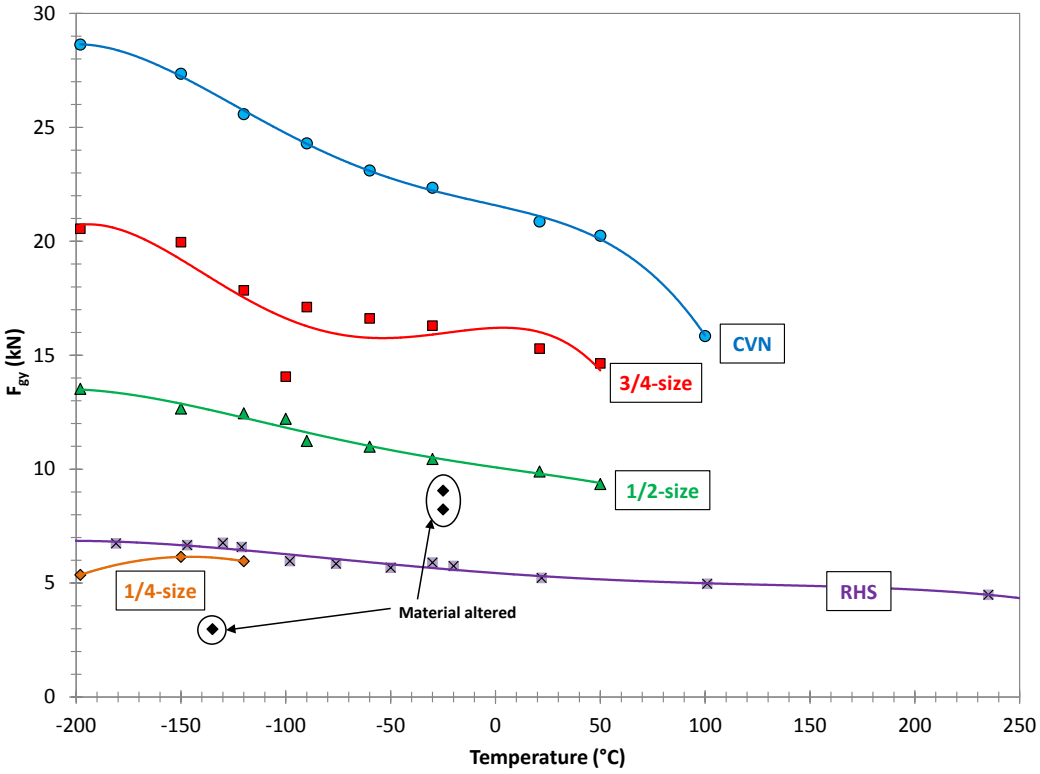

Figure 17 - Forces at general yield for 4340 high energy. Specimens altered by the machining process are indicated by black symbols.

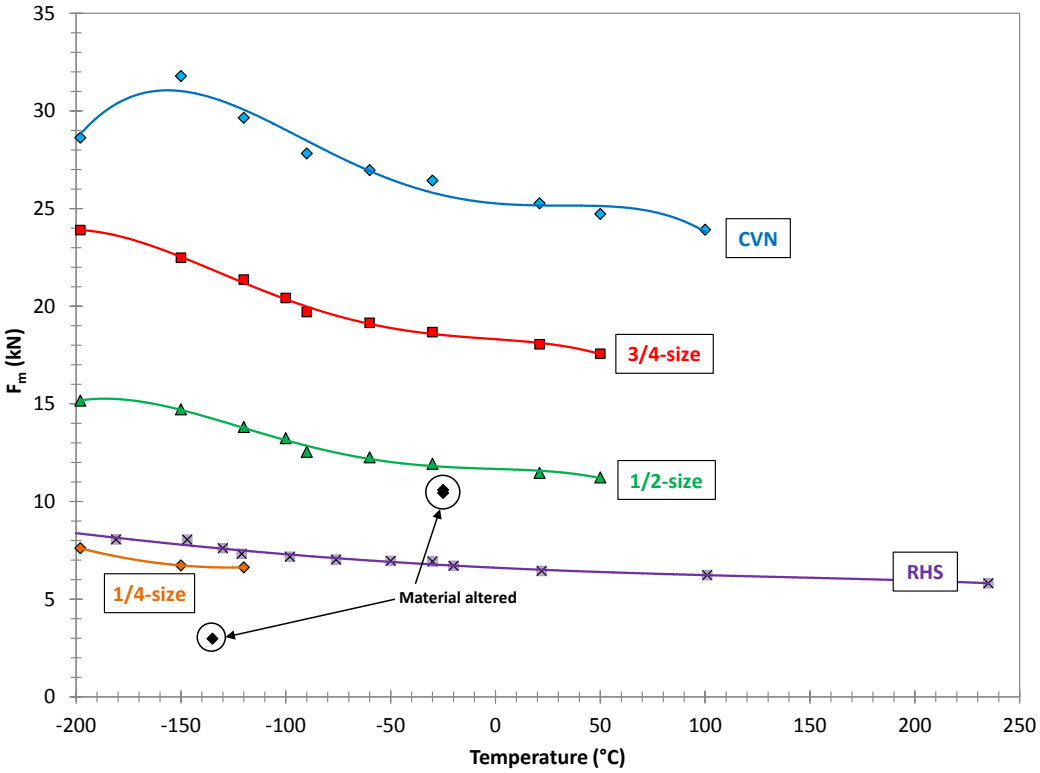

Figure 18 – Maximum forces for 4340 high energy. Specimens altered by the machining process are indicated by black symbols.

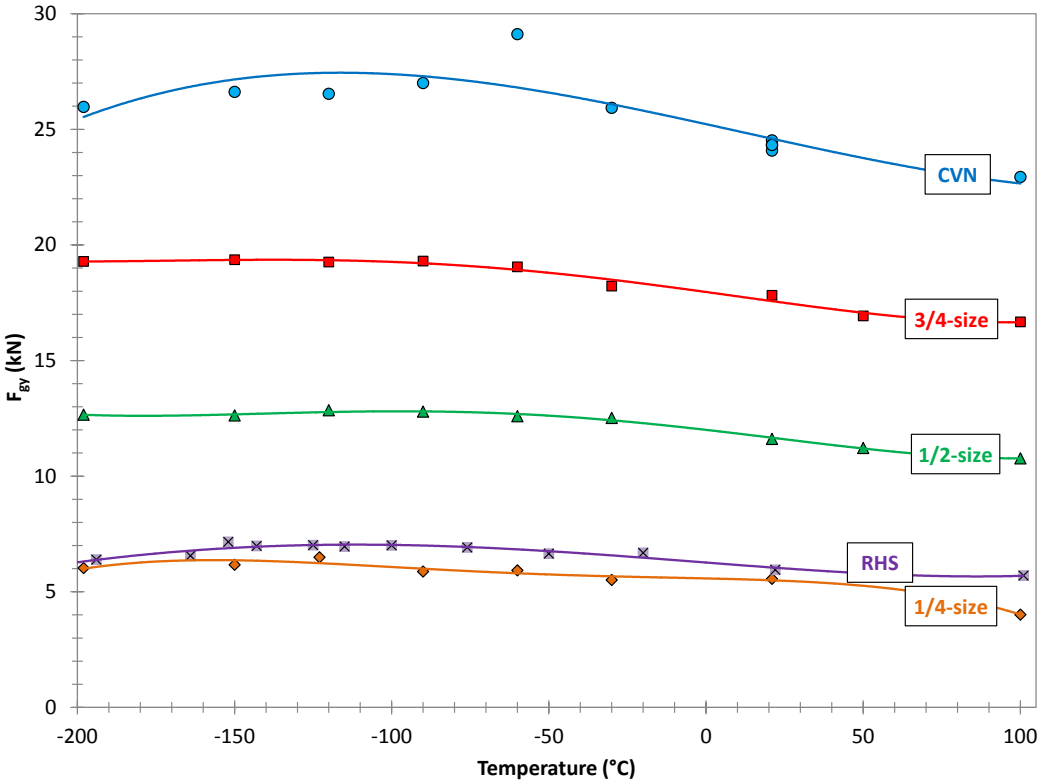

Figure 19 - Forces at general yield for T200.

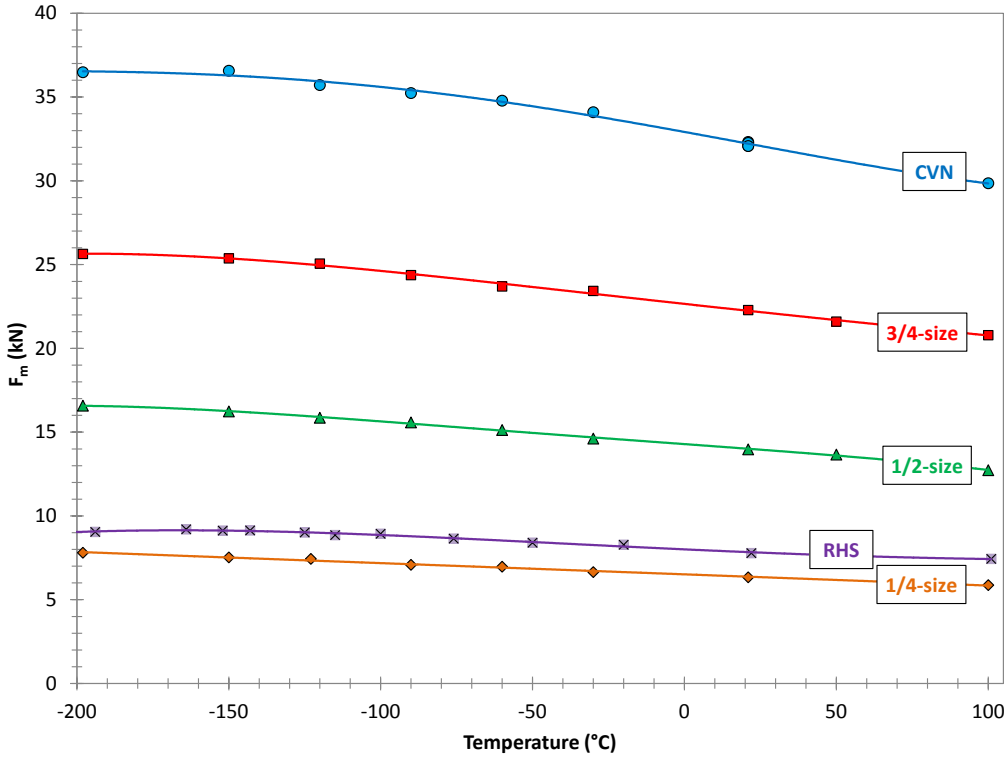

Figure 20 – Maximum forces for T200.

4.2.2 Normalization of characteristic forces

We applied several normalization approaches to general yield and maximum forces measured from SCVN and RHS specimens, to determine if any of these is successful in causing force values obtained from specimens of different size and geometry to become similar.

The general approach we followed was based on the ratio between geometrical parameters, as already proposed by several researchers for correlating upper shelf energies between miniaturized and full-size Charpy specimens (see also Section 5.2):

(a) ratio of nominal fracture areas, expressed as $B \cdot b$, where B is the specimen thickness and b is the specimen width below the notch (or ligament size);
(b) ratio of nominal fracture volumes, expressed as $B \cdot b^2$;
(c) ratio of nominal fracture volumes, expressed as $(B \cdot b)^{3/2}$.

The values of the above listed quantities are summarized in Table 14 for the different specimen geometries; the corresponding normalization factors obtained for each specimen geometry (with respect to CVN specimens) are listed in Table 15.

Table 14 - Values of nominal fracture areas and volumes for the Charpy specimen geometries used in this study.

Specimen type	$B \cdot b$ (mm^2)	$B \cdot b^2$ (mm^3)	$(B \cdot b)^{3/2}$ (mm^3)
CVN	80	640	715.54
3/4-size	60	480	464.76
1/2-size	40	320	252.98
1/4-size	20	160	89.44
RHS	18.64	71.97	80.50

Table 15 – Normalization factors, based on the ratio of nominal fracture areas and volumes for the SCVN and RHS specimens used in this study.

Geometrical parameter	Non-standard Charpy specimen type			
	3/4-size	1/2-size	1/4-size	RHS
Area, $B \cdot b$	1.33	2.00	4.00	4.29
Volume, $B \cdot b^2$				8.89
Volume, $(B \cdot b)^{3/2}$	1.54	2.83	8.00	

Note that:

- for any sub-size specimen the normalization factors corresponding to $B \cdot b$ and $B \cdot b^2$ are identical, since the ligament size b is the same as for CVN (only the thickness B varies);
- for RHS specimens, which are scaled down with respect to CVN, the two volume-based normalization factors turn out to be identical.

The results of the force normalization process on F_{gy} and F_m values are illustrated in Figures 21-26 (4340 low energy), Figures 27-32 (4340 high energy), and Figures 33-38 (T200).

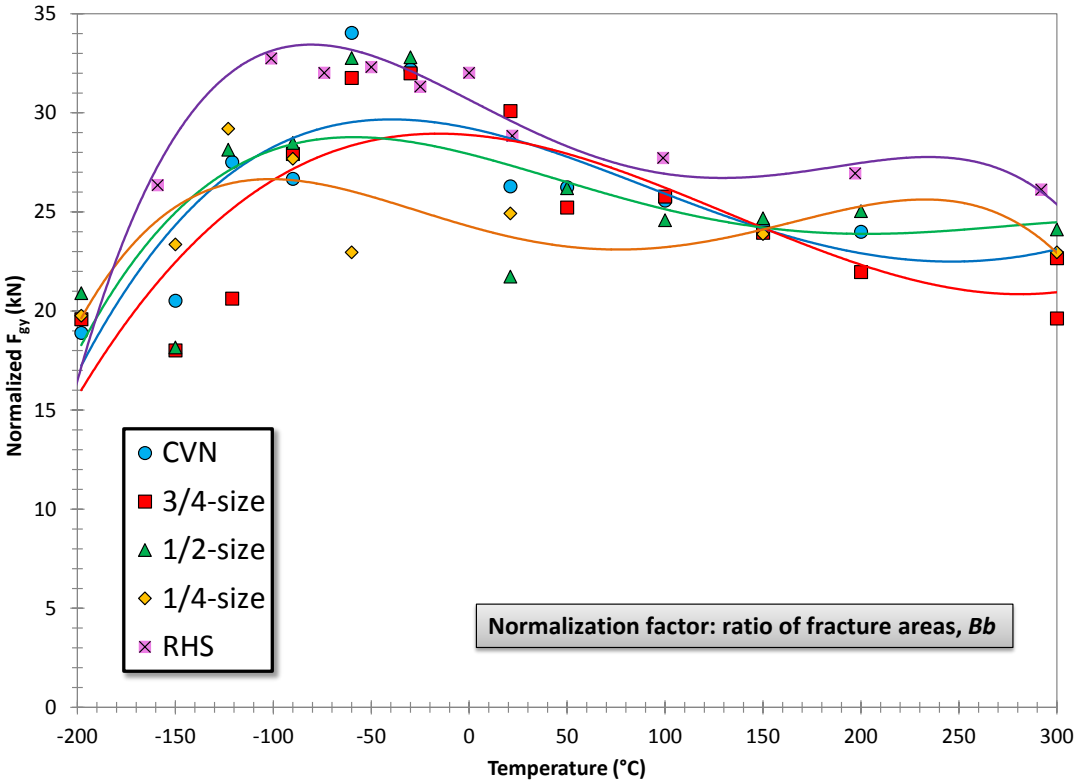

Figure 21 - Forces at general yield for 4340 low energy, normalized by the ratio of fracture areas.

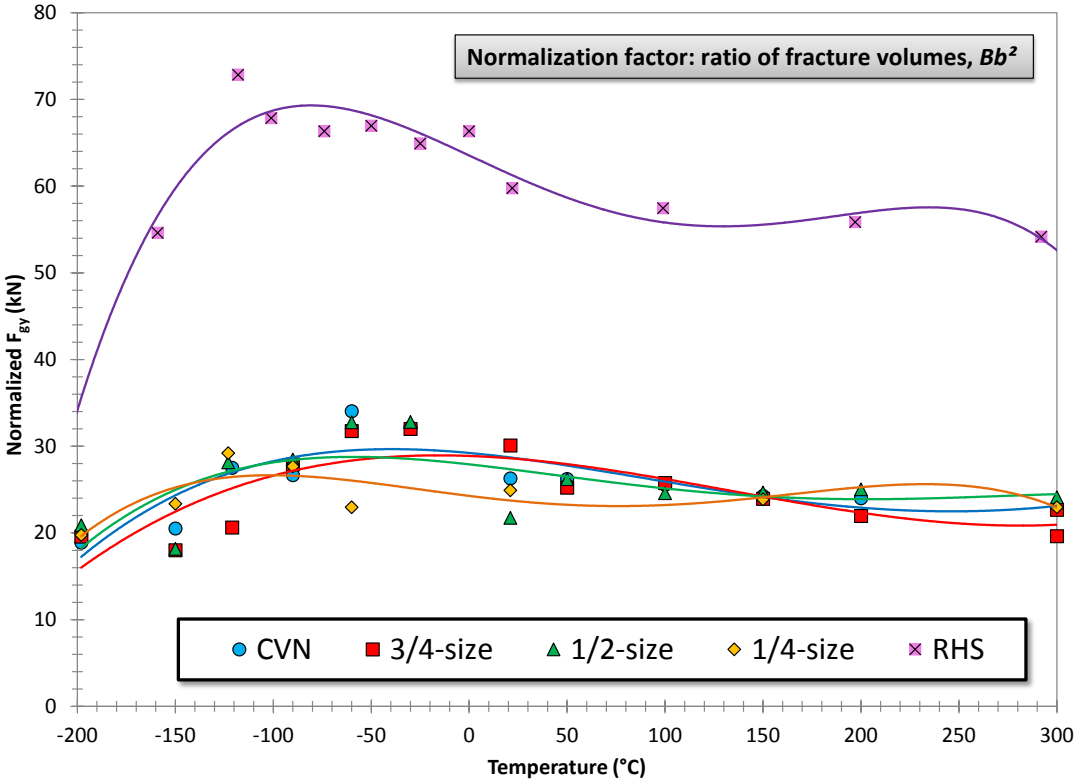

Figure 22 - Forces at general yield for 4340 low energy, normalized by the ratio of fracture volumes, Bb^2.

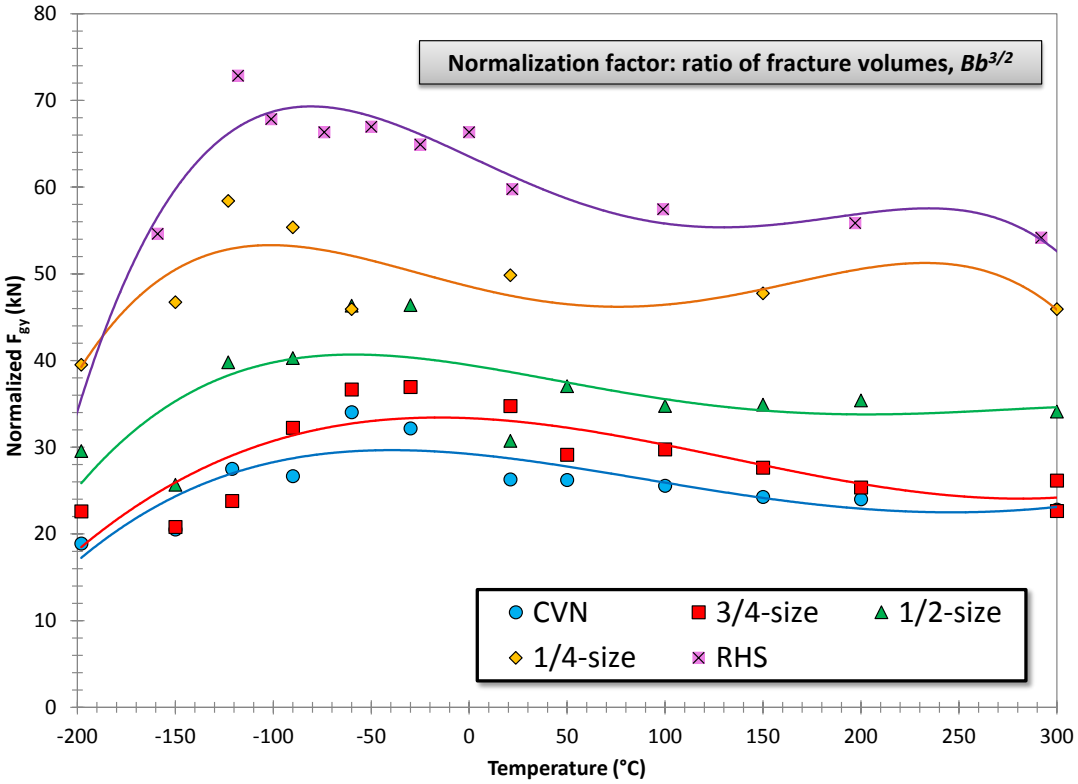

Figure 23 - Forces at general yield for 4340 low energy, normalized by the ratio of fracture volumes, $(Bb)^{3/2}$.

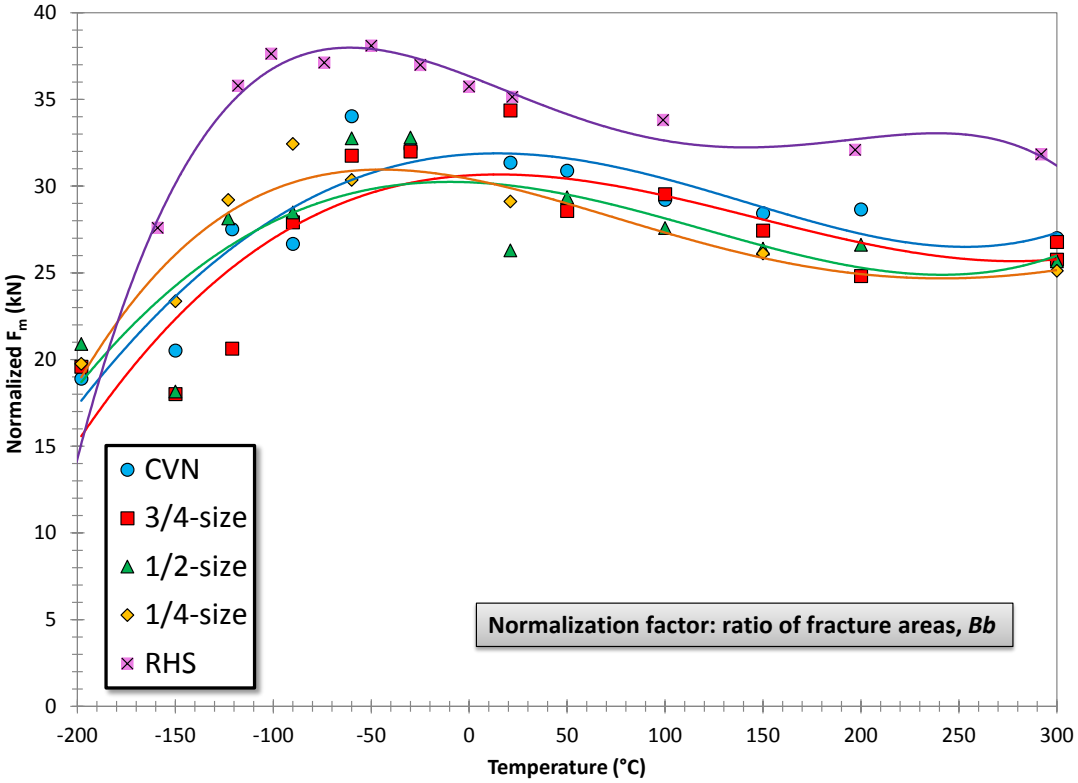

Figure 24 – Maximum forces for 4340 low energy, normalized by the ratio of fracture areas.

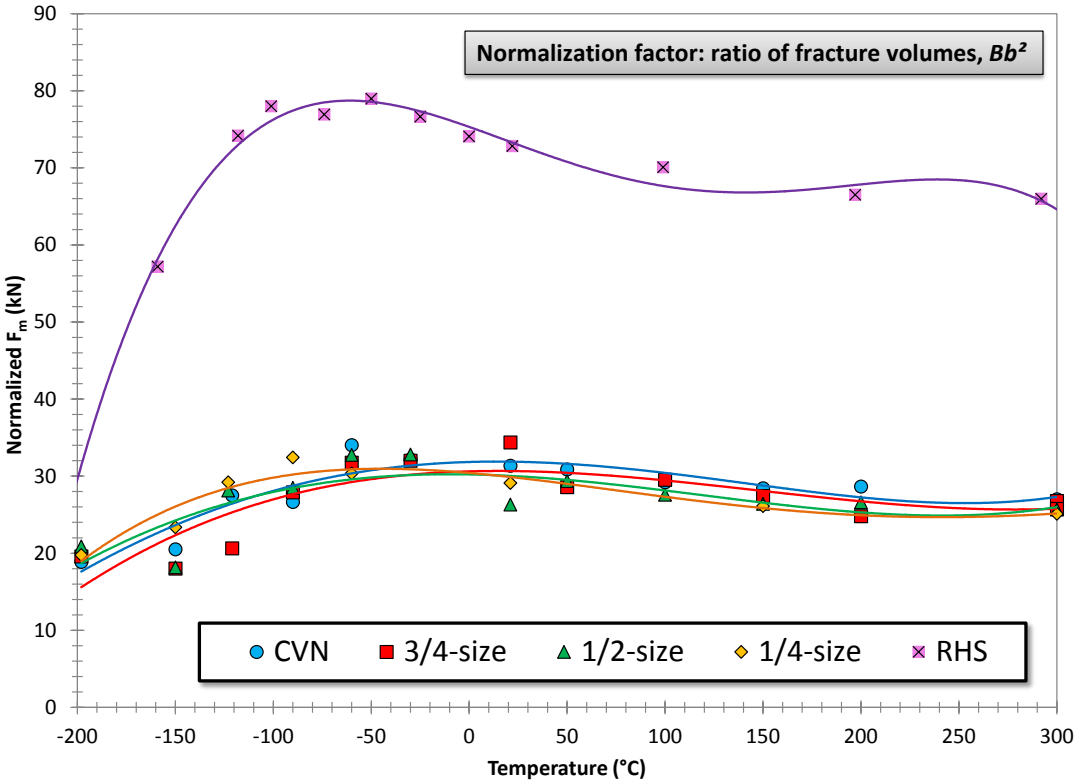

Figure 25 – Maximum forces for 4340 low energy, normalized by the ratio of fracture volumes, Bb^2.

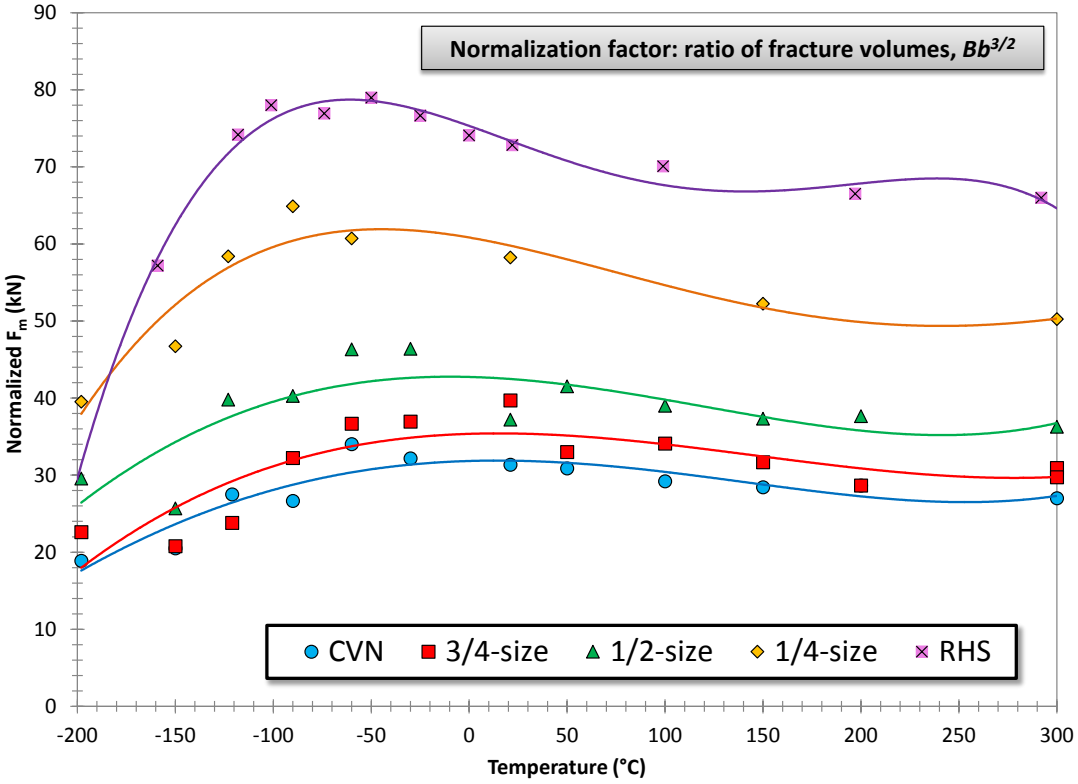

Figure 26 – Maximum forces for 4340 low energy, normalized by the ratio of fracture volumes, $(Bb)^{3/2}$.

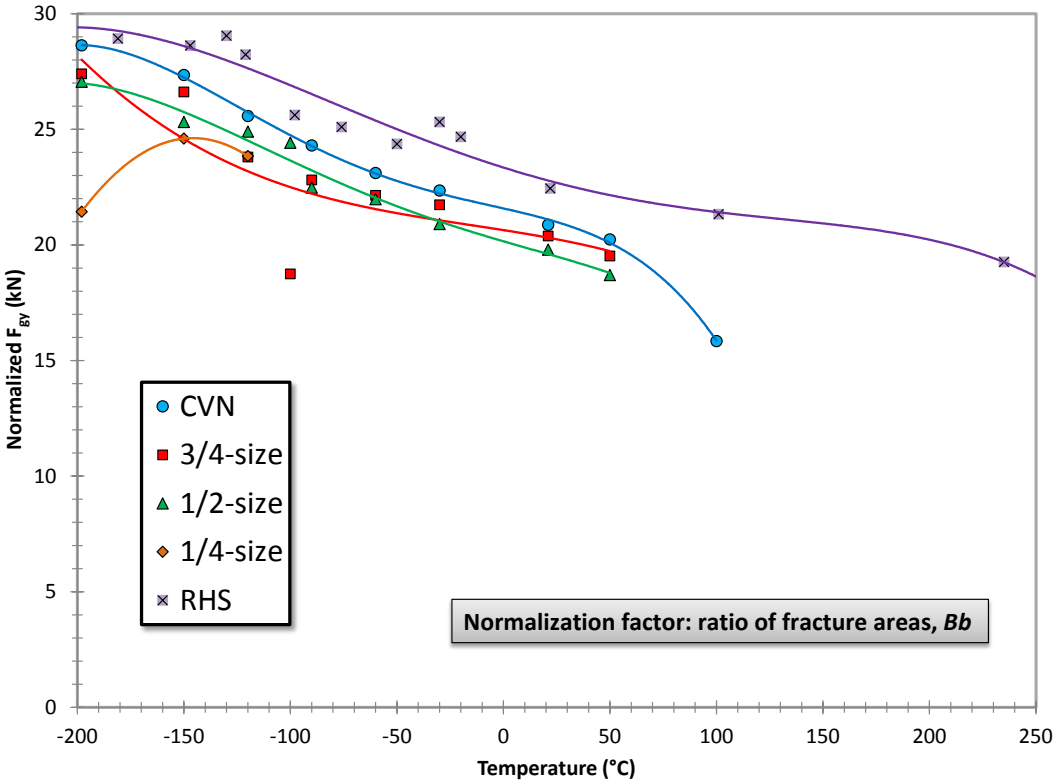

Figure 27 - Forces at general yield for 4340 high energy, normalized by the ratio of fracture areas.

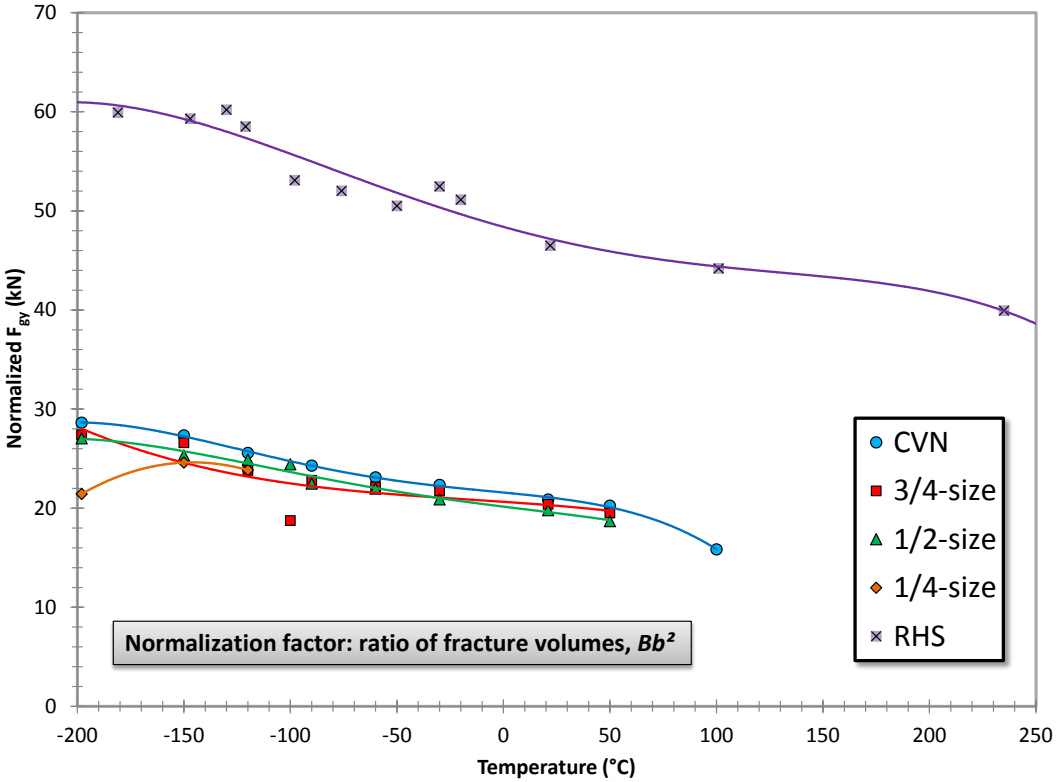

Figure 28 - Forces at general yield for 4340 high energy, normalized by the ratio of fracture volumes, Bb^2.

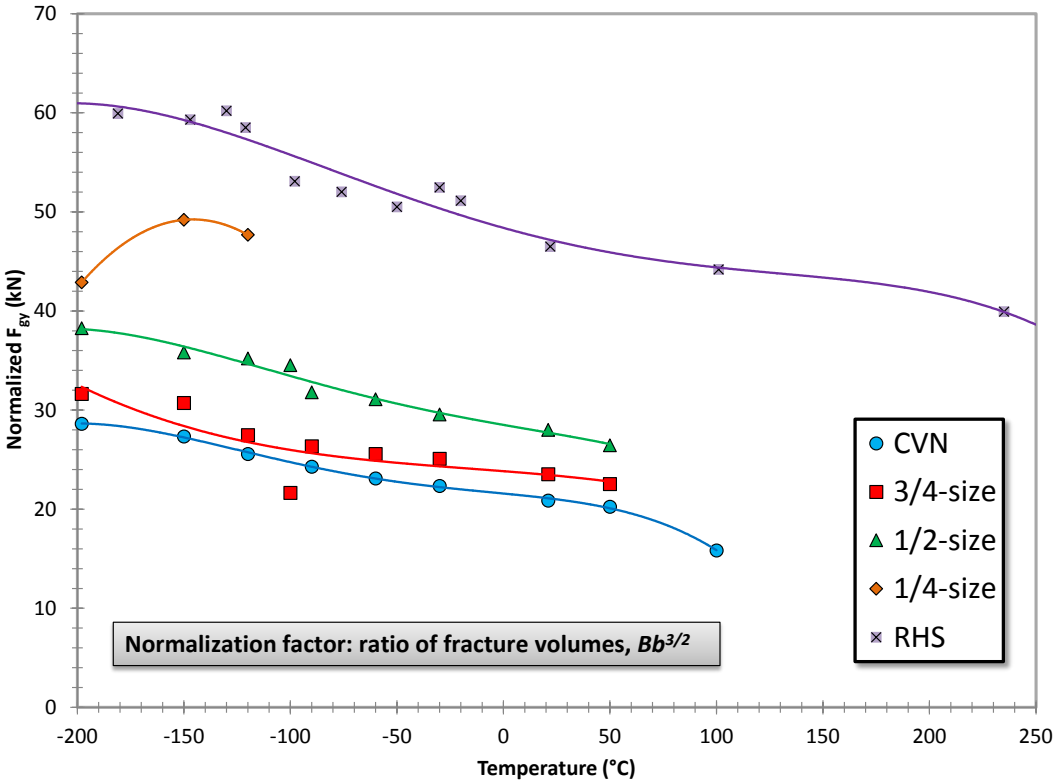

Figure 29 - Forces at general yield for 4340 high energy, normalized by the ratio of fracture volumes, $(Bb)^{3/2}$.

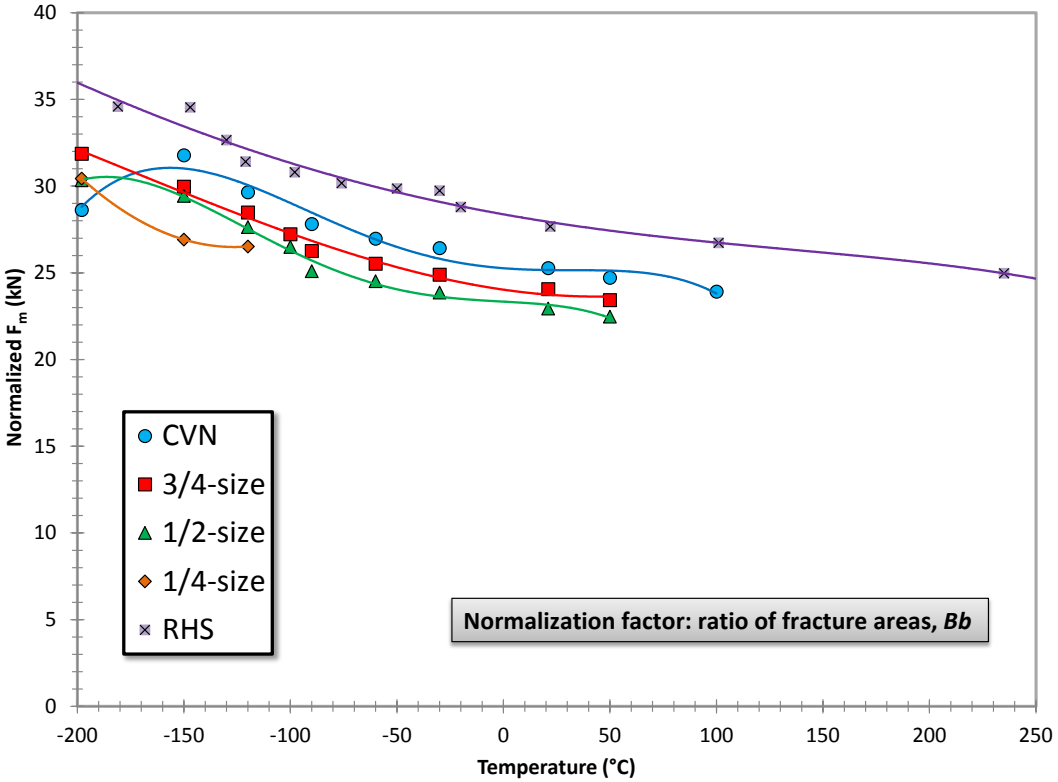

Figure 30 – Maximum forces for 4340 high energy, normalized by the ratio of fracture areas.

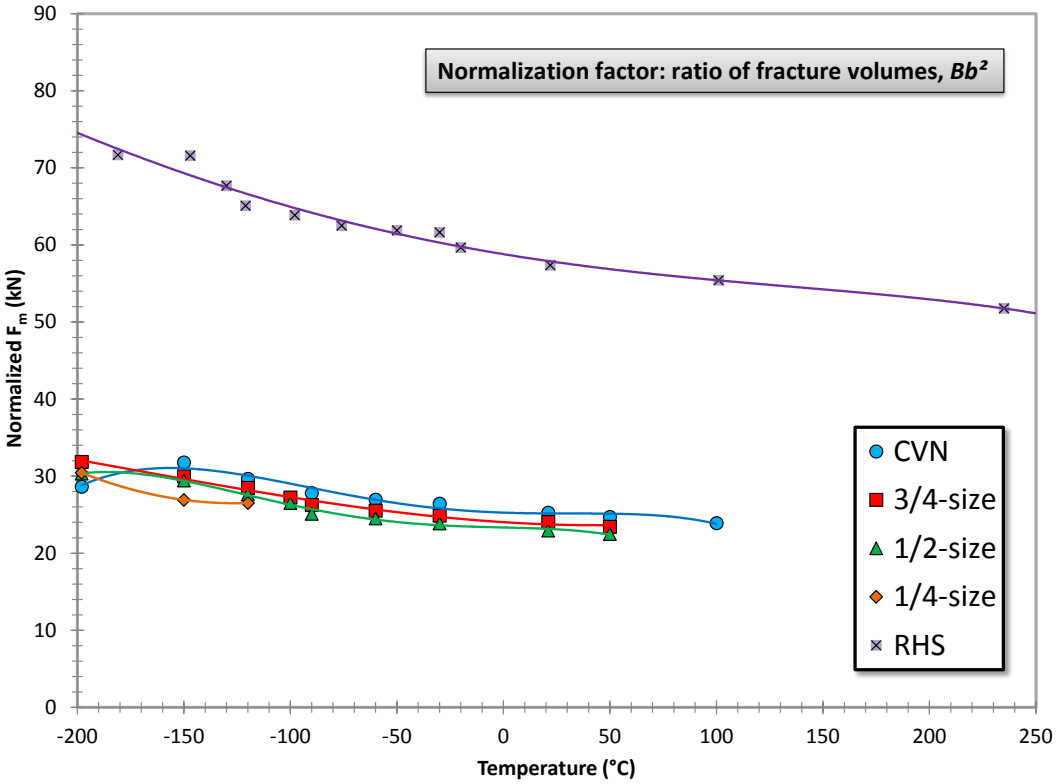

Figure 31 – Maximum forces for 4340 high energy, normalized for by ratio of fracture volumes, Bb^2.

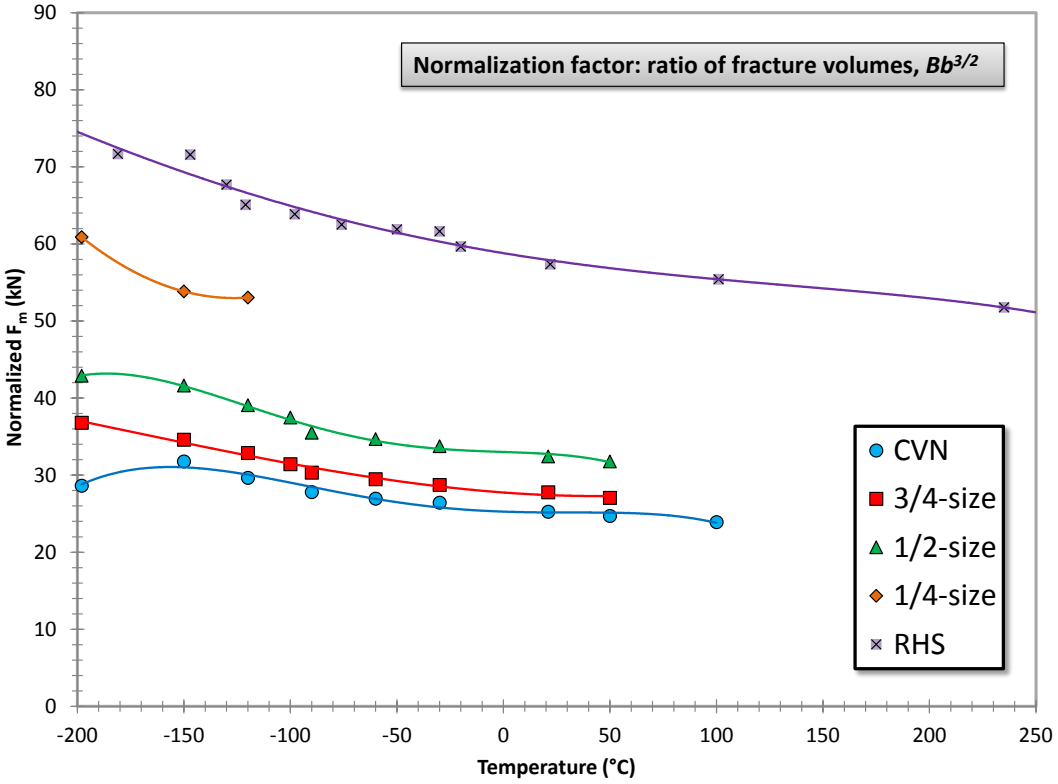

Figure 32 – Maximum forces for 4340 high energy, normalized by the ratio of fracture volumes, $(Bb)^{3/2}$.

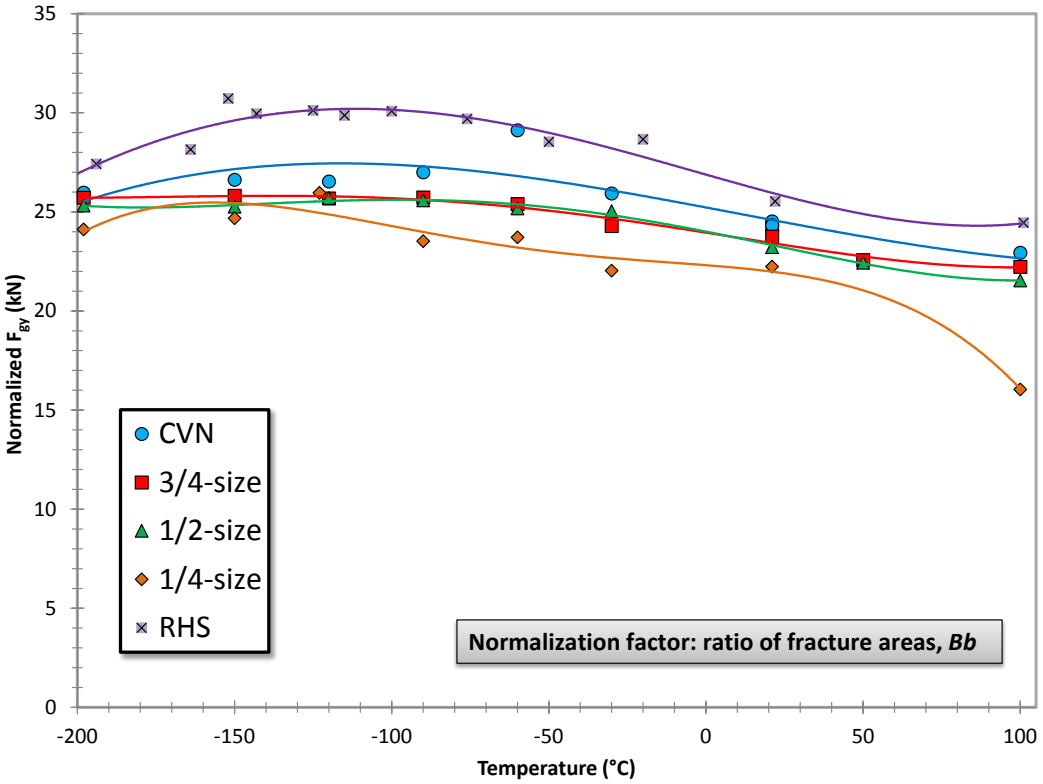

Figure 33 - Forces at general yield for T200, normalized by the ratio of fracture areas.

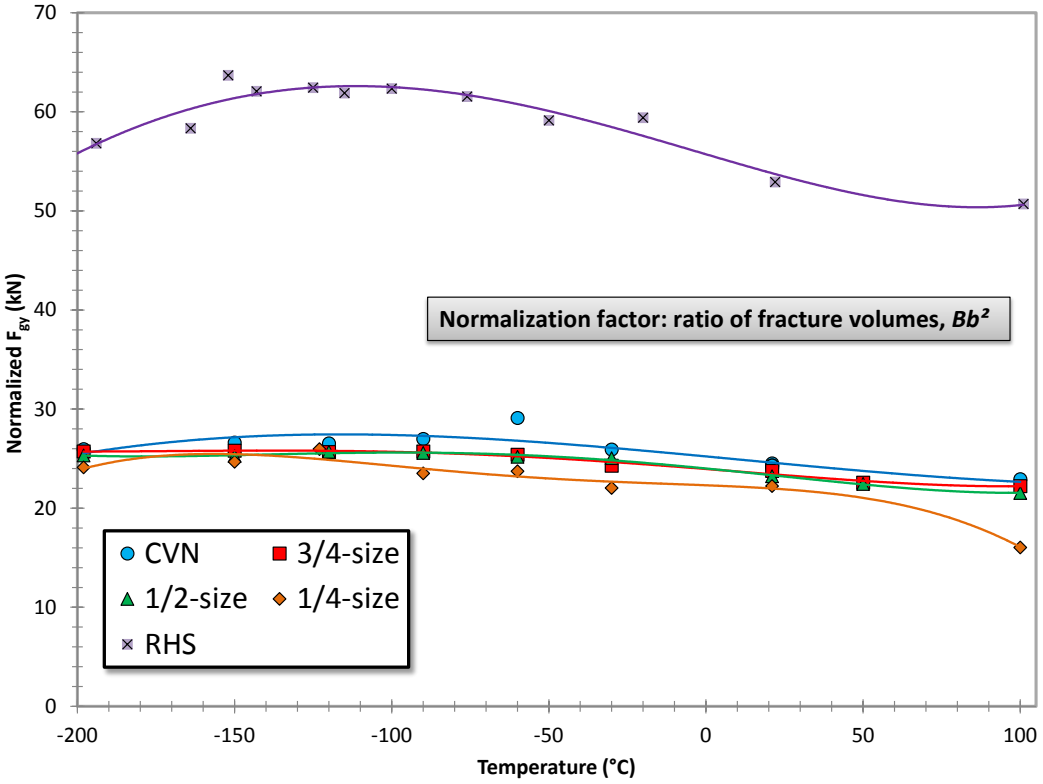

Figure 34 - Forces at general yield for T200, normalized by the ratio of fracture volumes, Bb^2.

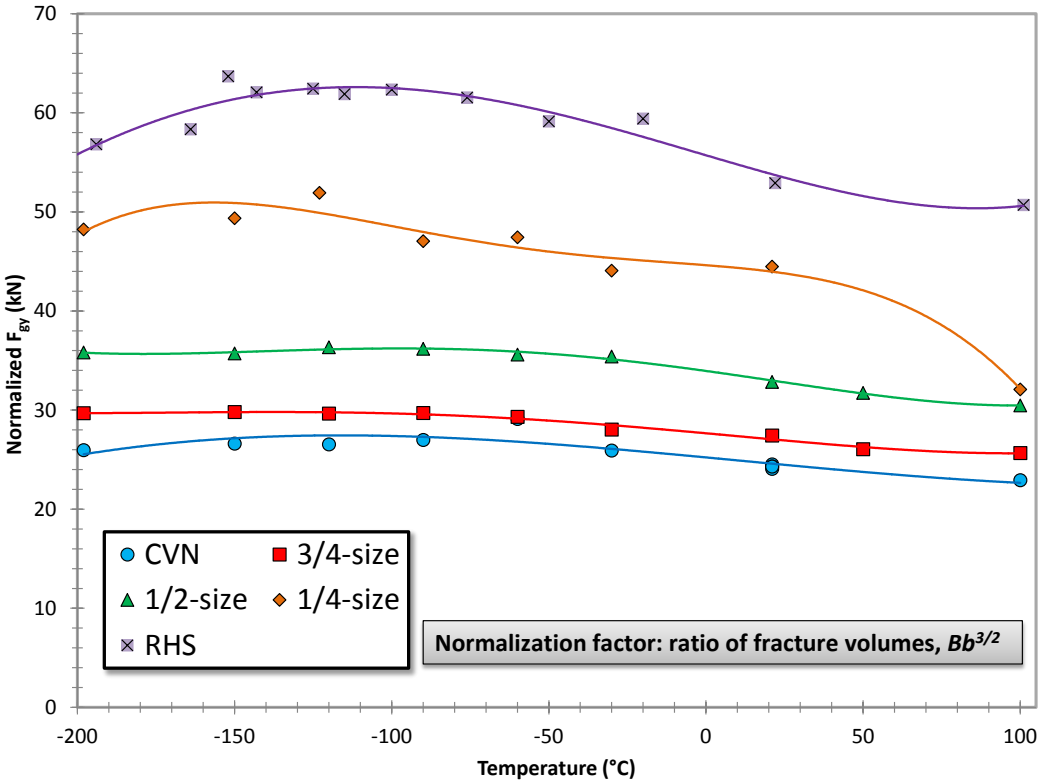

Figure 35 - Forces at general yield for T200, normalized by the ratio of fracture volumes, $(Bb)^{3/2}$.

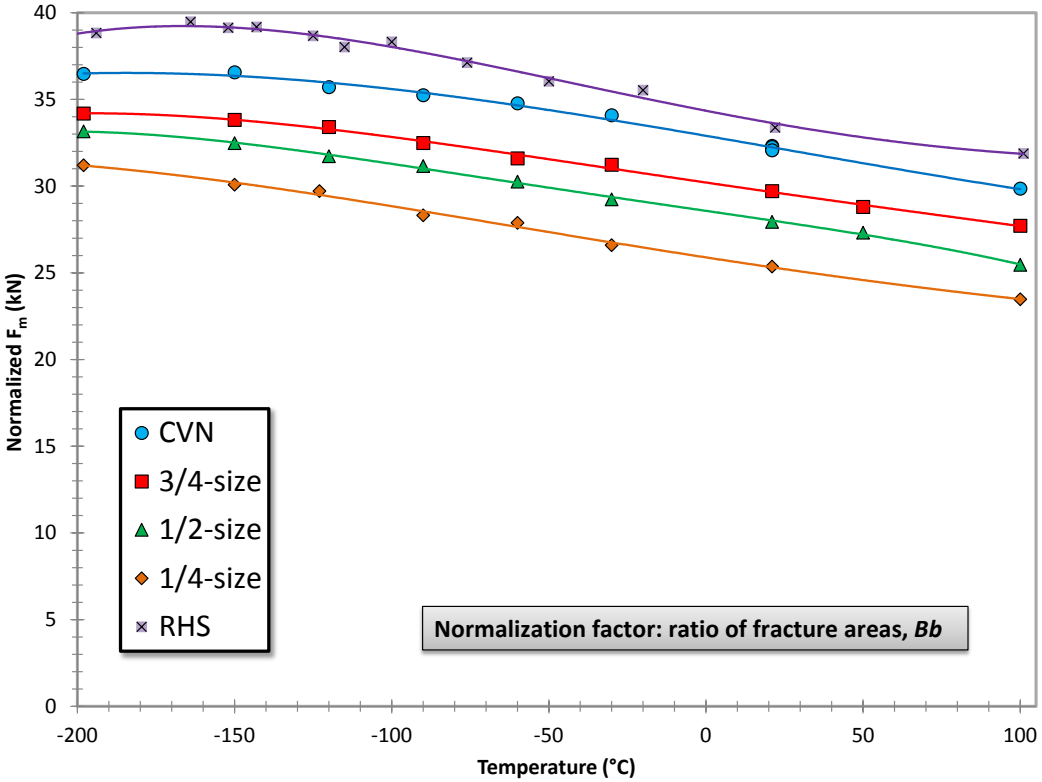

Figure 36 – Maximum forces for T200, normalized by the ratio of fracture areas.

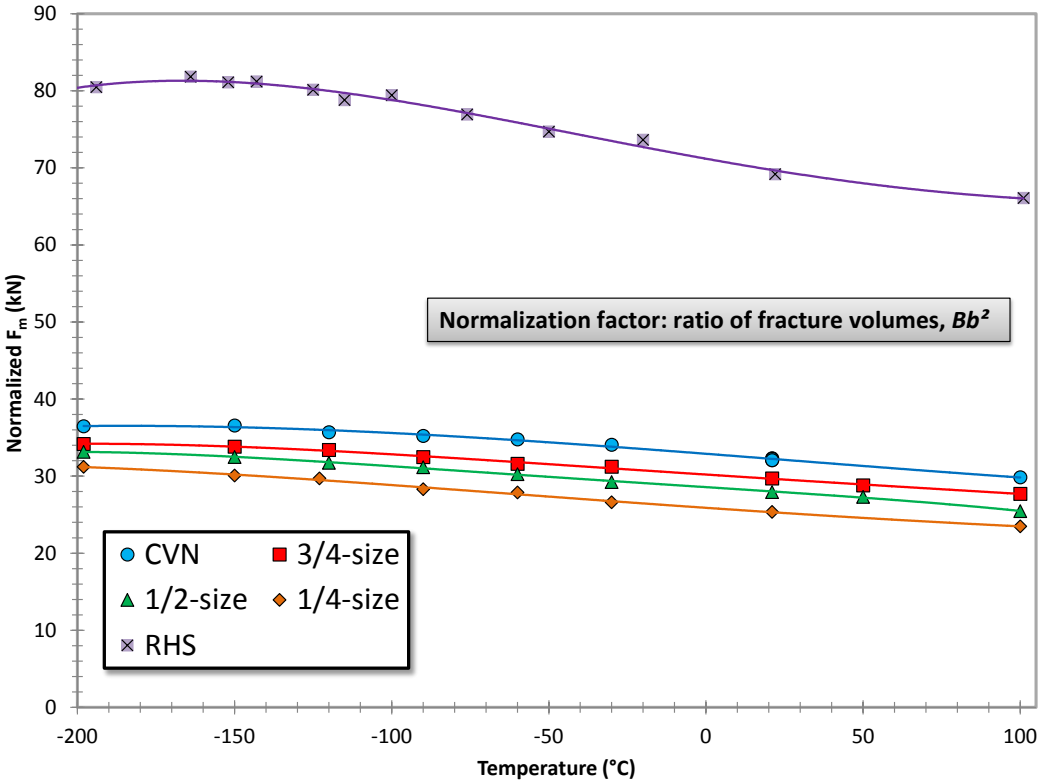

Figure 37 – Maximum forces for T200, normalized by the ratio of fracture volumes, Bb^2.

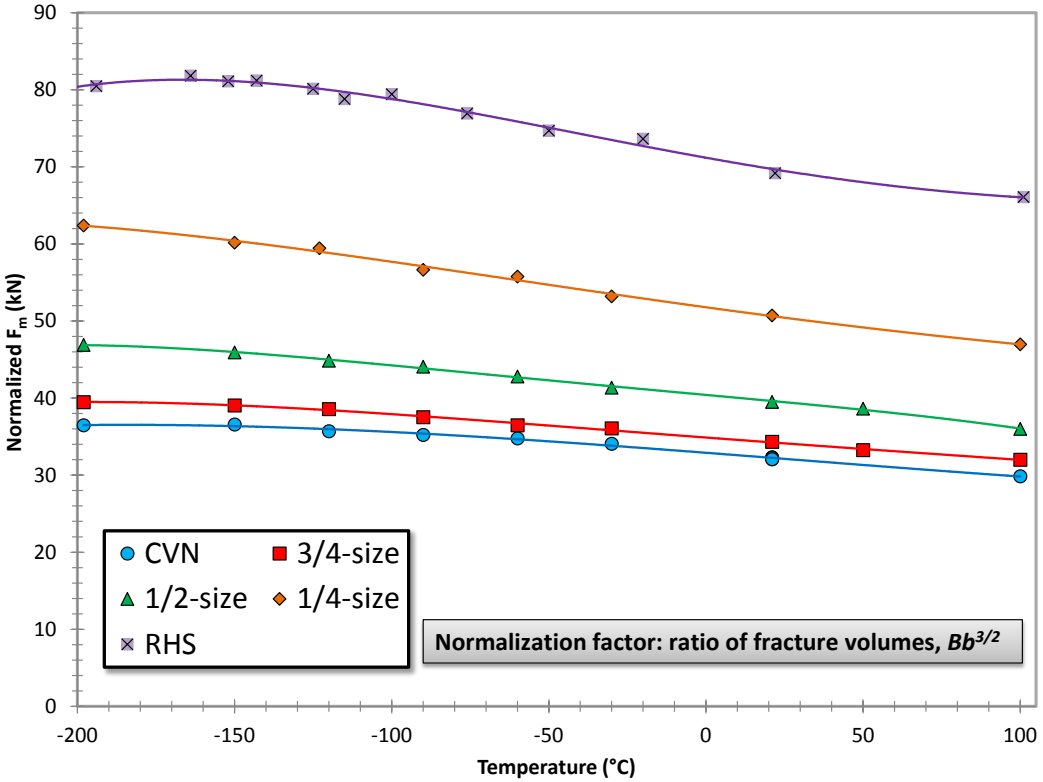

Figure 38 – Maximum forces for T200, normalized by the ratio of fracture volumes, $(Bb)^{3/2}$.

Examination of Figures 21 to 38 leads to the following observations.

(a) For SCVN specimens, irrespective of their thickness, the normalization based on fracture areas ***Bb*** (which coincide with $\boldsymbol{Bb}^2$) produces acceptable results for all materials, considering also the significant scatter of the characteristic force values measured, particularly for the 4340 low energy steel.

(b) For SCVN specimens, when the ratio of fracture volumes is expressed in the form $\boldsymbol{(Bb)}^{3/2}$, a clear tendency of the normalized forces to overestimate the values measured on CVN specimens (*i.e.*, overcorrection) is evident. The overestimation is more pronounced for the thinner specimens (1/2-size, and particularly 1/4-size).

(c) None of the approaches considered appears to be particularly effective for RHS specimens, especially when fracture volumes are used (as previously mentioned, the two expressions of fracture volume coincide for the CVN-scaled RHS specimen). Even when the ratio of fracture areas ***Bb*** is used, RHS-normalized forces are still too high with respect to CVN forces. When tests performed on CVN and RHS specimens at similar temperatures (within ±10 °C) are considered, the average overcorrection for F_{gy} and F_m values ranges between 6 % and 20 %, with the largest values (14 % for F_{gy} and 20 % for F_m) associated with the 4340 low energy steel and the lowest values (8 % and 6 % respectively) corresponding to the highest toughness T200 steel.

(d) Based on the previous considerations, the ratio of nominal fracture areas *Bb* needs to be multiplied by an empirical coefficient $\alpha \approx 0.88$, for an effective normalization of characteristic forces measured from RHS specimens.

4.3 Relationship between different measures of absorbed energy (*KV* and W_t)

The ratio KV/W_t (last column in Tables 9 to 13) is plotted as a function of measured *SFA* in Figure 39 (CVN and SCVN specimens) and Figure 40 (RHS specimens). Each plot refers to a specific combination of impact machine and instrumented striker. In Figure 40, the different steels investigated are separately indicated.

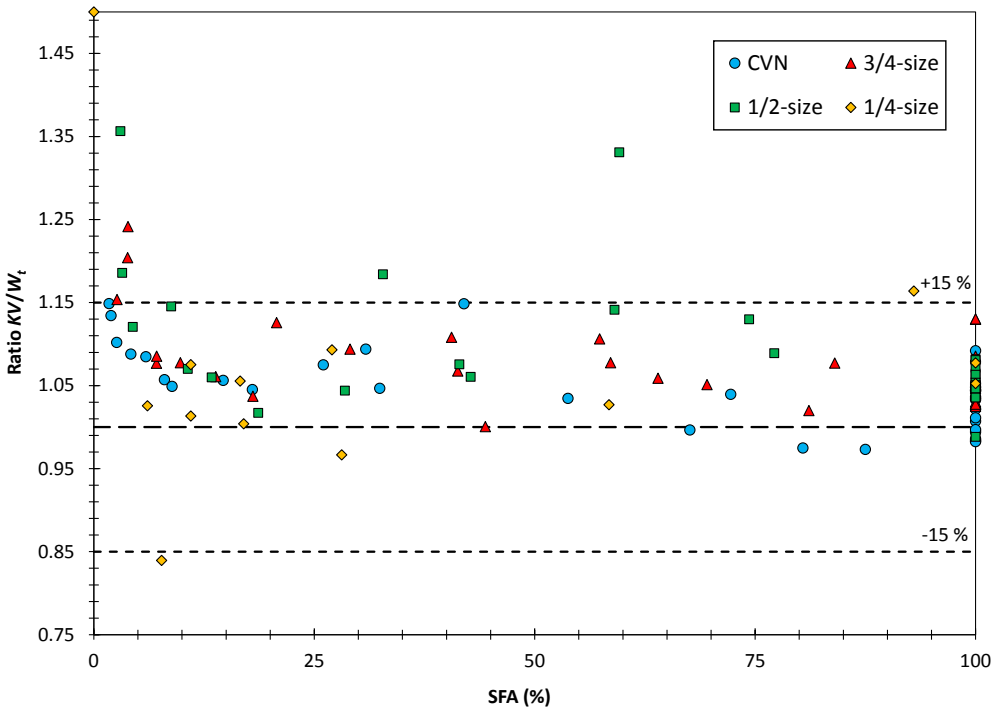

Figure 39 - Values of KV/W_t as a function of *SFA* for CVN and SCVN tests.

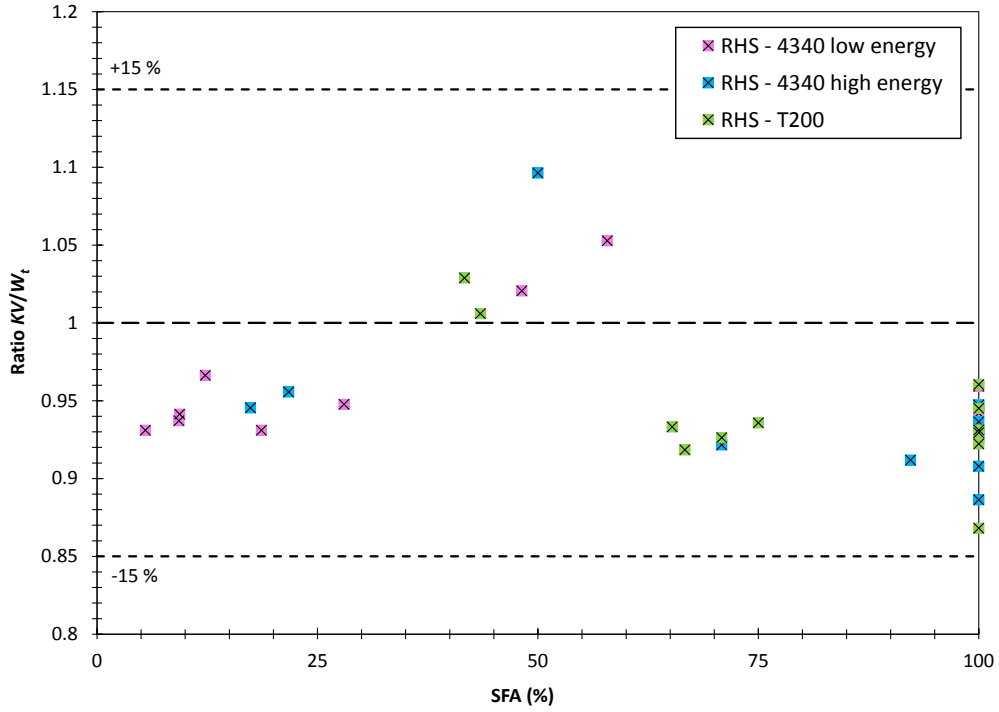

Figure 40 - Values of KV/W_t as a function of *SFA* for RHS tests.

For CVN and SCVN specimens (Figure 39), the vast majority of the tests yielded values of KV/W_t within ±15 % (0.85 to 1.15), which according to ASTM E2298-13a is the range for which no correction to instrumented

forces is required. Most of the outliers correspond to low *SFA* values (typically *SFA* < 10 %), which correspond to brittle tests, which are typically more difficult to analyze[†††]. A tendency of $W_t > KV$ can be observed.

In the case of RHS tests, all tests performed exhibit very good consistency between encoder and instrumented energy, irrespective of degree of ductility or steel tested. The opposite tendency ($W_t < KV$) can be observed.

5. Correlations between specimen types

5.1 Ductile-to-brittle transition temperatures

The values of $DBTT_{KV}$ calculated from SCVN and RHS specimens are plotted in Figure 41 as a function of the corresponding transition temperatures for full-size specimens. $DBTT_{LE}$ or $FATT_{50}$ values were not considered, given that most of them were associated with considerable uncertainty (see the data points outside ±25 °C limits in Figure 11) were not included in the analyses. Essentially linear relationships ($R^2 \geq 0.96$) are observed in Figure 41. Individual *DBTT* shifts, with mean values and standard deviations, are presented in Table 16 and Figure 42.

Table 16 - Shifts of ductile-to-brittle-transition temperature calculated for different steels, specimen types and Charpy parameters. NOTE: shifts involving values excluded from the analyses are marked in italic and contained in shaded cells.

		Specimen type			
Parameter	Material	3/4-size	1/2-size	1/4-size	RHS
KV	LL-141	17.6	19.6	-7.0	-20.1
	HH-143	-3.7	-6.4	-35.3	-25.2
	SH-38	-0.5	-15.8	-29.0	-45.8
	Mean	4.5	-0.8	-23.8	-30.4
LE	LL-141	*85.4*	*18.6*	*44.3*	*14.3*
	HH-143	6.6	-12.9	-35.1	-26.1
	SH-38	-12.3	-25.4	-48.6	-56.0
	Mean	-2.8	-19.2	-41.9	-41.0
SFA	LL-141	*-19.9*	-43.5	-87.7	*-42.1*
	HH-143	2.7	-5.0	-39.5	-29.3
	SH-38	*-4.0*	*-48.6*	*-80.5*	-40.9
	Mean	2.7	-24.2	-63.6	-35.1
Overall mean		1.7	-12.8	-40.3	-34.8
Overall st. dev.		10.1	19.4	24.5	13.1

Despite a considerable amount of data scatter, the magnitude of the downward shift predictably increases as the specimen size decreases, which confirms the well-known shift of *DBTT* to lower temperatures because of a reduction in specimen size [10,11]. The relationship between 1/4-size and RHS specimens (*i.e.*, relative position of diamonds and triangles in Figure 42) is variable, and is attributable to the loss of constraint experienced by the extremely thin specimen (1/4-size) when compared with the fully scaled-down (proportional) Charpy sample (RHS).

[†††]According to several researchers, brittle tests that feature less than 3 dynamic force oscillations before specimen fracture should not be analyzed, since the striker signal does not accurately represent the true specimen behavior.

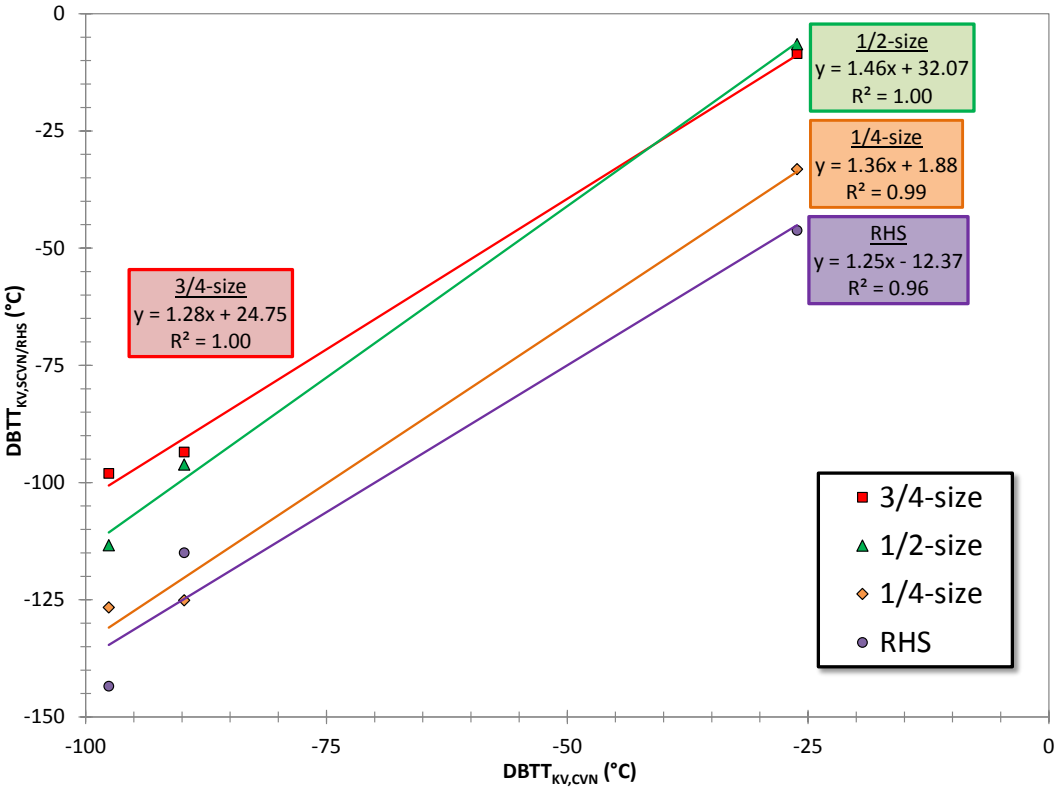

Figure 41 - Values of *DBTT*$_{KV}$ calculated from different specimen types.

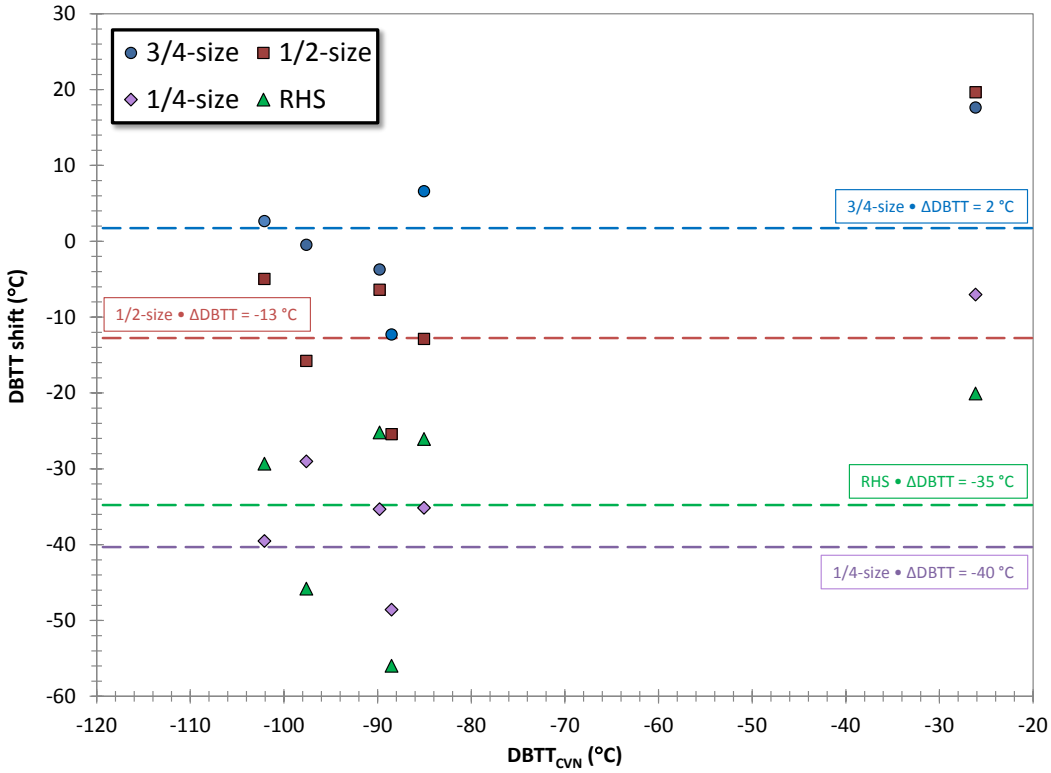

Figure 42 - Values of *DBTT* shift (from *KV*, *LE*, and *SFA*) obtained from different specimen types.

The feasibility of a simple empirical model such as:

$$DBTT_{CVN} = DBTT_{SCVN/MCVN} + M \quad (2)$$

(where M is the *DBTT* shift due to specimen size reduction) was checked by performing a simple statistical *t*-test on the slope of the linear fits which correlated in Figure 43 all reliable values of $DBTT_{SCVN/MCVN}$ and $DBTT_{CVN}$ (*i.e.*, excluding the shaded values in Table 16). In two out of four cases (Table 17), the calculated slope cannot be statistically distinguished from 1 at a confidence level of 95 % ($\alpha = 0.95$). However, a visual examination of the correlations in Figure 43 shows that most data points are clustered in a relatively narrow temperature range (between -102 °C and -85 °C), and therefore the uncertainty in the slope of the linear fits is elevated. Consequently, we have decided to use eq.(2), which is the model commonly used in the literature (see 5.1.1).

Table 17 - Results of the *t*-test on the slope of the linear correlations shown in Figure 43. The slope is not statistically different from 1 if $t_0 < t_{crit,\alpha=0.95}$.

X-variable	Y-variable	Specimen	Slope (1/°C)	Intercept (°C)	t_0	$t_{crit,\alpha=0.05}$	Result of *t*-test
$DBTT_{SCVN/MCVN}$	$DBTT_{CVN}$	3/4-size	1.264	23.229	2.124	2.132	Slope is not statistically different from 1
		1/2-size	1.443	28.517	2.756		Slope is statistically different from 1
		1/4-size	1.424	2.136	3.121		Slope is statistically different from 1
		RHS	1.167	-17.294	0.788		Slope is not statistically different from 1

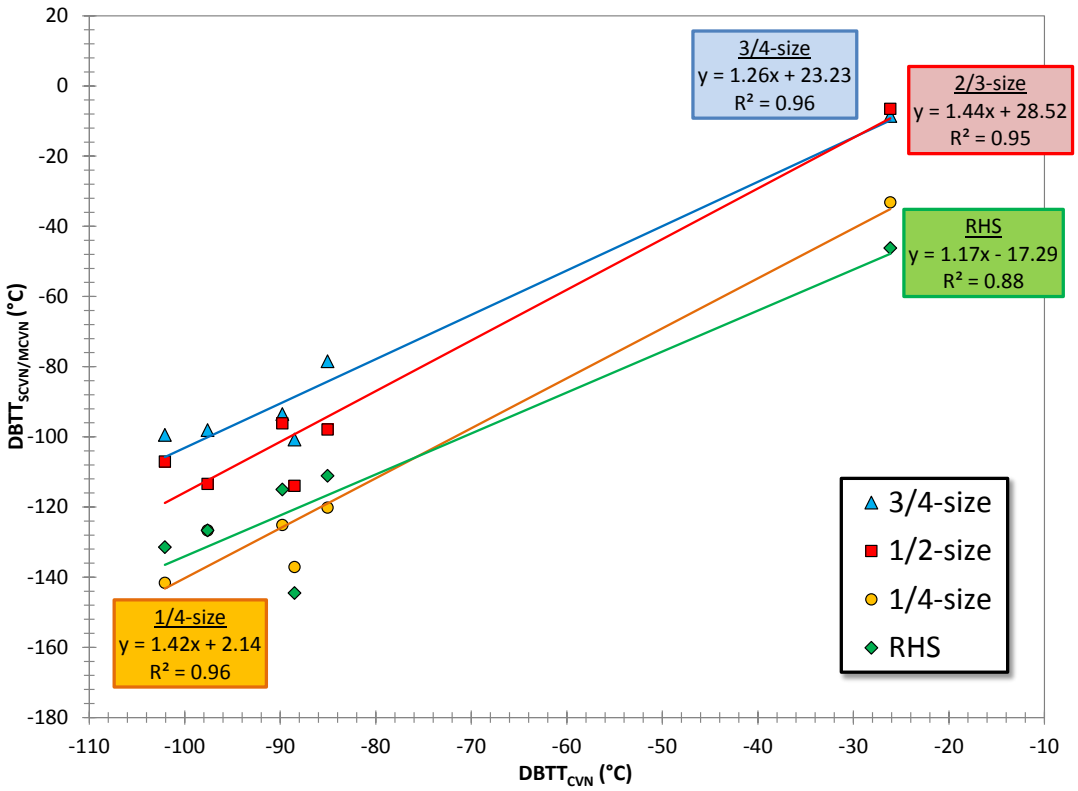

Figure 43 - Linear correlations between *DBTT* values from SCVN, MCVN, and CVN specimens. NOTE: data shaded in Table 16 are not included in the correlations presented.

5.1.1 Comparison with the literature

By analyzing test results obtained from CVN and four different types of MCVN specimens[‡‡‡] for 10 base and weld metals from reactor pressure vessel steels, Sokolov and Alexander [10] proposed the following correlation between the factor M in eq.(2) and the nominal fracture volume, expressed as Bb^2 (B = specimen thickness, b = ligament size):

$$M = 98 - 15.1 \cdot \ln\left(Bb^2\right) \tag{3}$$

In [10], eq.(3) was obtained by fitting values of M that corresponded to four different definitions of transition temperature: (a) temperature corresponding to 41 J absorbed energy; (b) temperature corresponding to 68 J absorbed energy; (c) temperature corresponding to the midpoint of the transition curve; and (d) temperature corresponding to 50 % *SFA*.

The values of the *DBTT* shift obtained in this investigation and listed in Table 16 are compared to eq.(3) in Figure 44, where excellent agreement with Sokolov/Alexander's original fit can be observed for only the 1/2-size and RHS specimens. We recalculated the coefficients of eq.(3) with both sets of results, subject to the constraint $M = 0$ for $Bb^2 = 640$ mm^3 (*i.e.*, for CVN specimens), and the following modified relationship was obtained:

$$M = 101.1 - 15.65 \cdot \ln\left(Bb^2\right) \tag{4}$$

Figure 44 illustrates our test results, the data points obtained by Sokolov/Alexander in [10] for MCVN specimens of 4 different geometries, their original relationship, eq.(3), and the modified fitting line, eq.(4).

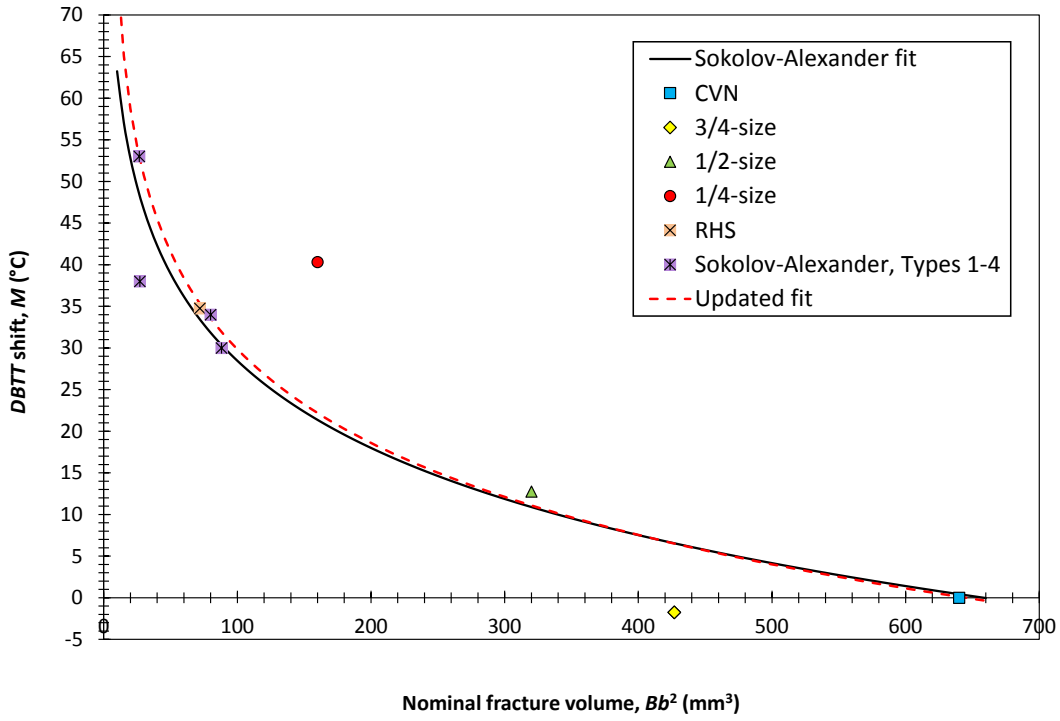

Figure 44 - Transition temperature correction for SCVN/MCVN specimens as a function of nominal fracture volume.

[‡‡‡]Type 1: B = 5 mm, b = 4.2 mm; type 2: B = 3.3 mm, b = 2.83 mm; type 3: B = 5 mm, b = 4 mm; type 4 (KLST): B = 3 mm, b = 3 mm.

An earlier investigation by Gross [12] studied the relationship between different measures of transition temperature that were obtained from standard and sub-size Charpy specimens of five structural steels with different strengths and ductilities. The sub-size geometries that were considered were 1/2-size (denominated HW, or *half-width*[§§§]) and 1/4-size (QW, *quarter-width*). Specimens with B = 20 mm were also used (DW, *double-width*). The criteria used to define and calculate *DBTT*s were: absorbed energy [KV = 15 ft.lb (20.3 J) and 3.8 ft.lb /0.1 in. (5.2 J/2.5 mm) width], lateral expansion [LE = 10 mils (0.25 mm), 15 mils (0.38 mm), and 20 mils (0.51 mm)], and shear fracture appearance (SFA = 10 %, 30 %, and 50 %). In addition, values of Nil-Ductility Temperature (*NDT*) were measured by drop-weight testing in accordance with ASTM E208 and were also reported. The average values of M for each steel investigated in [12] and the overall mean shift values are given in Table 18.

Table 18 - *DBTT* shifts measured by Gross [12] on five structural steels using different types of Charpy specimens.

Steel	Specimen type	Mean M (°C)
ABS-C	QW	-37
	HW	-14
	DW	4
A302-B	QW	-36
	HW	-15
	DW	2
HY-80	QW	-44
	HW	-12
	DW	-3
A517-F	QW	-67
	HW	-23
	DW	4
HY-130	QW	-56
	HW	-8
	DW	-2
All	**QW**	**-48**
	HW	**-14**
	DW	**1**

Both sub-size specimen geometries considered by Gross, the 1/2-size (or HW) and the 1/4-size (or QW), are in common with our investigation. The average shifts reported by Gross (-48 °C for 1/4-size and -14 °C for 1/2-size) are in good agreement with the mean values reported in Table 16, -40.3 °C for 1/4-size and -12.8 °C for 1/2-size. Note that in Gross' investigation, the change in *DBTT* was negligible (1 °C) when the thickness of the specimen was doubled.

If we add Gross' data to the M vs. Bb^2 plot shown in Figure 44, the values corresponding to 3/4-size and 1/4-size specimens do not appear well represented by Sokolov/Alexander's original fit or by our modified fit (Figure 45).

However, examination of Figure 45 leads to formulate a different hypothesis, based on the assumption that SCVN specimens follow a different trend than MCVN specimens, and therefore it should be more appropriate to separately fit SCVN and MCVN data.

[§§§]Note that in [11], the specimen dimension parallel to the notch is denominated "width". However, in this investigation the same dimension (B) is called "thickness", following the conventional fracture toughness designation.

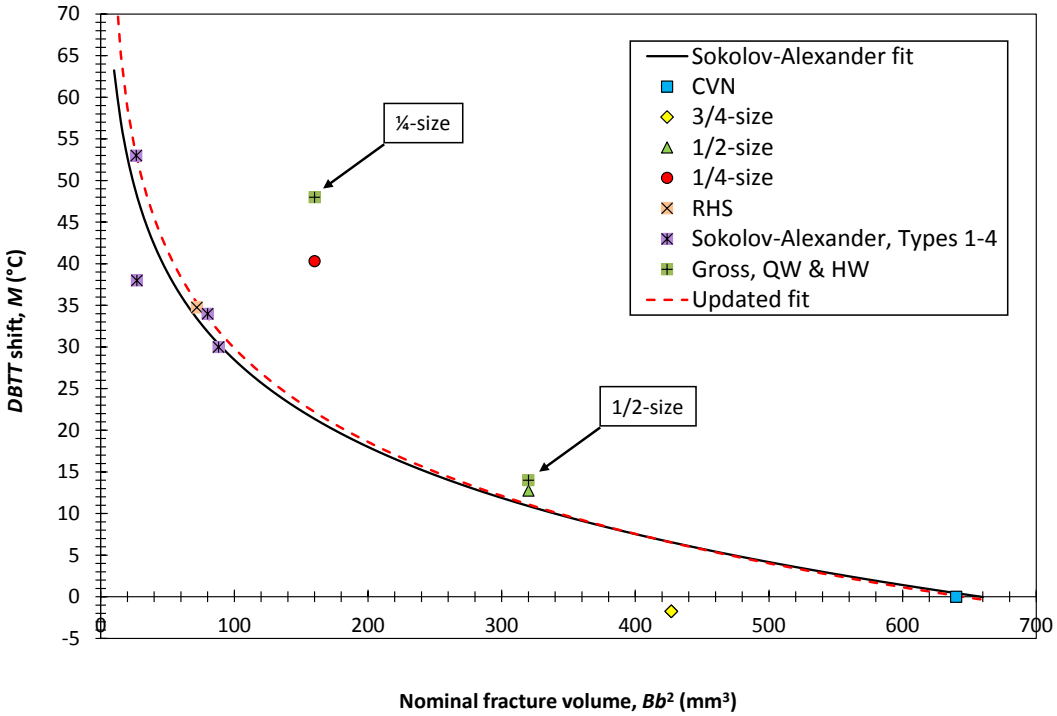

Figure 45 - Transition temperature correction for SCVN/MCVN specimens, with Gross' results added.

In Figure 46 we present an attempt at separately fitting SCVN and MCVN data, using the same formulation as eqs.(3) and (4) and still imposing $M = 0$ for CVN specimens. The quality of the SCVN fit is relatively poor, and more experimental data are needed to verify the applicability of this formulation for fitting SVCN test results.

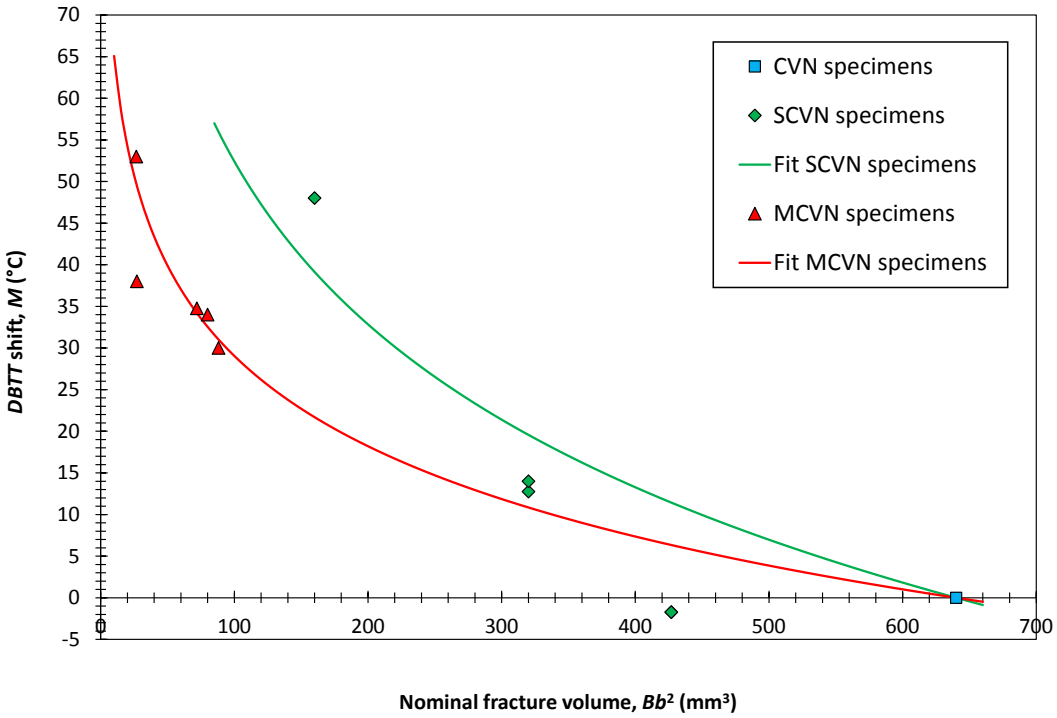

Figure 46 – *DBTT* shifts from [10], [12], and this investigation, fitted separately for SCVN and MCVN specimens.

5.2 Upper Shelf Energy

The most commonly used approach for correlating *USE* values between Charpy specimens of different geometries involves the use of a normalization factor, *NF*, which can be empirically derived from experimental data or calculated as the ratio between specific geometric parameters (see also Section 4.2.1):

$$USE_{CVN} = NF \times USE_{SCVN/MCVN} \tag{5}$$

Published values of *NF* include:

- NF_1 = ratio of fracture areas, expressed as Bb [13,14];
- NF_2 = ratio of nominal fracture volumes, expressed as $(Bb)^{3/2}$ [13,14];
- NF_3 = ratio of nominal fracture volumes, expressed as Bb^2 [15,16];
- NF_4 = ratio of Bb^2/SK_t (with S = span, or distance between the anvils, and K_t = elastic stress concentration factor, which depends on ligament size and notch root radius) [17];
- NF_5 = ratio of $(Bb)^{3/2}/QK_t$ (with Q = plastic stress concentration factor, given by $Q = 1 + (\pi - \theta)/2$, where θ is the notch angle in radians) [18].

Additionally, empirical normalization factors were published by Sokolov and Alexander for four types of miniaturized Charpy specimens [10] (NF_6).

In this investigation, the empirical normalization factors NF_7 obtained by fitting *USE* values with eq.(5), see Figure 47, are listed in Table 19, where they are compared with the previously listed geometrical and empirical factors.

Table 19 - Normalization factors published in the literature (NF_1 to NF_6) and calculated in this investigation (NF_7). For the definition of NF_1 to NF_7, see above.

Specimen type	NF_1	NF_2	NF_3	NF_4	NF_5	NF_6	$\mathbf{NF_7}$
3/4-size	1.33	1.54	1.33	1.33	1.54	-	**0.77**
1/2-size	2.00	2.83	2.00	2.00	2.83	-	**0.42**
1/4-size	4.00	8.00	4.00	4.00	8.00	-	**0.14**
RHS	4.29	8.89	8.89	3.30	6.84	6.3****	**0.15**

All of he calculated normalization factors are much lower than any of the values published in the literature. The behavior of 1/4-size and RHS specimens is almost identical, as can be appreciated in Figure 47. The degree of linearity of the relationships between *USE* values is generally high, except for 1/4-size specimens.

One possible explanation for this result is that the "true" Upper Shelf Energy might not have been established for some of the steels and some of the specimen geometries employed. Particularly if the experimental values of USE_{CVN} are underestimated, the normalization factor *NF* from equation (5) will also be underestimated. This appears as a plausible circumstance when looking at Figure 48, which compares *KV*-based transition curves obtained from CVN specimens for the three steels. Particularly in the case of 4340 low and high energy, one might wonder if higher *KV* values could be obtained by testing at higher temperatures, even though at least three tests corresponding to fully ductile fracture, *i.e.*, *SFA* = 100 %, are available. Indeed, three tests corresponding to *SFA* ≥ 95 % is the minimum requirement commonly used for calculating a reliable value of *USE*, see for example ASTM E185-10 [19].

****This value corresponds to Type 3 in [6], which is dimensionally almost identical to a RHS specimen (thickness = 5 mm, width = 5 mm, length = 27 mm, notch angle = 45°, notch depth = 1 mm, notch root radius = 0.25 mm).

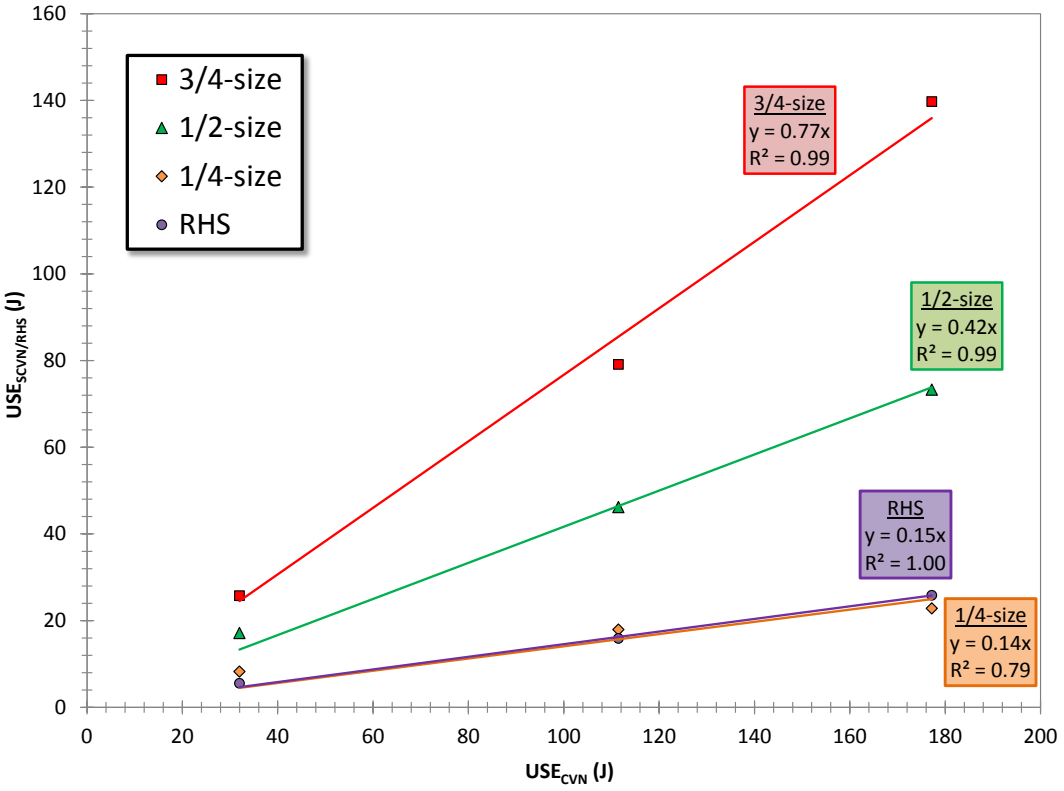

Figure 47 - Correlation between USE values measured on CVN, SVCN, and RHS specimens.

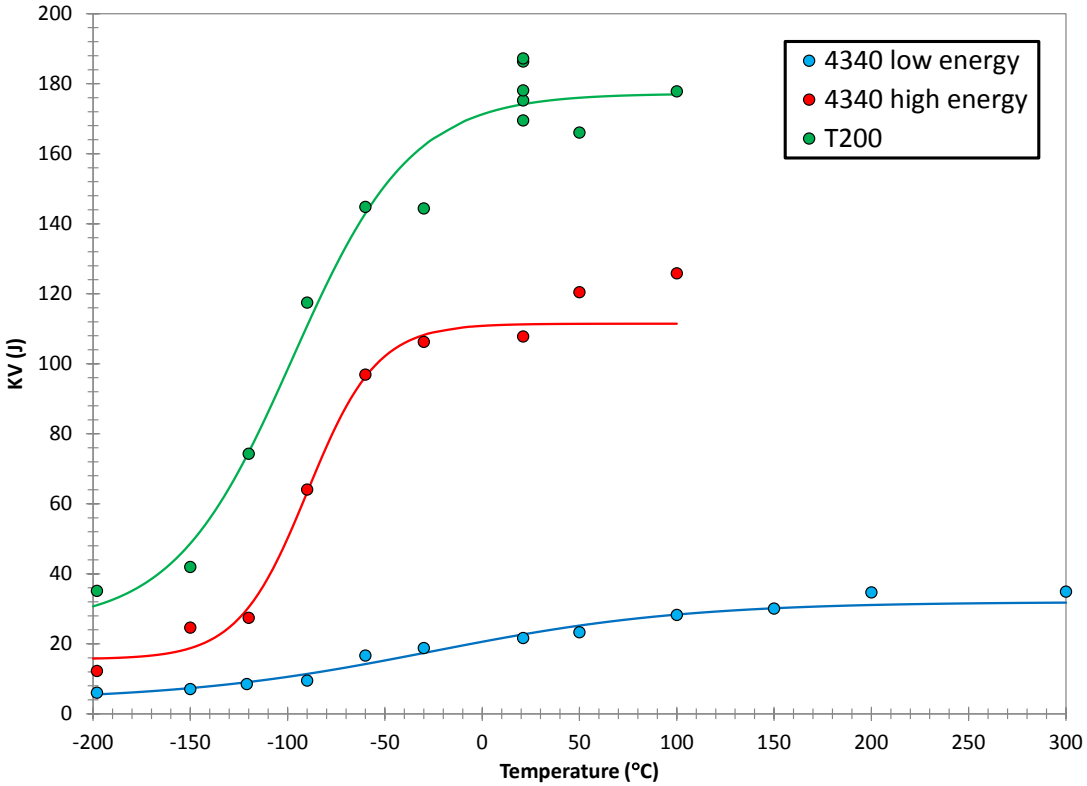

Figure 48 – Comparison between *KV* transition curves obtained from CVN specimens, which show that the highest values of absorbed energy might not have been attained for some of the steels.

6. Validation of Table 9 from ASTM A370-14, *Standard Test Methods and Definitions for Mechanical Testing of Steel Products*

ASTM Standard A370-14 covers procedures and definitions for the mechanical testing of steels, stainless steels, and related alloys. The mechanical tests described include tension, bend, hardness, and impact, and are used to determine properties required in the product specifications.

In the impact (Charpy) section of the standard, both standard size (CVN) and subsize (SCVN) specimens are covered. These latter are to be used for tubular materials, when the relationship between diameter and wall thickness does not permit obtaining CVN specimens (the largest feasible SCVN specimen should be used). The SCVN geometries listed are: 1/4-size (B = 2.5 mm), 1/3-size (B = 3.3 mm), 1/2-size (B = 5 mm), 2/3-size (B = 6.7 mm), and 3/4-size (B = 7.5 mm). Three of these specimen configurations were used for the investigations described in this report.

Oftentimes, the acceptance criterion for impact tests is specified as a minimum average *KV* value from three specimens from one location, and at a given temperature. When SCVN specimens have to be used, the specified minimum *KV* test requirements must be modified in accordance with Table 9 of ASTM A370-14, which is given in Figure 1 and also reproduced below. Note *A* limits the table to 54 J (40 ft-lb), stating that beyond this limit the relationship between KV_{CVN} and KV_{SCVN} "has been reported to be non-linear."

A370 – 13

TABLE 9 Charpy V-Notch Test Acceptance Criteria for Various Sub-Size Specimens

Full Size, 10 by 10 mm		¾ Size, 10 by 7.5 mm		⅔ Size, 10 by 6.7 mm		½ Size, 10 by 5 mm		⅓ Size, 10 by 3.3 mm		¼ Size, 10 by 2.5 mm	
ft·lbf	[J]	ft·lbf	[J]	ft·lbf	[J]	ft·lbf	[J]	ft·lbf	[J]	ft·lbf	[J]
40[A]	[54]	30	[41]	27	[37]	20	[27]	13	[18]	10	[14]
35	[48]	26	[35]	23	[31]	18	[24]	12	[16]	9	[12]
30	[41]	22	[30]	20	[27]	15	[20]	10	[14]	8	[11]
25	[34]	19	[26]	17	[23]	12	[16]	8	[11]	6	[8]
20	[27]	15	[20]	13	[18]	10	[14]	7	[10]	5	[7]
16	[22]	12	[16]	11	[15]	8	[11]	5	[7]	4	[5]
15	[20]	11	[15]	10	[14]	8	[11]	5	[7]	4	[5]
13	[18]	10	[14]	9	[12]	6	[8]	4	[5]	3	[4]
12	[16]	9	[12]	8	[11]	6	[8]	4	[5]	3	[4]
10	[14]	8	[11]	7	[10]	5	[7]	3	[4]	2	[3]
7	[10]	5	[7]	5	[7]	4	[5]	2	[3]	2	[3]

[A] Table is limited to 40 ft-lbf because the relationship between specimen size and test results has been reported to be non-linear for higher values.

A Task Group was initiated within ASTM Subcommittee A01.13 (*Mechanical and Chemical Testing and Processing Methods of Steel Products and Processes*) with the objective of verifying and updating the information provided in Table 9 of A370. The source of the data provided in the current Table 9 is unknown, and needed to be verified with actual Charpy results, and also the possibility of extending the applicability of the table to values higher than 54 J needed to be assessed.

During one of the ASTM Committee meetings in 2012, the A01.13 Task Group and NIST decided to verify the applicability and reliability of Table 9 by performing instrumented Charpy tests on full-size and sub-sized specimens of the three steels used at NIST for producing reference specimens (4340 low energy, 4340 high energy, and T200 maraging steel). The implications of our tests for Table 9 of A370-14 are discussed in this section.

Additionally, the same analyses were undertaken on instrumented Charpy tests performed on four line pipe steels (X52, X65, X70, and X100), which have been described in detail in a separate report [24].

6.1 Procedure for correlating *KV* values between CVN and SCVN specimens

The verification of Table 9 of ASTM A370-14 implies establishing a correlation between absorbed energy values measured from CVN and SCVN specimens, based on the results obtained on the NIST reference steels.

The simple procedure applied for this correlation is illustrated in Figure 49, and can be summarized as follows:

(a) for each of the materials tested, the reference value of *KV* from Table 9 is associated to a test temperature on the *CVN* transition curve (upper part of Figure 49, for example KV_{CVN} = 43 J);

(b) this test temperature corresponds to a specific value of KV_{SCVN} on the corresponding transition curve for each of the sub-sized specimens tested (lower part of Figure 49, for example KV_{SCVN} = 26 J).

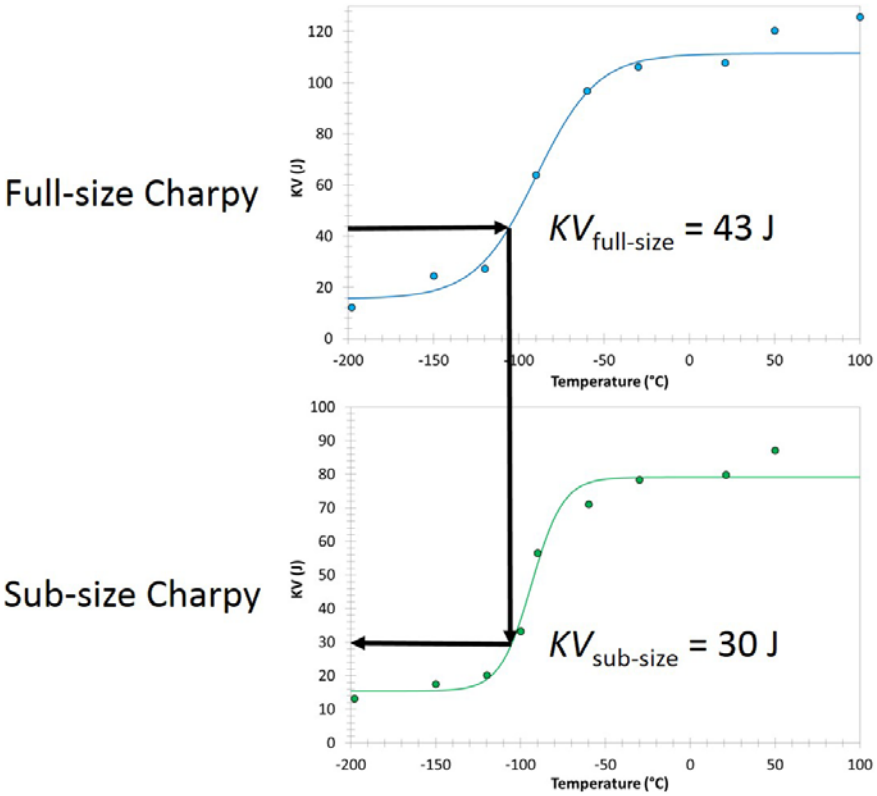

Figure 49 - Procedure for correlating *KV* values from CVN and SCVN specimens.

As a result of this correlation procedure, we obtained the values reported in Table 20 (NIST reference steels) and Table 21 (line pipe steels) for the sub-sized specimens used (3/4-size, 2/3-size[††††], 1/2-size, 1/4-size). We also extended this analysis to the miniaturized specimens (KLST[‡‡‡‡] and RHS) used in the two studies. In Table 20, the KV_{CVN} values correspond to the numbers given in Table 9 of A370. Note that, for many combinations of KV_{CVN} and specimen type, the corresponding $KV_{SCVN/RHS}$ is not available because the test temperature falls outside the limits of the experimentally measured transition curve.

[††††]2/3-size specimens (B = 6.67 mm) of the four line pipe steels were tested in the study described in [24].

[‡‡‡‡]KLST specimens of the four line pipe steels were tested in the study described in [24]. KLST (from the German "*Kleinstprobe*", or "small specimens" is a miniaturized Charpy specimen which has the following dimensions: length = 27 mm, thickness = 3 mm, width = 4 mm, notch depth = 1 mm, notch angle = 60°, and notch root radius = 0.1 mm. It is the reference MCVN geometry for ISO 14556:2000, but is also mentioned in ASTM E2248-13. Its characteristic feature is that, unlike the RHS specimen, it is not a scaled-down (proportional) specimen with respect to the full-size Charpy.

Table 20 – Values of absorbed energy for CVN, SCVN, and RHS specimens obtained for the NIST reference steels by means of the procedure outlined in Figure 49.

4340 low energy *KV* (J)					4340 high energy *KV* (J)					T200 *KV* (J)				
CVN	3/4-size	1/2-size	1/4-size	RHS	CVN	3/4-size	1/2-size	1/4-size	RHS	CVN	3/4-size	1/2-size	1/4-size	RHS
54					54	40.8	26.8	16.7	12.1	54	38.0	28.4	15.5	14.3
48					48	32.5	17.6	16.1	11.3	48	33.1	25.1	14.8	12.6
41					41	24.7	13.2	15.0	10.3	41	27.6	21.3	13.9	10.3
34	25.1	16.9	8.2	5.4	34	19.5	12.3	13.2	9.0	34	22.3	17.9	12.8	7.4
27	21.0	14.7	7.8	4.7	27	16.7	12.1	10.4	7.3	27	17.5	15.1	11.4	3.9
22	16.8	11.7	6.8	4.0	22	15.8	12.1	7.9	5.9	22				
20	15.0	10.3	6.2	3.7	20	15.6	12.1	6.9	5.3	20				
18	13.2	8.9	5.5	3.4	18	15.5	12.1	6.1	4.7	18				
16	11.5	7.5	4.7	3.0	16	15.4	12.1	5.4	4.0	16				
14	9.8	6.3	4.0	2.7	14	15.4	12.1	5.1	3.3	14				
10	6.8	4.4	2.8	1.9	10					10				

Table 21 – Values of absorbed energy for CVN, SCVN, and MCVN specimens obtained for the line pipe steels by means of the procedure outlined in Figure 49.

X52 *KV* (J)					X65 *KV* (J)				
CVN	2/3-size	1/2-size	KLST	RHS	CVN	2/3-size	1/2-size	KLST	RHS
54	39.4	29.9	4.2	11.7	54	88.1	62.2	8.0	43.5
48	36.9	28.3	4.2	11.2	48	77.2	57.2	7.7	43.3
41	33.8	26.3	4.2	10.6	41	63.9	50.7	7.4	42.7
34	30.3	24.1	4.1	9.6	34	50.4	43.4	6.9	41.5
27	26.4	21.6	4.1	8.3	27	36.9	35.2	6.3	38.3
22	23.2	19.5	4.1	7.1	22	27.6	28.7	5.7	33.0
20	21.8	18.6	4.0	6.5	20	24.0	26.0	5.4	29.6
18	20.3	17.6	4.0	5.9	18	20.6	23.1	5.0	25.2
16	18.7	16.5	3.9	5.2	16	17.2	20.3	4.6	19.9
14	17.0	15.3	3.9	4.5	14	14.0	17.3	4.1	14.2
10	13.2	12.4	3.5	2.9	10	8.3	11.3	3.0	4.5

X70 *KV* (J)					X100 *KV* (J)				
CVN	2/3-size	1/2-size	KLST	RHS	CVN	2/3-size	1/2-size	KLST	RHS
54	85.5	67.3	10.0	47.1	54	53.8	28.7	8.9	28.9
48	77.2	65.7	10.0	47.1	48	50.0	26.5	8.9	28.9
41	66.9	63.5	10.0	47.1	41	45.4	23.8	8.9	28.9
34	56.0	60.9	10.0	47.1	34	40.2	20.9	8.8	28.6
27	44.4	57.8	10.0	47.1	27	34.5	17.8	8.6	20.3
22	35.8	55.0	10.0	47.1	22	30.0	15.4	8.2	3.4
20	32.3	53.7	10.0	47.1	20	28.0	14.4	8.0	1.7
18	28.8	52.3	10.0	47.1	18	25.9	13.4	7.5	1.3
16	25.2	50.6	10.0	47.1	16	23.8	12.3	6.9	1.2
14	21.6	48.8	10.0	47.1	14	21.5	11.1	6.0	1.2
10	14.3	44.0	10.0	47.1	10	16.5	8.7	3.0	1.2

As previously mentioned, higher energies were also investigated, so that the claim of Note A from Table 9 ("*Table is limited to 40 ft-lbf because the relationship between specimen size and test results has been reported to be non-linear for higher values.*") could be substantiated or refuted. The corresponding values for 60 J $\leq KV_{CVN} \leq$ 100 J are given in Table 22 for 4340 high energy and T200 (for 4340 low energy, the highest value which could be correlated was KV_{CVN} = 34 J) and in Table 23 for the line pipe steels.

Table 22 – Values of absorbed energy in the range 60 J ≤ KV_{CVN} ≤ 100 J for 4340 high energy and T200.

4340 high energy *KV* (J)					T200 *KV* (J)				
CVN	3/4-size	1/2-size	1/4-size	RHS	CVN	3/4-size	1/2-size	1/4-size	RHS
60	49.7	37.1	17.1	12.8	60	43.0	31.8	16.1	16.1
70	62.8	44.7	17.5	13.6	70	51.4	37.3	16.9	16.9
80	71.6	46.0	17.7	14.3	80	60.0	42.7	17.7	17.7
90	76.3	46.2	17.9	14.9	90	68.7	47.7	18.4	18.4
100	78.4	46.2	17.9	15.3	100	77.3	52.3	19.0	19.0

Table 23 – Values of absorbed energy in the range 60 J ≤ KV_{CVN} ≤ 100 J for the line pipe steels.

X52 *KV* (J)					X65 *KV* (J)				
CVN	2/3-size	1/2-size	KLST	RHS	CVN	2/3-size	1/2-size	KLST	RHS
60	41.8	31.5	4.2	12.0	60	98.6	66.6	8.1	43.7
70	46.0	34.6	4.2	12.3	70	114.9	73.1	8.4	43.8
					80	129.6	78.6	8.6	43.9
					90	142.8	83.4	8.7	43.9
					100	154.5	87.4	8.8	43.9

X70 *KV* (J)					X100 *KV* (J)				
CVN	2/3-size	1/2-size	KLST	RHS	CVN	2/3-size	1/2-size	KLST	RHS
60	93.4	68.8	10.0	47.1	60	57.2	30.8	8.9	28.9
70	105.8	71.0	10.0	47.1	70	62.6	34.1	8.9	28.9
80	117.1	73.0	10.0	47.1	80	67.6	37.2	8.9	28.9
90	127.4	74.7	10.0	47.1	90	72.1	40.1	8.9	28.9
100	136.9	76.3	10.0	47.1	100	76.4	43.0	8.9	28.9

6.2 Comparisons between data from Table 9 data and experimental results

The comparisons between the values reported in Table 9 of ASTM A370-14 and in Tables 31 to 34 of this report are provided in Figures 63 to 65 for the NIST reference steels and Figures 66 to 69 for the line pipe steels.

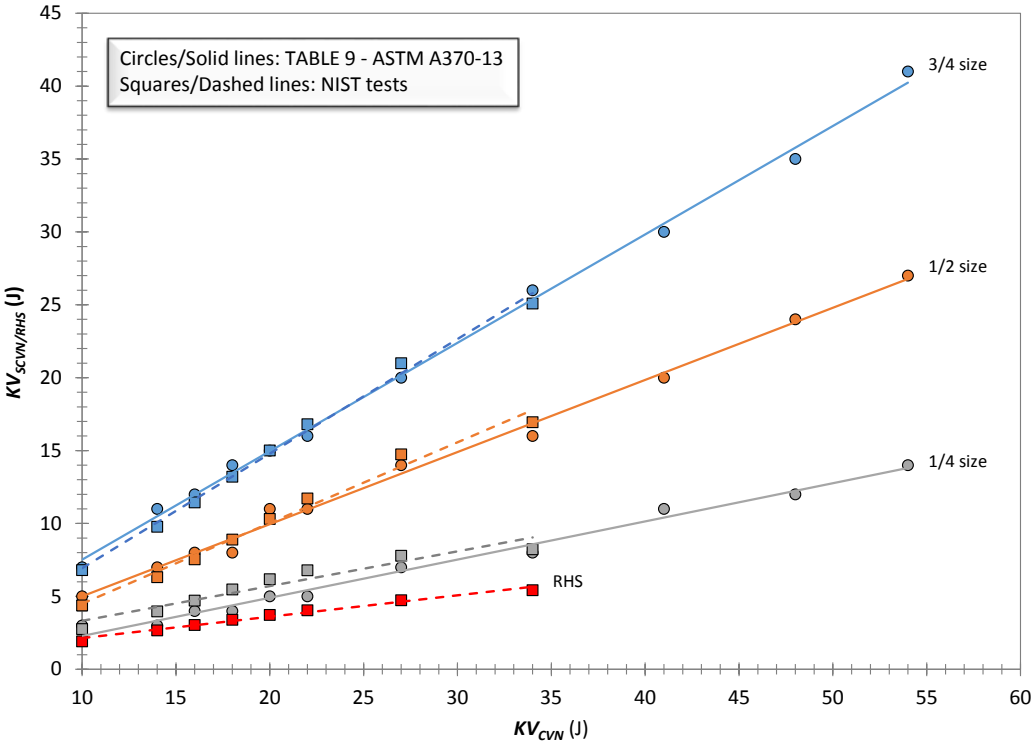

Figure 50 – Comparison between Table 9 of ASTM A370-14 and Charpy test results from 4340 low energy.

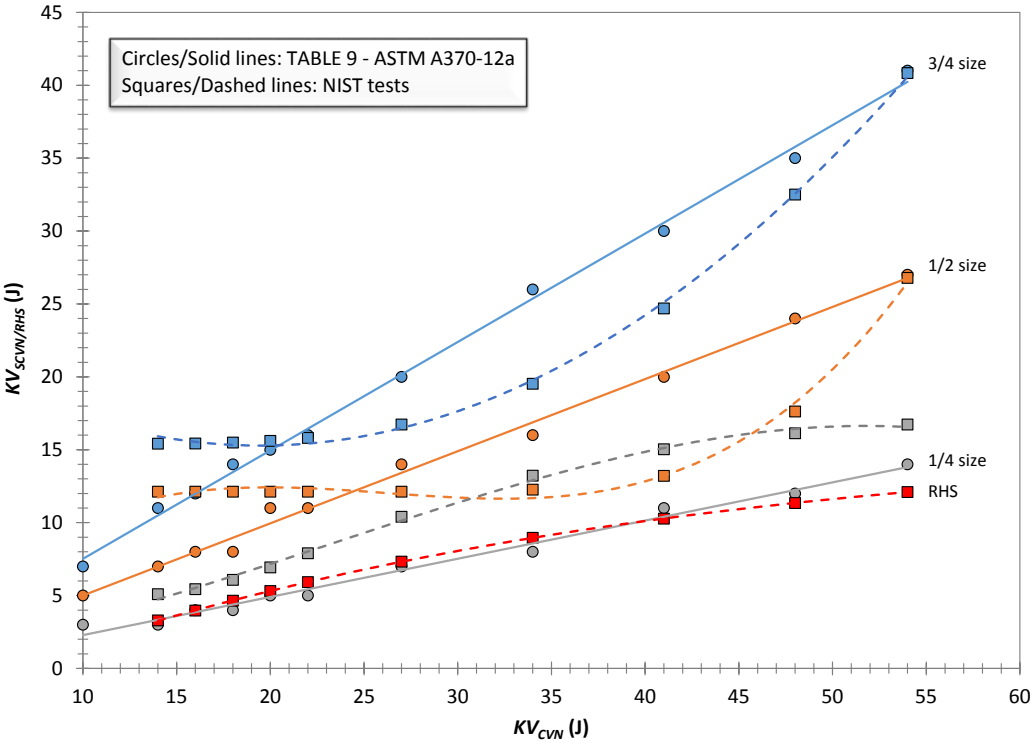

Figure 51 – Comparison between Table 9 of ASTM A370-14 and Charpy test results from 4340 high energy.

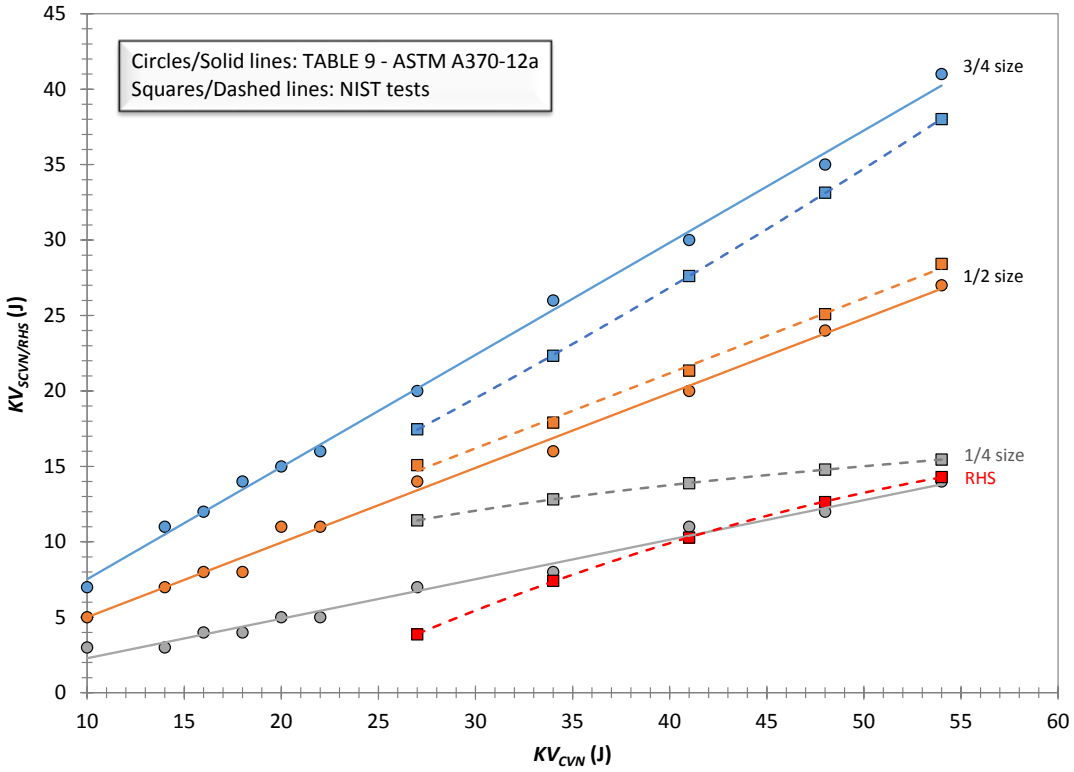

Figure 52 – Comparison between Table 9 of ASTM A370-14 and Charpy test results from T200.

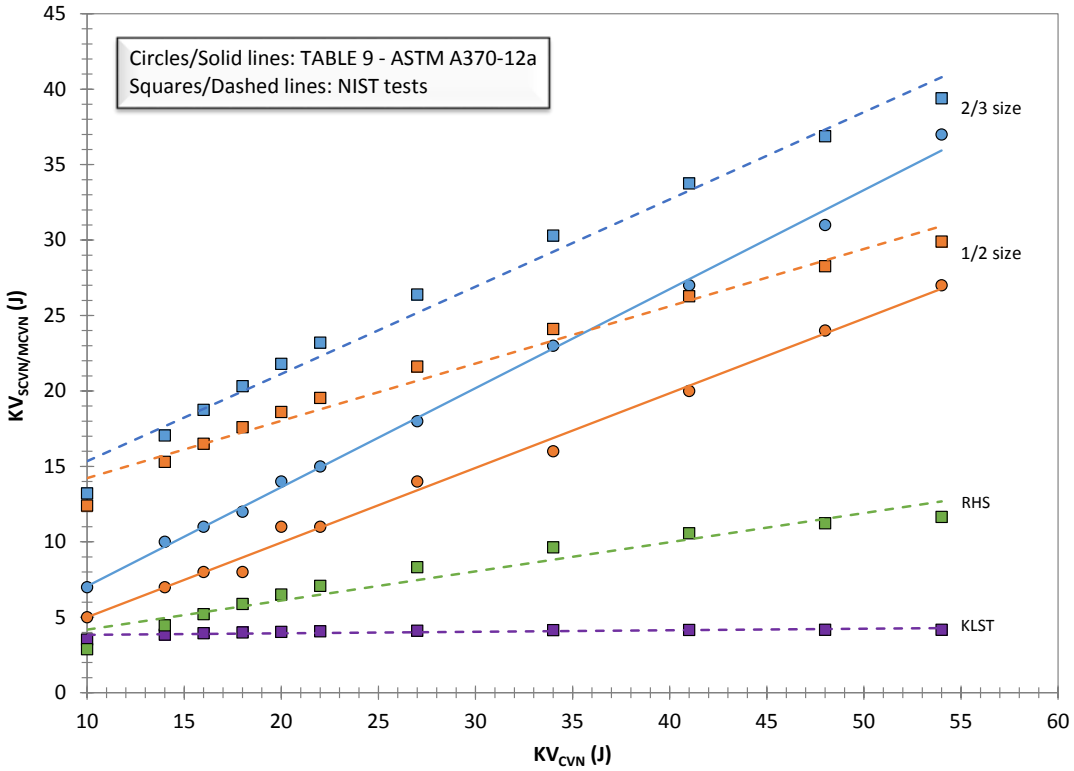

Figure 53 – Comparison between Table 9 of ASTM A370-14 and Charpy test results from X52 line pipe steel.

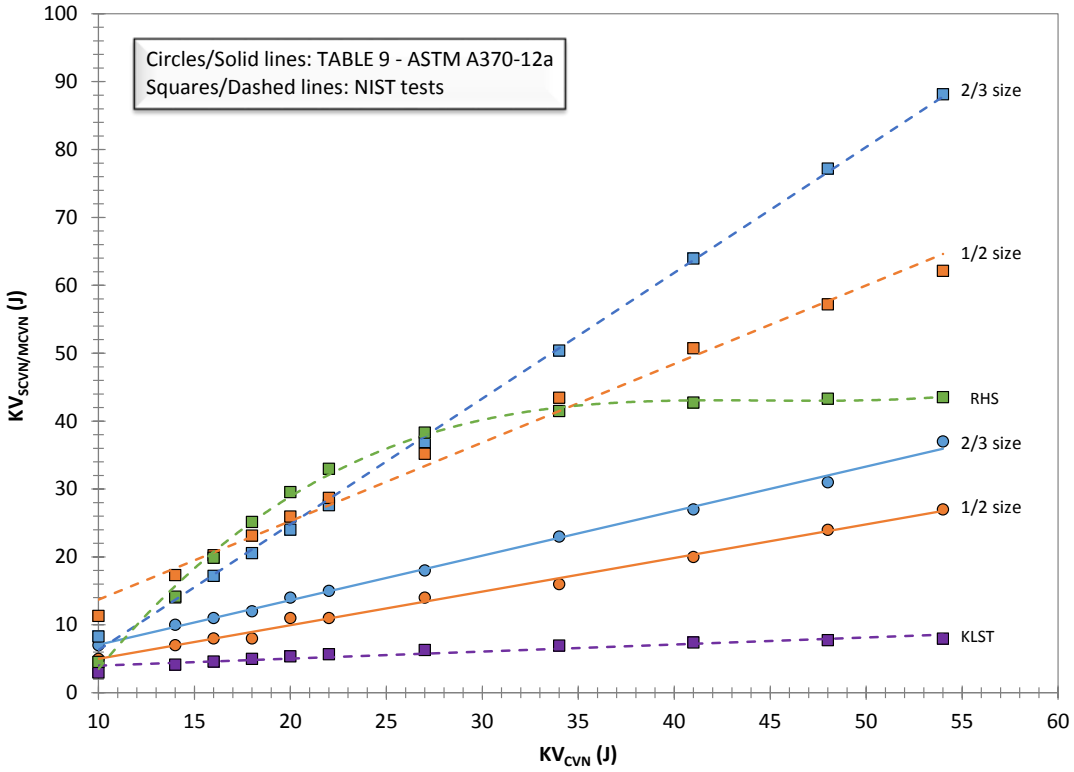

Figure 54 – Comparison between Table 9 of ASTM A370-14 and Charpy test results from X65 line pipe steel.

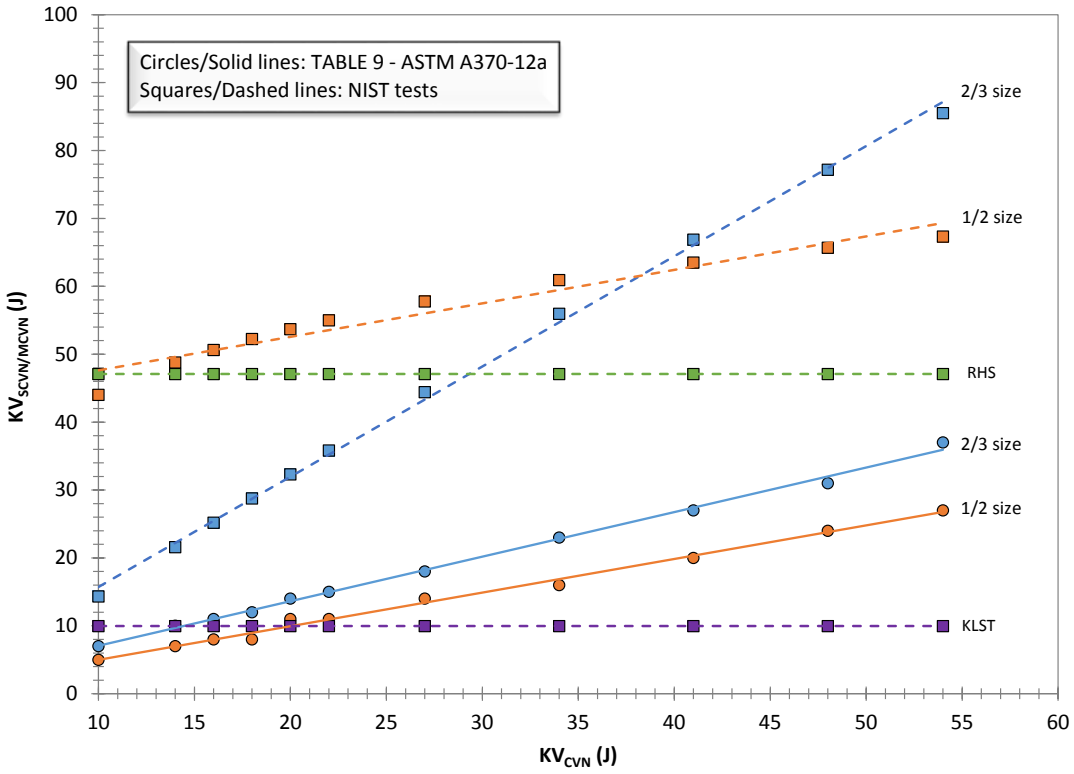

Figure 55 – Comparison between Table 9 of ASTM A370-14 and Charpy test results from X70 line pipe steel.

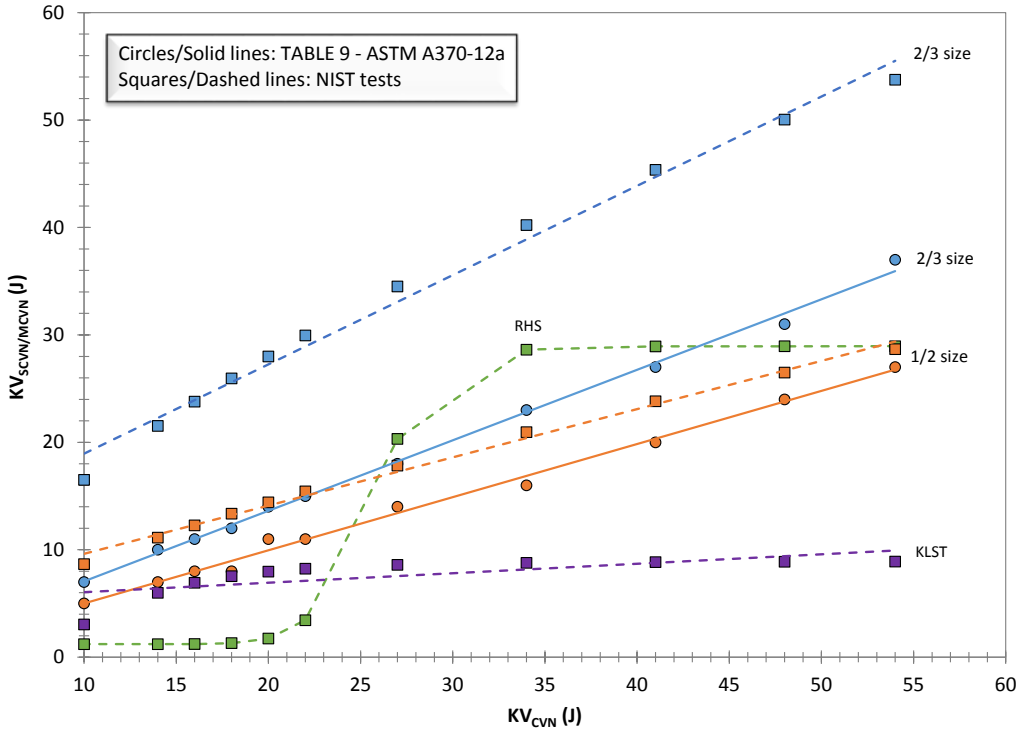

Figure 56 – Comparison between Table 9 of ASTM A370-14 and Charpy test results from X100 line pipe steel.

A different analytical approach is proposed in Figures 70 to 75, where for each non-standard specimen configuration, KV_{CVN} and $KV_{SCVN/MCVN}$ from each of the steels investigated are compared with Table 9 values.

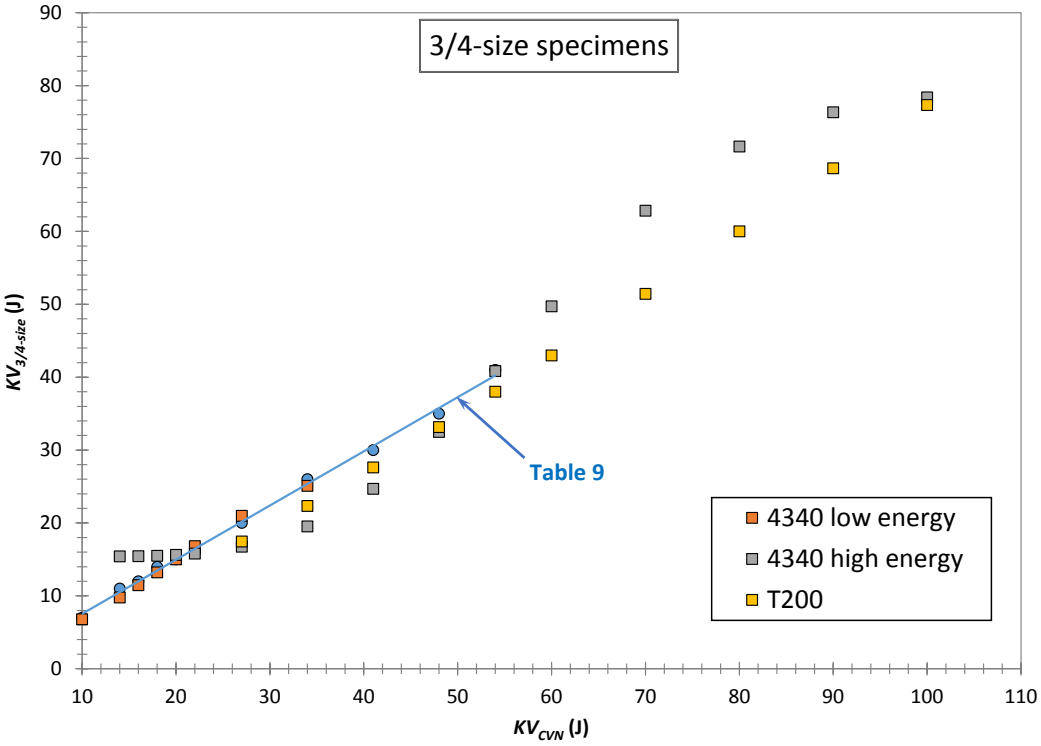

Figure 57 – Comparison between Table 9 of ASTM A370-14 and Charpy test results for 3/4-size specimens.

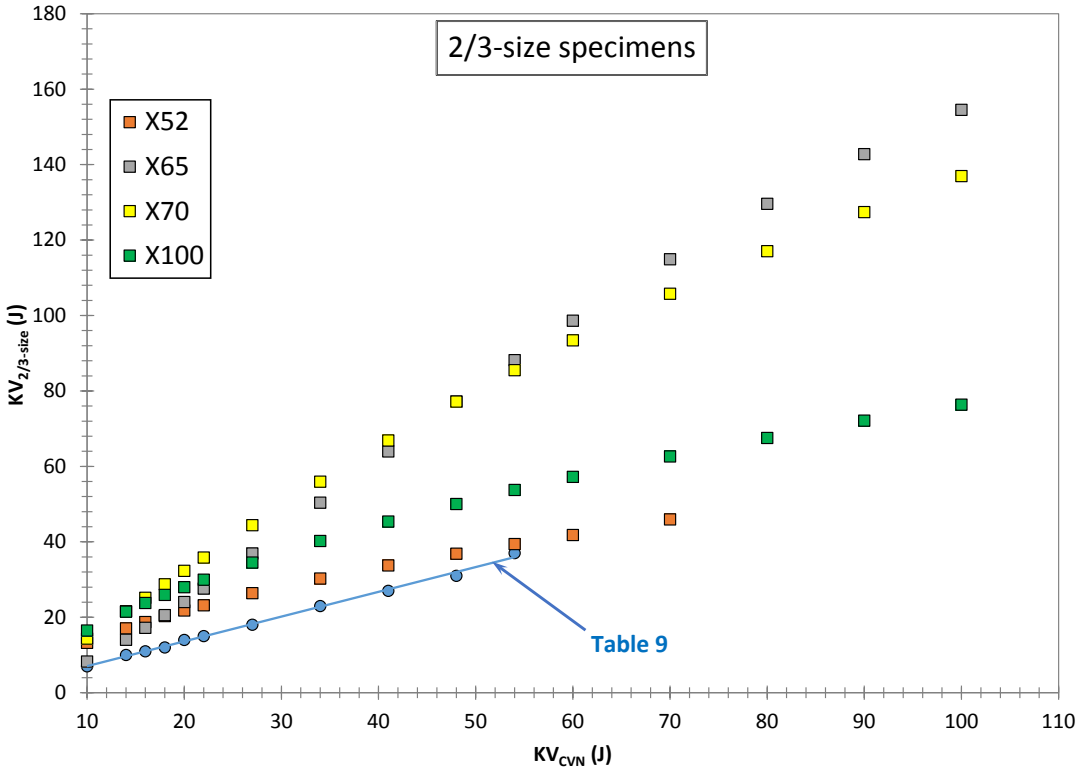

Figure 58 – Comparison between Table 9 of ASTM A370-14 and Charpy test results for 2/3-size specimens.

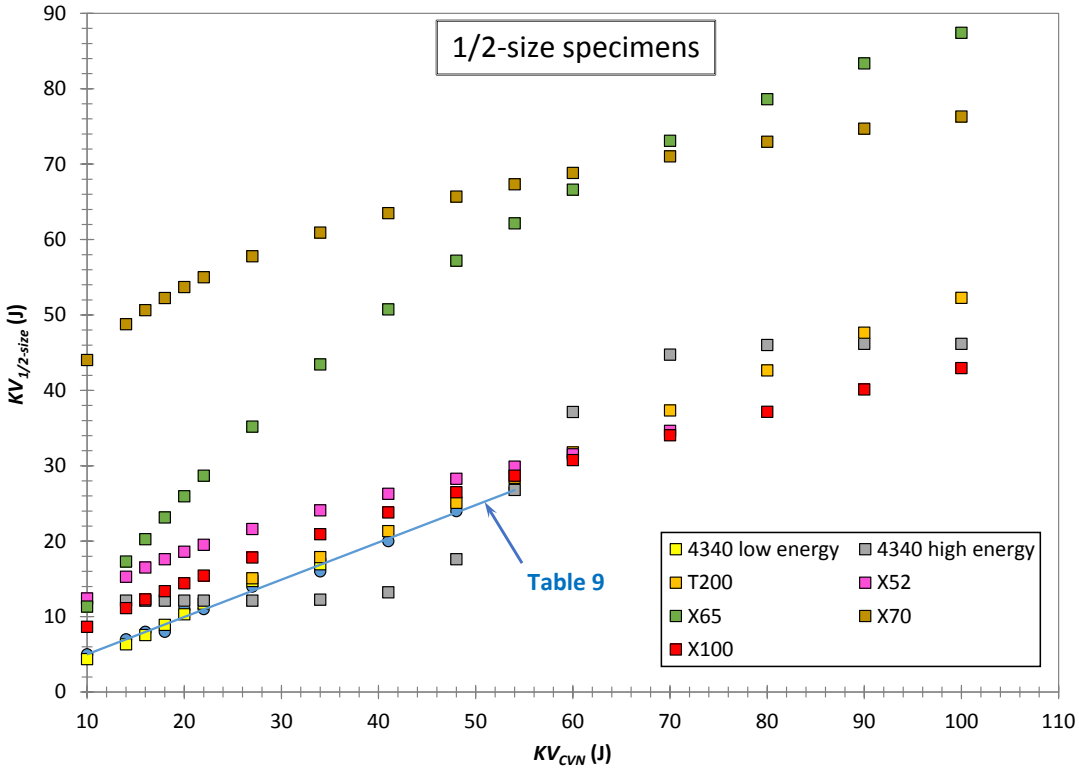

Figure 59 – Comparison between Table 9 of ASTM A370-14 and Charpy test results for 1/2-size specimens.

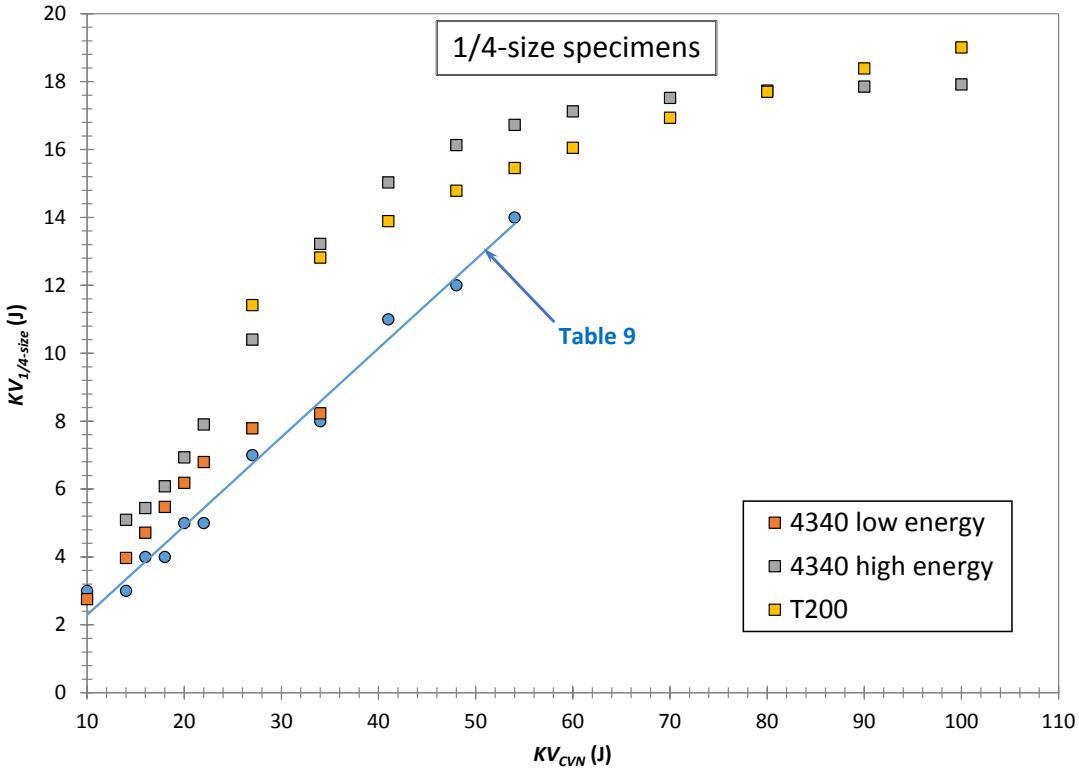

Figure 60 – Comparison between Table 9 of ASTM A370-14 and Charpy test results for 1/4-size specimens.

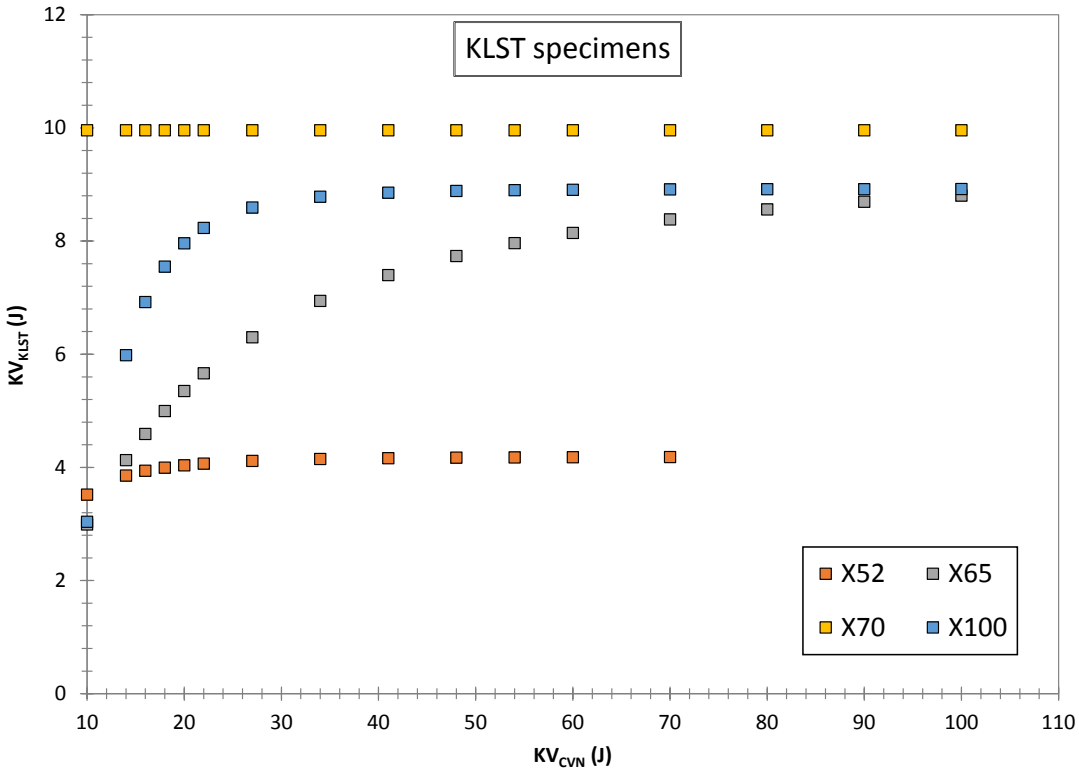

Figure 61 – Comparison between Charpy test results for KLST specimens.

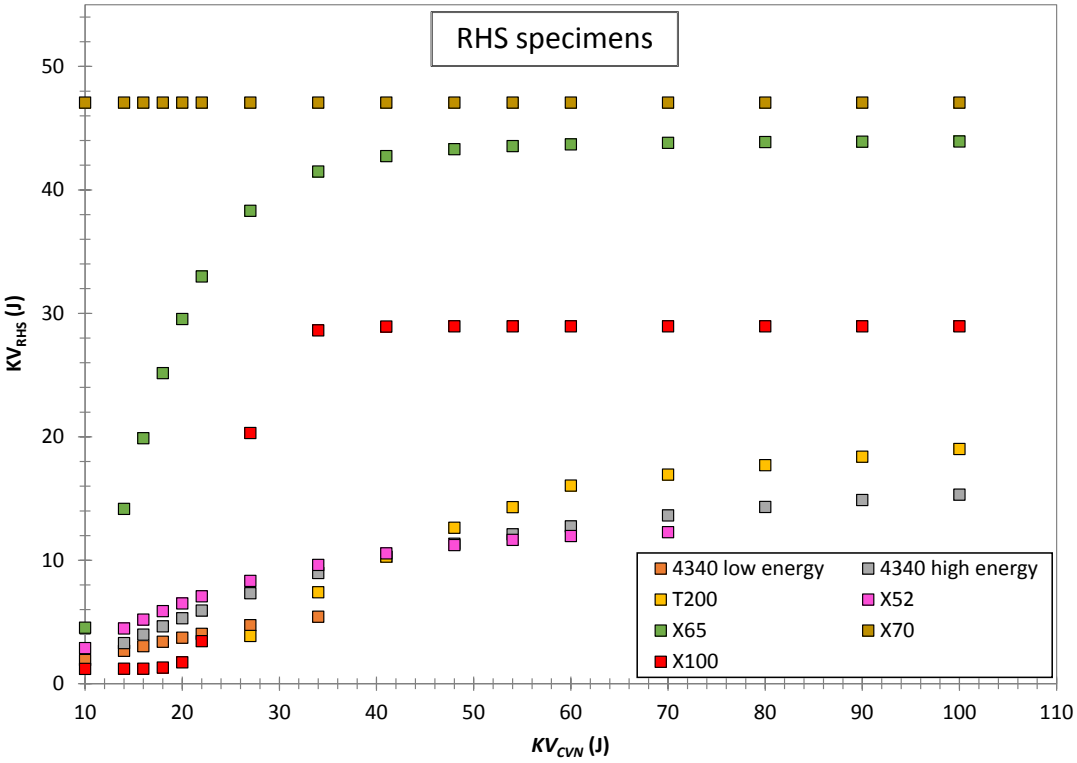

Figure 62 – Comparison between Charpy test results for RHS specimens.

The analyses presented in Figures 63 to 75 lead to the following observations.

(1) The agreement between our experimental data and Table 9 is satisfactory only for one of the seven steels tested, 4340 low energy. For the remaining materials, discrepancies are very large, particularly for very high toughness and ductility materials such as X65 and X70 line pipe steels.

(2) The trend shown by Table 9 data is substantially linear, whereas for many of the NIST experimental results the trends are clearly non-linear, due to some of the KV_{SCVN} values falling on the lower shelf or on the upper shelf of the transition curve. Significant non-linearity can already occur at KV_{CVN} values well below 54 J, thereby contradicting the statement provided in Note A.

(3) It appears plausible that Table 9 was developed for a material (or several materials) with characteristics similar to those of 4340 low energy. However, for higher ductility/toughness steels, the use of Table 9 is inadequate and equivalent data should be generated for the steel under investigation, or at least for a specific class of materials with similar mechanical properties.

(4) It's interesting to note that for two of the investigated steels (4340 high energy and T200), Table 9 values for 1/4-size specimens are in better agreement with test results from RHS than from 1/4-size specimens. Also in consideration of the additional issues which emerged concerning the use of 1/4-size specimens in this study, it could be contended that RHS should be used instead of 1/4-size specimens when thin-walled components have to be characterized.

In summary, the approach used by Table 9 does not seem useful for most steels. The main issue is that a fixed conversion/correlation factor between *KV* values from full-size and sub-size Charpy specimens can be envisaged only when both specimen types are in the same fracture regime (*i.e.*, lower shelf, transition, or upper shelf) at the test temperature for the material under investigation. The possibility of the two specimens being in different

regimes increases with increasing material toughness and decreasing sub-size specimen thickness. In this case, a completely different and probably more complex approach than a simple *KV* correction factor will have to be considered.

7. Conclusions

(1) Although tests on 4340 low energy steel were conducted up to 300 °C, a stable upper shelf plateau was not reached. This introduces significant uncertainty in the determination of parameters such as ductile-to-brittle transition temperatures and upper shelf levels.

(2) At the opposite end of the spectrum, relatively high percentages of ductile fracture (*SFA* values ≥ 25 %) were measured for T200 even at the lowest achievable test temperature (≈ -198 °C). This leads to a poor definition of the $FATT_{50}$ transition temperatures.

(3) The above mentioned uncertainties are confirmed by the fact that, in several cases, transition temperatures measured from lateral expansion or *SFA* are in poor agreement with values measured from absorbed energy (*KV*).

(4) For a number of instrumented Charpy tests performed on 1/4-size specimens, the instrumented striker signal could not be recorded. For this specimen geometry, the acquisition trigger level had to be lowered because of the lower magnitude of the signals, but this led to false triggers caused by noise or electrical instabilities. Additionally, we found evidence of material embrittlement due to overheating (bluing) for four 1/4-size specimens of 4340 high energy, which had to be removed from the overall analyses. Finally, transition curves from 1/4-size specimens were often less well-defined than those obtained from other specimen types, including RHS specimens, particularly for 4340 low energy. All these circumstances lead us to advise against the use of 1/4-size specimens. In the case of thin-walled structures, a miniaturized specimen such as KLST or RHS should be employed (even if the false triggering issue could be solved).

(5) Instrumented characteristic forces at general yield (F_{gy}) and maximum forces (F_m) tend to decrease with increasing test temperature and obviously with specimen size. For SCVN specimens, instrumented forces can be normalized to CVN values with acceptable results, by the use of a normalization factor corresponding to the ratio of the nominal facture areas, expressed as *Bb*. For RHS specimens, the ratio between fracture areas needs to be multiplied by an empirical factor $\alpha \approx 0.88$.

(6) The ratio between the two measures of absorbed energy (*KV* and W_t) was found to be quite consistent and independent of test temperature or specimen type for both instrumented strikers used. The exception was for some tests performed at very low temperatures, where the interpretation of the instrumented test record cab be difficult.

(7) Because of the uncertainties associated with many of the calculated transition temperatures, the variations in *DBTT* between different specimen types were found to be less consistent than for a similar investigation recently conducted on a number of line pipe steels [24]. Nonetheless, results obtained from RHS specimens were found to be in good agreement with results previously published by other authors. Our results also show that SCVN and MCVN specimens follow different trends in their relationship with full-size Charpy specimens.

(8) The ratio between the Upper Shelf Energies as measured on SCVN/RHS and CVN specimens was found to be much lower than what has been published in the literature. One possible explanation is that for several

combinations of steel and specimen configuration, the “true” value of *USE* might not have been established, see item (1) above.

(9) For all materials and specimen types, we have compared optical measurements of Shear Fracture Appearance with estimates provided by four empirical formulae based on instrumented forces at general yield, maximum force, unstable fracture initiation, and crack arrest. All the empirical relationships tend to underestimate the measured *SFA* values, which leads to the calculation of conservative $FATT_{50}$. The second formula (designated F2 in this report) provides the best agreement with optically measured *SFA* values. Its accuracy is best for CVN specimens. Discrepancies between measured and estimated values are particularly significant for 4340 low energy, whose instrumented curves are the most difficult to analyze.

We used the results obtained on the NIST reference materials, as well as from the line pipe steels in [24], to verify the relationship between absorbed energy from CVN and SCVN specimens, as provided in Table 9 of ASTM A370-14 (*Charpy V-Notch Test Acceptance Criteria for Various Sub-Size Specimens*).

We observed that Table 9 works acceptably only for the least tough material investigated (4340 low energy). For tougher materials, the values in Table 9 are unacceptably low and the difference increases with the material’s toughness. The linearity of the relationship between KV_{CVN} and KV_{SCVN} is also extremely questionable, and a completely different approach appears warranted. The main issue is that, in most cases, different specimen types tested at the same temperature exhibit significantly different fracture behaviors, because of the shift of the transition temperature caused by a reduction of specimen size/thickness. Only when it can be guaranteed that all tests correspond to the same fracture regime (brittle/transition/ductile), a simple correlation/conversion factor between absorbed energies can be employed. Further research in this direction is therefore required.

Bibliography

[1] ASTM A370-14, *Standard Test Methods and Definitions for Mechanical Testing of Steel Products*, ASTM Book of Standards 01.03, 2014.

[2] ASTM E140-12$^{b\varepsilon 1}$, *Standard Hardness Conversion Tables for Metals Relationship Among Brinell Hardness, Vickers Hardness, Rockwell Hardness, Superficial Hardness, Knoop Hardness, Scleroscope Hardness, and Leeb Hardness*, ASTM Book of Standards 01.03, 2014.

[3] C. McCowan, R. Santoyo, and J. Splett, "*Certification Report for SRMs 2112 and 2123*," NIST Special Publication 260-172, July 2009.

[4] C. N. McCowan, T. A. Siewert, and D. P. Vigliotti, "*The NIST Charpy V-notch Verification Program: Overview and Operating Procedures*," in: NIST Technical Note 1500-9, *Charpy Verification Program: Reports Covering 1989-2002*, September 2003, pp. 3-42.

[5] ASTM E2248-13, *Standard Test Method for Impact Testing of Miniaturized Charpy V-Notch Specimens*, ASTM Book of Standards 01.03, 2014.

[6] ISO 14556:2000, *Steel -- Charpy V-notch pendulum impact test -- Instrumented test method*, International Standards Organization, 2000.

[7] ASTM E2298-13a, *Standard Test Method for Instrumented Impact Testing of Metallic Materials*, ASTM Book of Standards 01.03, 2014.

[8] C. N. McCowan, E. Lucon, and R. L. Santoyo, "*Comparison of Charpy V-notch Specimens: Full Size, Sub-Size, and Mini – Part 2: Shear Fracture*," to be submitted to *Materials Performance and Characterization*, 2014 (in preparation).

[9] W. Oldfield, "*Curve Fitting Impact Test Data: A Statistical Procedure*," ASTM Standardization News, November 1975, pp. 24-29.

[10] M. A. Sokolov and D. J. Alexander, "*An Improved Correlation Procedure for Subsize and Full-Size Charpy Impact Specimen Data*," NUREG/CR-6379, ORNL-6888, Oak Ridge National Laboratory, March 1997.

[11] E. Lucon, R. Chaouadi, A. Fabry, J.-L. Puzzolante, and E. van Walle, "*Characterizing Material Properties by the Use of Full-Size and Subsize Charpy Tests: An Overview of Different Correlation Procedures*," in ASTM STP 1380, "*Pendulum Impact Testing: A Century of Progress*," T. A. Siewert and M. P. Manahan, Eds., ASTM, West Conshohocken, PA, 2000, pp.146-163.

[12] J. H. Gross, "*Effect of Strength and Thickness on Notch Ductility*," in ASTM STP 466, "*Impact Testing of Metals*," D. E. Driscoll, Ed., ASTM, Philadelphia, 1970, pp. 21-52.

[13] W. R. Corwin and A. M. Hougland, "*Effect of Specimen Size and Material Condition on the Charpy Impact Properties of 9Cr-1Mo-V-Nb Steel*," in ASTM STP 888, "*The Use of Small-scale Specimens for Testing Irradiated Material*," W. R. Corwin and G. E. Lucas, Eds., ASTM, Philadelphia, 1986, pp. 325-338.

[14] W. R. Corwin, R. L. Klueh, and J. M. Vitek, "*Effect of Specimen Size and Nickel Content on the Impact Properties of 12 Cr-1 MoVW Ferritic Steel*," Journal of Nuclear Materials **122-123**, 1984, pp. 343-348.

[15] G. E. Lucas, G. R. Odette, J. W. Sheckherd, P. McConnell, and J. Perrin, "*Subsized Bend and Charpy V-Notch Specimens for Irradiated Testing*," in ASTM STP 888, "*The Use of Small-scale Specimens for Testing Irradiated Material*," W. R. Corwin and G. E. Lucas, Eds., ASTM, Philadelphia, 1986, pp. 304-324.

[16] G. E. Lucas, G. R. Odette, J. W. Sheckherd, and M. R. Krishnadev, "*Recent Progress in Subsized Charpy Impact Specimen Testing for Fusion Reactor Materials Development*," Fusion Technology **10**, 1986, pp. 728-733.

[17] B. S. Louden, A. S. Kumar, F. A. Garner, M. L. Hamilton, and W. L. Hu, "*The Influence of Specimen Size on Charpy Impact Testing of Unirradiated HT-9*," Journal of Nuclear Materials **155-157**, 1988, pp. 662-67.

[18] H. Kayano, H. Kurishia, A. Kimura, M. Narui, M. Yamazaki, and Y. Suzuki, "*Charpy Impact Testing Using Miniature Specimens and Its Application to the Study of Irradiation Behavior of Low-Activation Ferritic Steels*," Journal of Nuclear Materials **179-181**, 1991, pp. 425-88.

[19] ASTM E185-10, *Standard Practice for Design of Surveillance Programs for Light-Water Moderated Nuclear Power Reactor Vessels*, ASTM Book of Standards 12.02, 2014

[20] E. Lucon, C. N. McCowan, and R. L. Santoyo, "*Impact Characterization of Line Pipe Steels by Means of Standard, Sub-Size and Miniaturized Charpy Specimens*," NIST Technical Note, Publication id 917096, September 2014.